AFCRL-64-929

AFCRL-64-929

61(052)-490

December 1963

THIRD TECHNICAL ANNUAL SUMMARY REPORT

ON THE PROPAGATION OF VLF WAVES IN SOLIDS

Dr. W. Bitterlich
Innsbruck, Austria

The research reported in this document has been sponsored by the United States Government.

Preface

The main problem scheduled for the year 1963 by the team working on VLF problems since December 1960 is the explanation and elimination of discrepancies between the results of theoretical calculations and experimental measurements that still existed. For this purpose all factors influencing the propagation of VLF waves had to be studied theoretically and the experimental methods of measurement had to be further developed. The improvement of all apparatus used so far as well as the expansion of measurements over much greater distances at which clear effects are to be expected according to theoretical considerations, are of special importance. Measurements were conducted in German and Dutch mines to explain the effect of different geological bodies on wave propagation; furthermore, a number of conductivity measurements were made. We mainly thank our "landlord" Bergrat Dipl. Ing. Kettner, director of the Montan Werke Brixlegg for making it possible for us to work and move about freely with our measuring equipment in the mines of Schwaz and St. Gertraudi.
He also gave us permission to install our mine lab, and some of his miners did the necessary blasting. We again want to express our best thanks.
The directors of the Dutch coal pit Oranje Nassau III made it possible for us (by special safety measures and by unsupported galleries) to conduct an interesting measurement along a coal seam. We want to thank them very much for their great efforts.
Furthermore I want to express my special thanks to the directors of the Salzgitter ore mine, Vereinigte Kaliwerke Saldetfurth, Siegerland ore mine and all those who assisted us in our subsurface measurements.

Innsbruck, December 1963 Wolfram Bitterlich

of a new VLF receiver. A completely new way was chosen to build antenna circuits, amplifier circuits, and selective circuits from different viewpoints and by means of nuvistors. (See Fig. III). The first results which are promising show a progress in our efforts to build an optimum receiving device. The sensitivity, band width, and the signal-to-noise ratio were improved. These studies will probably be published in 1964, as the development is still being continued.

An easily portable measuring device was built and numerous experiments in different geological bodies were made in order to determine the electrical data of the rock, especially the conductivity.

In 1963, 45 expeditions to mines and underground measurements were made.

1.2 Field strength measuring device

The field strength measuring device built in 1962 had to be improved in various respects. In principle, however, the construction remained the same. The following items have to be pointed out:

(1.) Redesign of the input stage; lowering of the noise level, and at the same time increase of amplification. A limiter circuit at the input prevents this stage to be overdriven.

(2.) The selectivity was increased by building in a helical potentiometer, simultaneously, the amplification was made more constant (better than $\pm$ 2 db when tuning over a frequency range of 1 : 10). The frequency range of 30 cps - 30 kc/sec can now be covered continuously in three ranges.

(3.) The use of a millivoltmeter proved to be very suitable so that the antenna voltage on the amplifier input in this developed

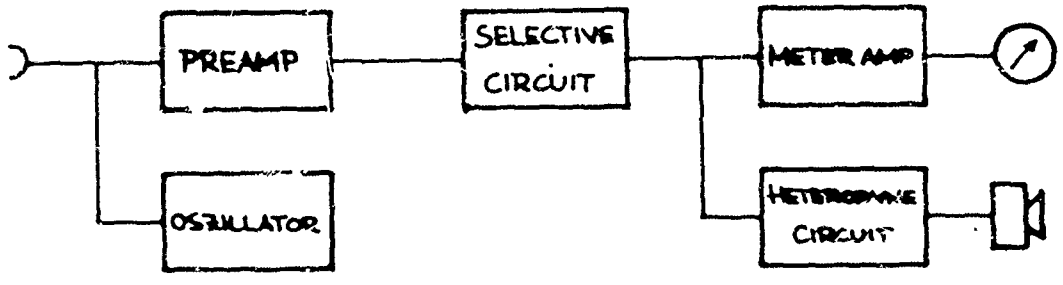

VLF FIELD STRENGTH METER

SCHEME S 2:

1 OFF
2 SUPPLY
3 METER
4 HETERODYNE
5 CALIBRATE

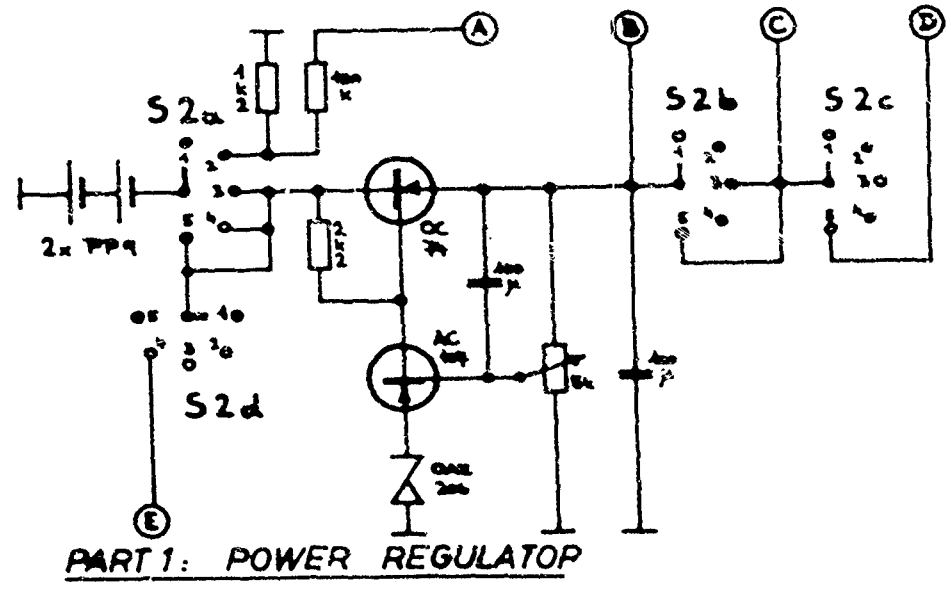

PART 1: POWER REGULATOP

FIG. 1.1

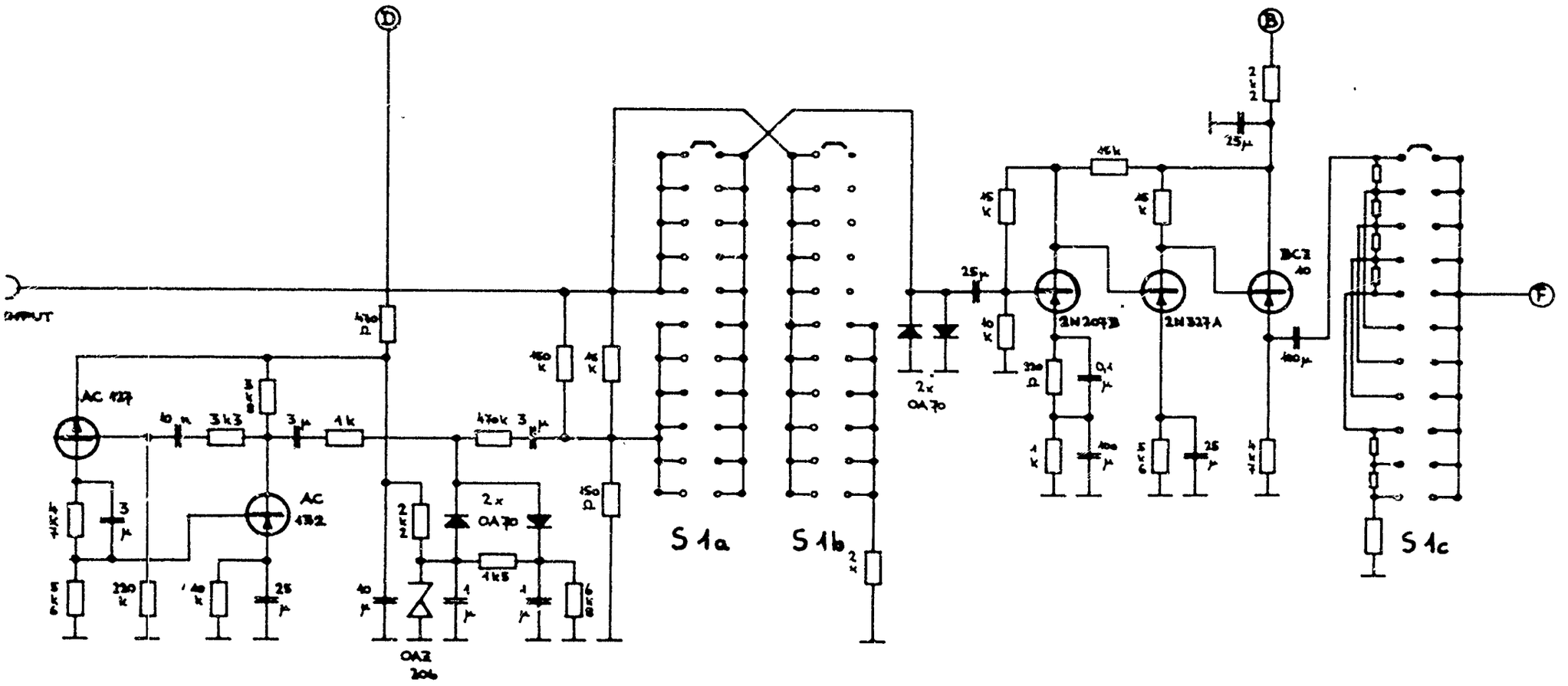

PART 2: PREAMP + OSZILLATOR

FIG. 1, 2

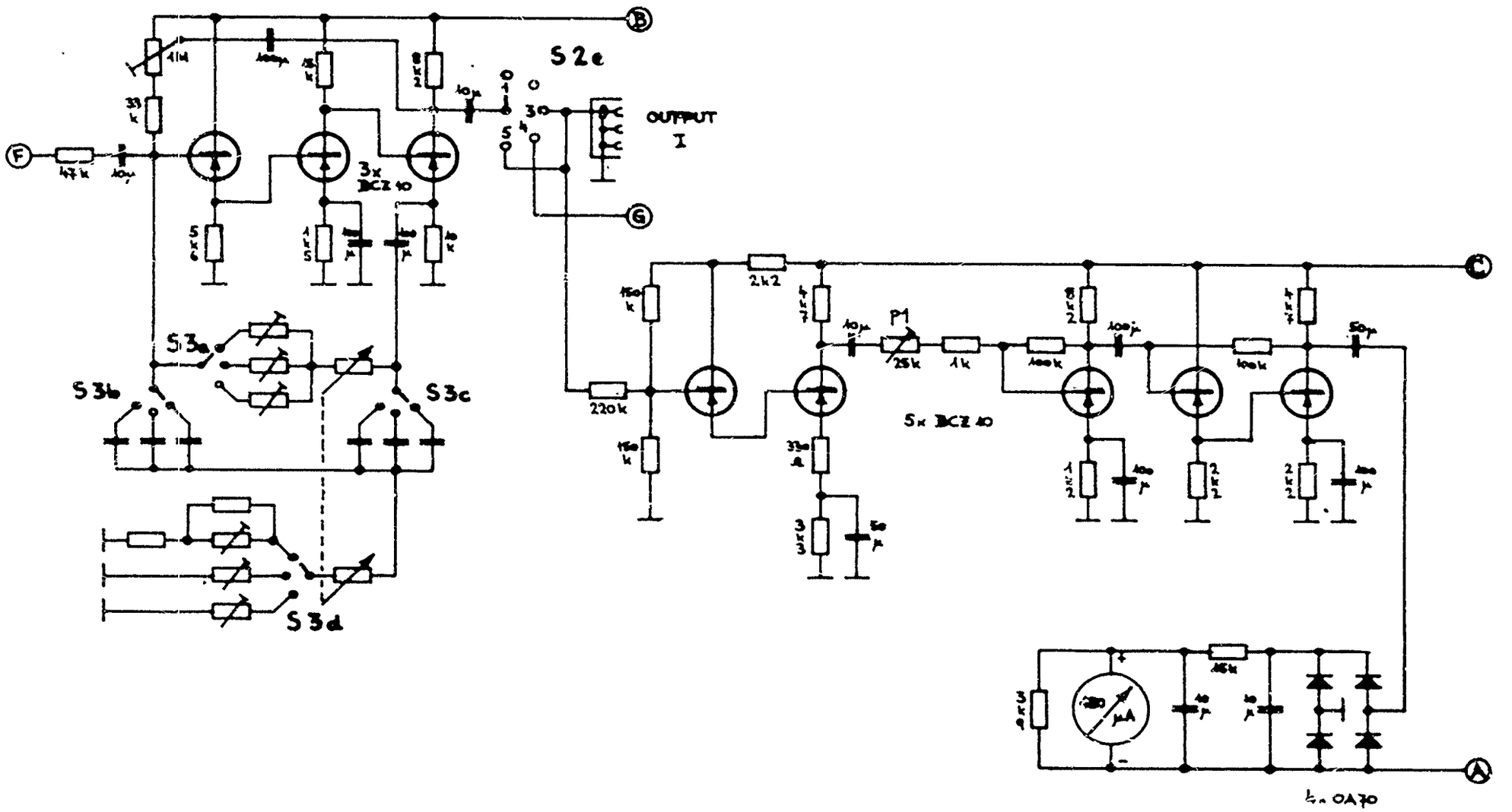

PART 3: SELECTIVE CIRCUIT + METER AMP

FIG: 43

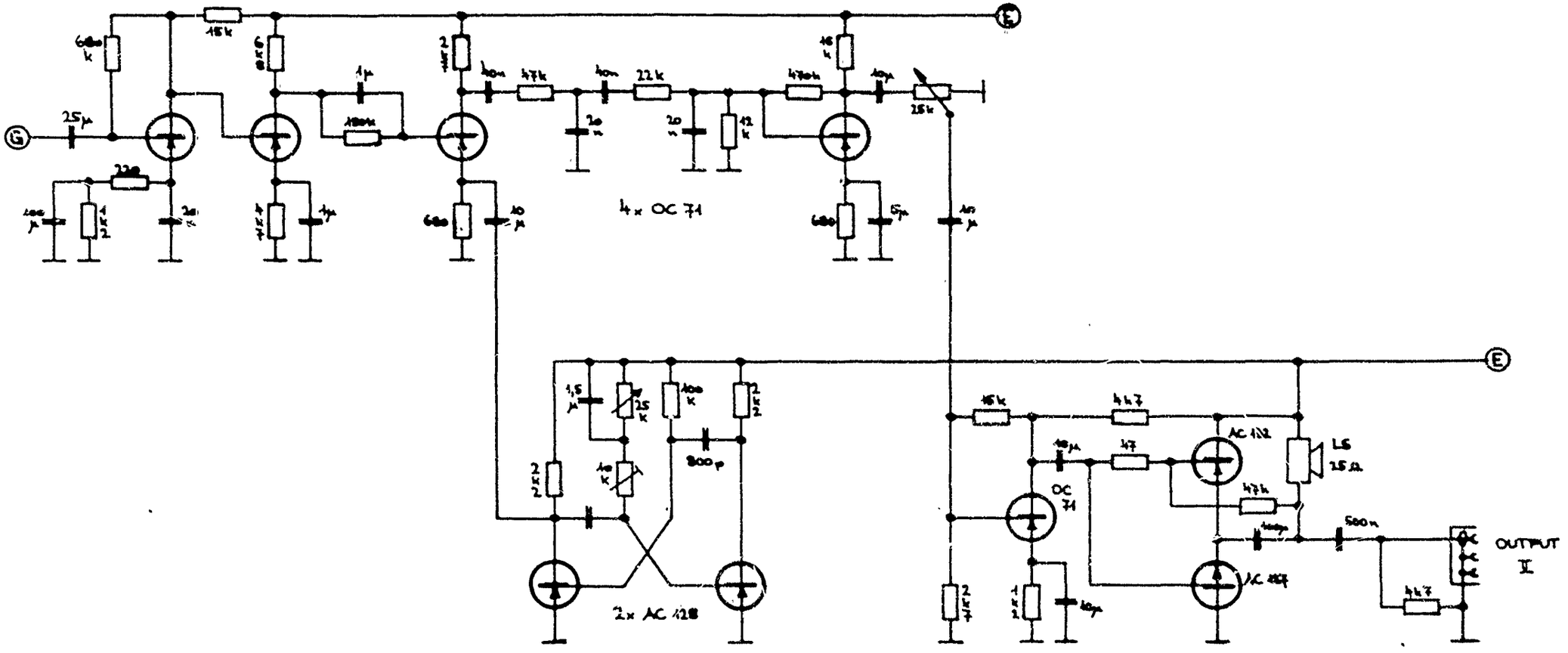

PART 4: HETERODYNE CIRCUIT

FIG.1.4

device can be read directly from the instrument. The scale is calibrated in microvolts or millivolts. Voltages between 0.1 μv and 100 mv can be measured.

(4.) Special attention was paid to the temperature stability of the device, as the environmental temperature varied from 4°C to 35°C. The circuit diagrams of Figs. 1,1 to 1,4 show that considerable independence of temperature and fluctuations of the operating voltage was reached by means of directly coupled amplifier stages and sufficiently dimensioned negative feedbacks. The operating voltage is kept constant by an electronic circuit, battery voltage fluctuations from 20 v to 14 v having no effect on the measuring accuracy.

(5.) A special calibrated oscillator was provided to make it possible that the device can be recalibrated any time. It produces rectangular voltage pulses of approximately 1.3 kc/sec whose value is made independent of the environmental temperature by means of careful stabilization.

This calibrated voltage is fed to the amplifier input in "calibration" position. The indicator of the instrument can be adjusted to the corresponding calibration value by means of the potentiometer P_1.

(6.) In principle, the superheterodyne unit shown in Fig. 1,4 remained unchanged. The only difference occurs in the output amplifier which now contains complementary transistors in order to avoid the use of any transformers whose magnetic stray field might affect the antenna stages.

The field strength meter built according to these principles is shown in Fig. IV. The great advantage of this device is its reliable construction and its low weight.

1,3 The amplifiers of the transmitter and the transmitting antennas

In principle, the battery-operated device remained unchanged, but an autotransformer made it possible to reach a higher output power. Fig. 1,5 shows that the antenna circuit can thus be directly connected with the output transistors, without involving any additional drawbacks. The operating reliability was improved by using an overvoltage fuse for output transistors. This is to avoid that short-term voltage peaks which might occur e.g. by tuning to resonance by means of the capacitor decade, destroy the power transistors. This protective circuit consists of heavy-duty diodes and a sufficiently dimensioned buffer capacitor (11 mF).

As the capacitor decade in the improved amplifier of the transmitter had been made stronger so that resonance voltages up to 2000 v could occur without any damage, the mechanical construction of the device had also to be changed correspondingly. The device was used mainly for measurements in Germany and Holland. An amplifier of 1000 w was installed in the St. Gertraudi mine in order to transmit over larger distances. The device delivered by the firm Bryan SAVAGE is mains supplied. The frequency range of the amplifier at full output power reaches 20 cps - 10 kc/sec. Especially in connection with the transmitter antenna SA VIII (which will be described below) with a winding surface of approximately 480 m^2, distance of more than 3000 m could be bridged without any difficulties.

As we have mentioned before, this transmitter was set up in a special mine laboratory. This was necessary because of

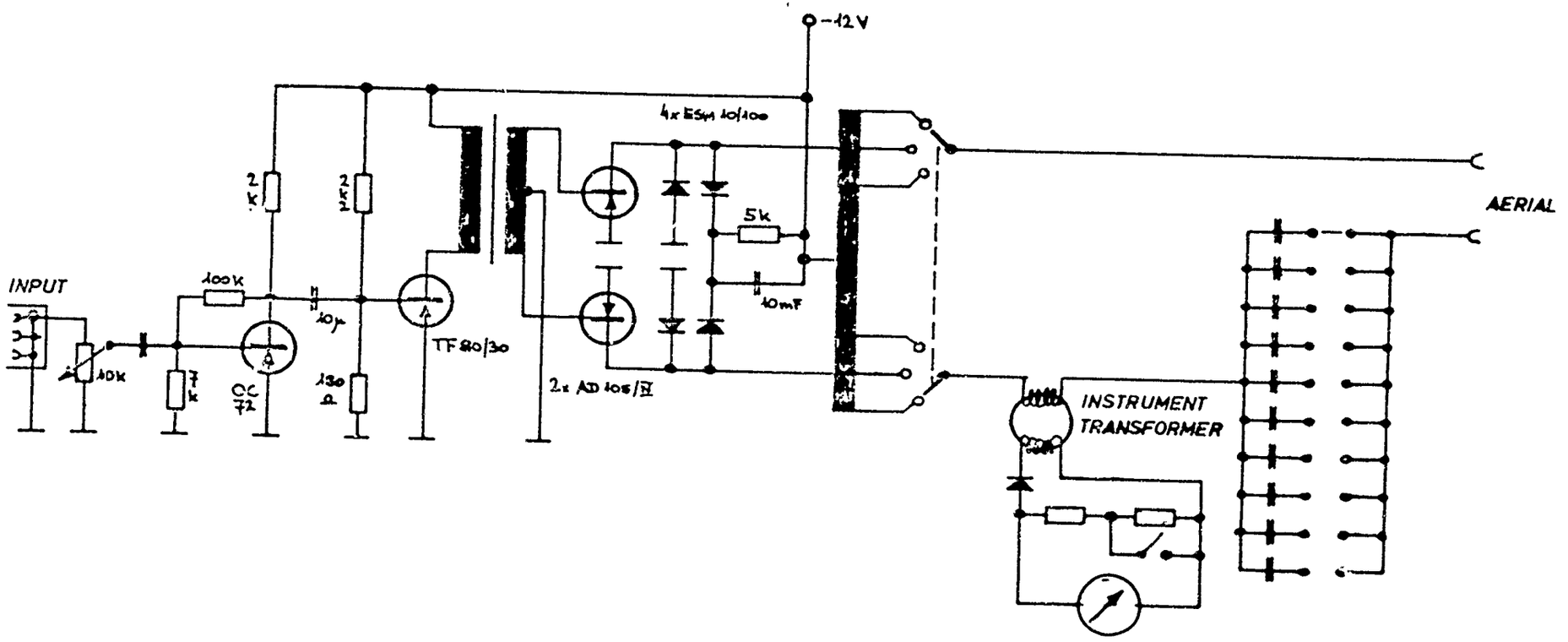

FIG. 1.5

TRANSMITTER

the available power and also because such a device has to be set up under certain climatic conditions. The atmospheric humidity had to be reduced from 100% to standard values, and the installations had to be made with special care for such powers. Fig. I shows the transmitter and the mine lab. Two separate antennas were fed with this device.

1. Pivoted frame: SA VII.

In order to make possible measurements under different angles ϑ, the existing frame in the "Bunte Kluft", with a winding surface of 300 m^2, had to be reconstructed so that it can be used for the provided power of 1 kw. For this purpose, it was necessary to insulate the individual turns of the frame sufficiently. Voltages that occur between the individual turns or also with respect to ground exceed 2000 v, so that the plastics insulation of the wires becomes insufficient. Therefore, the individual wires were installed at a certain distance in order to avoid a direct contact of the wires. Fig. II shows the new antenna whose dimensions on the whole remained the same, namely 3.8 m x 4 m coil area.

2. Fixed frame: SA VIII.

For measurements over larger distances, a pivoted antenna (SA VII, see above) could not be used. The next step was therefore the construction of a threefold frame with a winding area of 480 m^2. The dimensions of this frame are approximately 40 m x 40 m. The antenna was laid through vertical shafts and the connecting galleries above and below. In this case it was also important to insulate the antenna wire perfectly from the

ground, otherwise a considerable portion of the output power would have been lost.

Sufficient dimensioning of the wire cross section (2.5 mm^2 Cu) allowed us to choose the resistance of the antenna so small that a current of more than 25 a passes through the antenna at full output power. The two transmitter antennas differ by a factor which can be expressed by winding area times antenna current. The following values are obtained:

SA VII : 750 $a \cdot m^2$

SA VIII : 1350 $a \cdot m^2$

SA VIII is thus superior to SA VII by the factor 1.8. The only drawback is the fact that SA VIII is not pivoted so that it can only be used for measurements at one single angle ϑ.

1,4 Mine laboratory

A special room with a power supply (380 v 50 cps) had to be equipped for setting up the large mains-supplied transmitter. As it was desirable that a number of measuring instruments should be left permanently in the new lab, the atmospheric humidity in the mine had to be reduced from 100% to standard values. This is done by two powerful air drying apparatus. In order to increase their efficiency, the room is permanently kept at a temperature of more than 25°C. It is very difficult to air-condition the laboratory because the surrounding rock is very damp and the floor of the gallery is covered with percolating water.

The mine lab shown in Fig. I is equipped with the following devices:

(1) Low-frequency amplifier ranging from 20 cps to 10 kc/sec with 1 kw output power.

(2) High frequency amplifier for frequencies ranging from 100 kc/sec to approximately 600 kc/sec with a maximum output power of 1200 w.

This transmitter is intended to be used for conductivity measurements. The theoretical bases of these measurements are outlined in our second annual report [1] and in [4].

(3) A number of instruments such as an oscilloscope, a multirange voltmeter, an RC generator, an AF amplifier, a VLF receiver, and a tube voltmeter.

The laboratory will become very important for future work, because measurements of VLF transmitters and atmospherics over extended periods of time are planned. The position of the lab in the mine is shown in Fig. 1,21 (A). This site was chosen because it offers the possibility of transporting heavy instruments with the mine railway right to the mine lab, and because antennas can easily be set up in its immediate neighborhood.

Propagation measurements of VLF waves

As we have briefly mentioned in the preface, the experimental studies of 1963 concentrated on two points:

1. The most important tasks were studies of propagation in geological media which differ largely from those examined so far. The excursion to Northern Germany and Holland yielded a number of interesting results concerning this sphere of problems. We conducted measurements in five different mines in media of high conductivity and also in well insulating rock. The possibility of measuring under simple geometrical conditions, i.e. conditions under which the earth's surface can actually be looked upon as a plane, was of great interest. Our theoretical calculations are all based on this simplified assumption so that the measurements made in the Tyrol are only approximately comparable to the results obtained theoretically.

2. Measurements over very large distances, i.e. more than one kilometer. They were expected to yield results concerning our apparatus and especially the construction of devices that would make possible transmission over still greater distances. At the same time another problem could be solved, namely the problem whether the sky wave or the ground wave is responsible for the propagation. This problem is to be discussed in part III.

1.5 Salzgitter mine Konrad I (Germany)

The measurements conducted in the iron ore mine Konrad I yielded a number of very interesting results, as the conductivity of the studied geological medium differs considerably from those studied so far.

The experimental results were compared with the theory given in [1] that holds for a dipole in an unbounded homogeneous medium. As the conductivity was unexpectedly high, the numerical data given in [1] had to be calculated again for the special values of conductivity and distance.

1. Theoretical considerations

According to the theory developed in the second Annual VLF Report (1962), which holds for a magnetic dipole in an unbounded and conducting medium, the magnetic field strength was calculated as dependent on the distance r, the angle ϑ and the conductivity σ. Below, the quantity Δ (see p.1 1 expression 40 and 41 in the above report) instead of the conductivity σ shall be considered to make the calculation more general, otherwise the results would be bound to a certain measuring frequency, but this is to be avoided. For this purpose, the function $h(r,\vartheta,\Delta)$ (expression 52 of the report) was calculated for a number of distances and conductivities.

The function

$$h(r,\vartheta,\Delta) = \frac{\exp(-\Delta r)}{r}\left\{\frac{4\cos^2\vartheta}{r^2}\left(\frac{1}{r^2}+\frac{2\Delta}{r}+2\Delta^2\right)+\right. \tag{1}$$

$$\left.+\sin^2\vartheta\left(\frac{1}{r^4}+\frac{2\Delta}{r^3}\quad\frac{2\Delta^2}{r^2}\quad\frac{4\Delta^2}{r}+4\Delta^2\right)\right\}^{1/2}$$

is calculated in Table I for the values $\Delta = 4.86\cdot10^{-2}$; $1.085\cdot10^{-2}$; $3.45\cdot10^{-2}$; $7.7\cdot10^{-2}$; $1.09\cdot10^{-1}$. For the frequency 3 kc/sec used for these measurements, the conductivity would be $\sigma = 10^{-2}$. 10^{-1}; $2\cdot10^{-1}$; $5\cdot10^{-1}$,

$1(\Omega^{-1}\ m^{-1})$. The graphical representations shown in Figs. 1,6 through 1,9 give a good illustration of the directional pattern as dependent on the distance at constant conductivity on the one hand, and at a given distance as dependent on the conductivity on the other hand. For a better survey, the value of the function $h(r,\vartheta,\Delta)$ was plotted in the diagram in radial direction (logarithmic scale). Fig. 1,8 clearly shows the result obtained previously, namely that the field strength component H (in the direction $\vartheta = 90^{\circ}$) for a certain conductivity has a maximum at a given distance and frequency.

The definition of the function $\varphi(r,\Delta)$ in the form

$$\varphi(r,\Delta) = \frac{|H|\ \vartheta = 0^{\circ}}{|H|\ \vartheta = 90^{\circ}} \qquad (2)$$

proved advantageous for further studies. Table II gives some computed values of this function which are plotted in Fig. 1,10. By means of this function which on the whole is consistent with the function V(r) in the report (see p. 16, expression 53), the conductivity can be determined from the value of $\varphi(r,\Delta)$ which can easily be measured by experiment, and from Fig. 1,10 via . The considerable decrease of the value of the function characterizing the far field of the dipole indicates the predominance of the component H_{ϑ}.

In the present report it shall not be discussed how far the boundary of the medium can be neglected and how great the error thus becomes, since the existing results at present are being compared with the experimental data.

2. Measurements in the Salzgitter mine (Germany)- shaft region Konrad I

The geological structure of this region is characterized by a

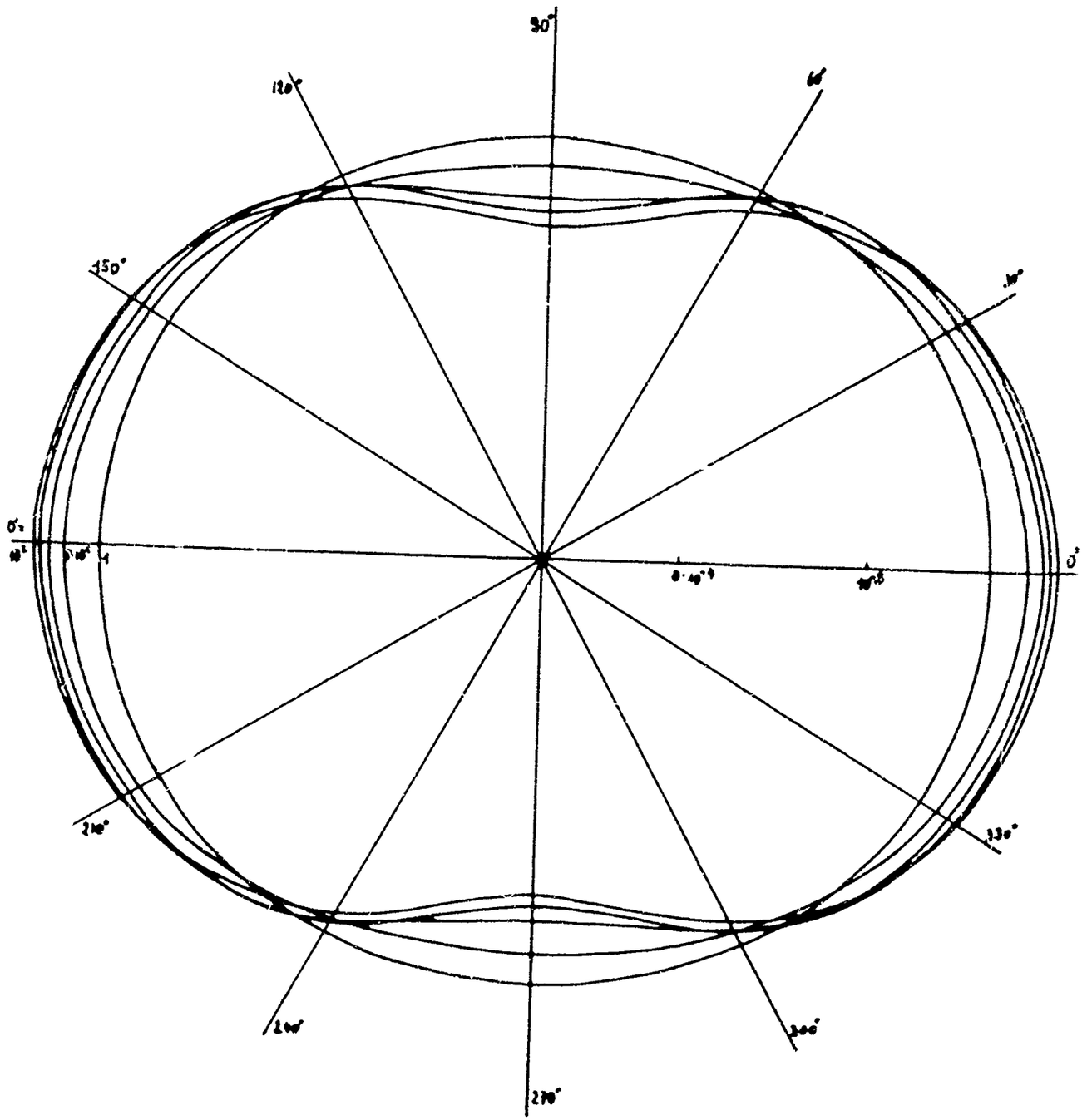

$R(x, \vartheta, \Delta)$

$f = 3$ kc $\quad r = 10$ m

Fig. 1,6

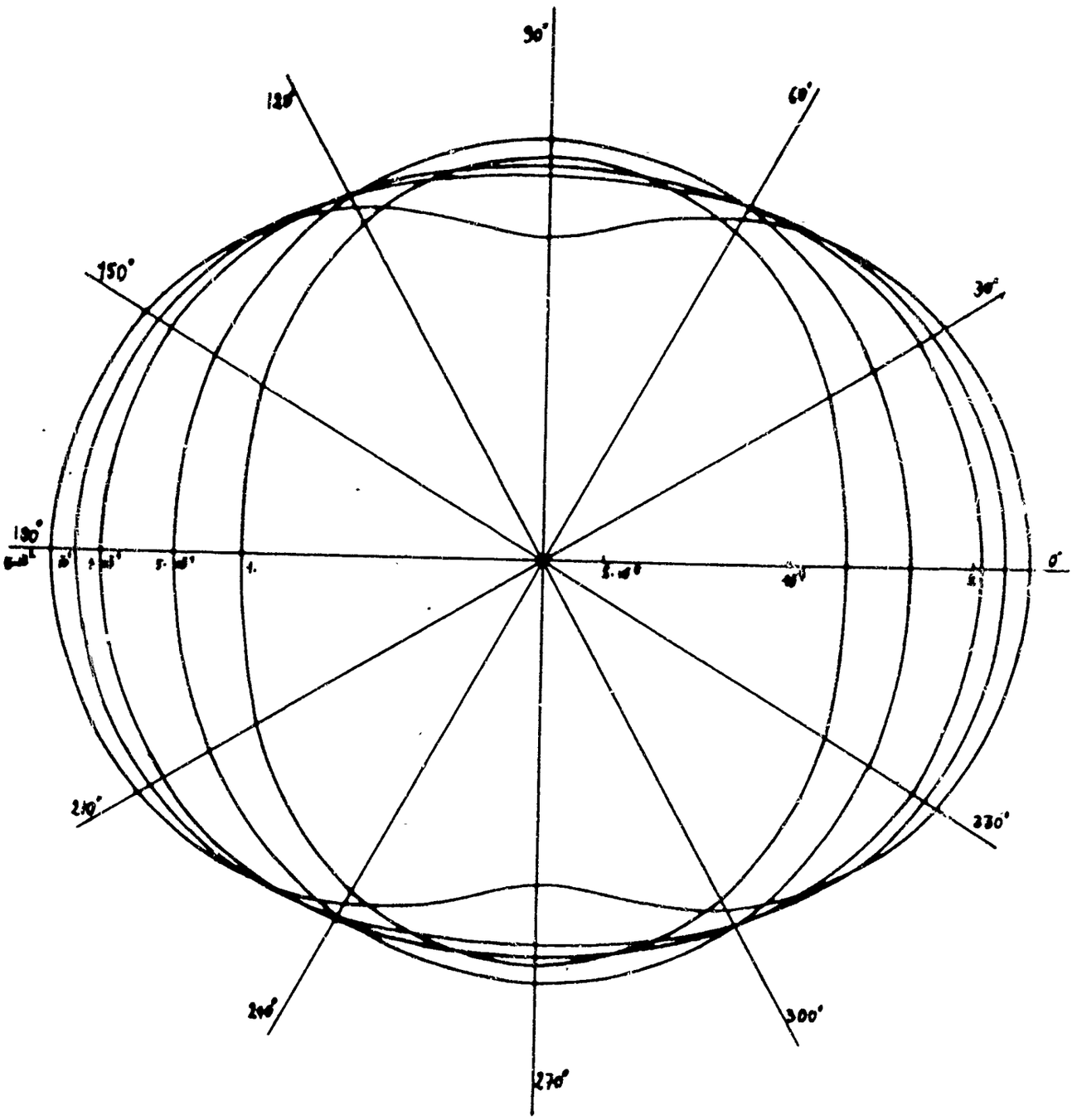

$R(x, \vartheta, \Delta)$
$f = 3\,kc$ $r = 2\,km$

Fig. 1,7

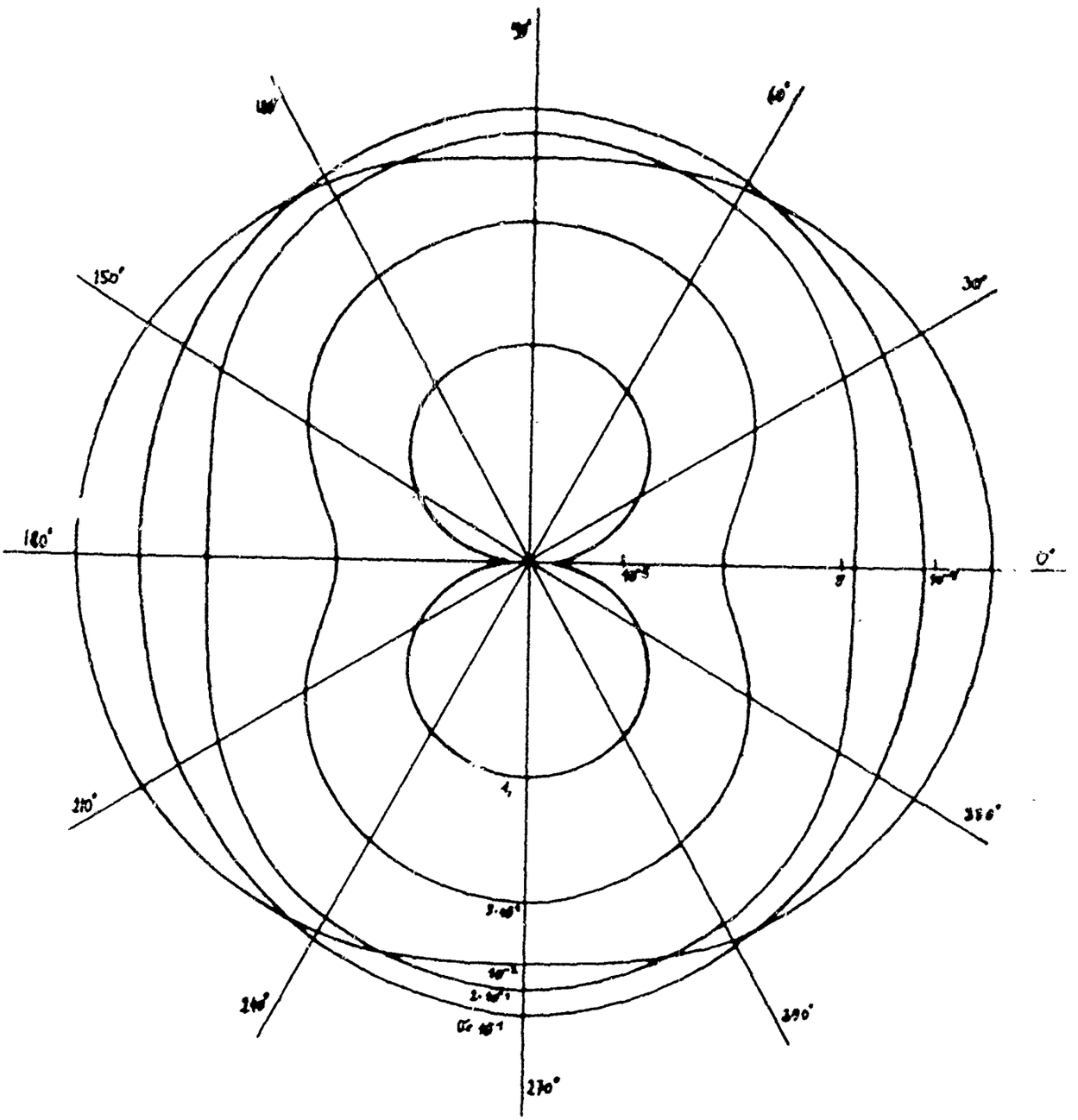

$h(x, \theta, \Delta)$
$f = 3\,kc$ $r = 50m$

Fig. 1,8

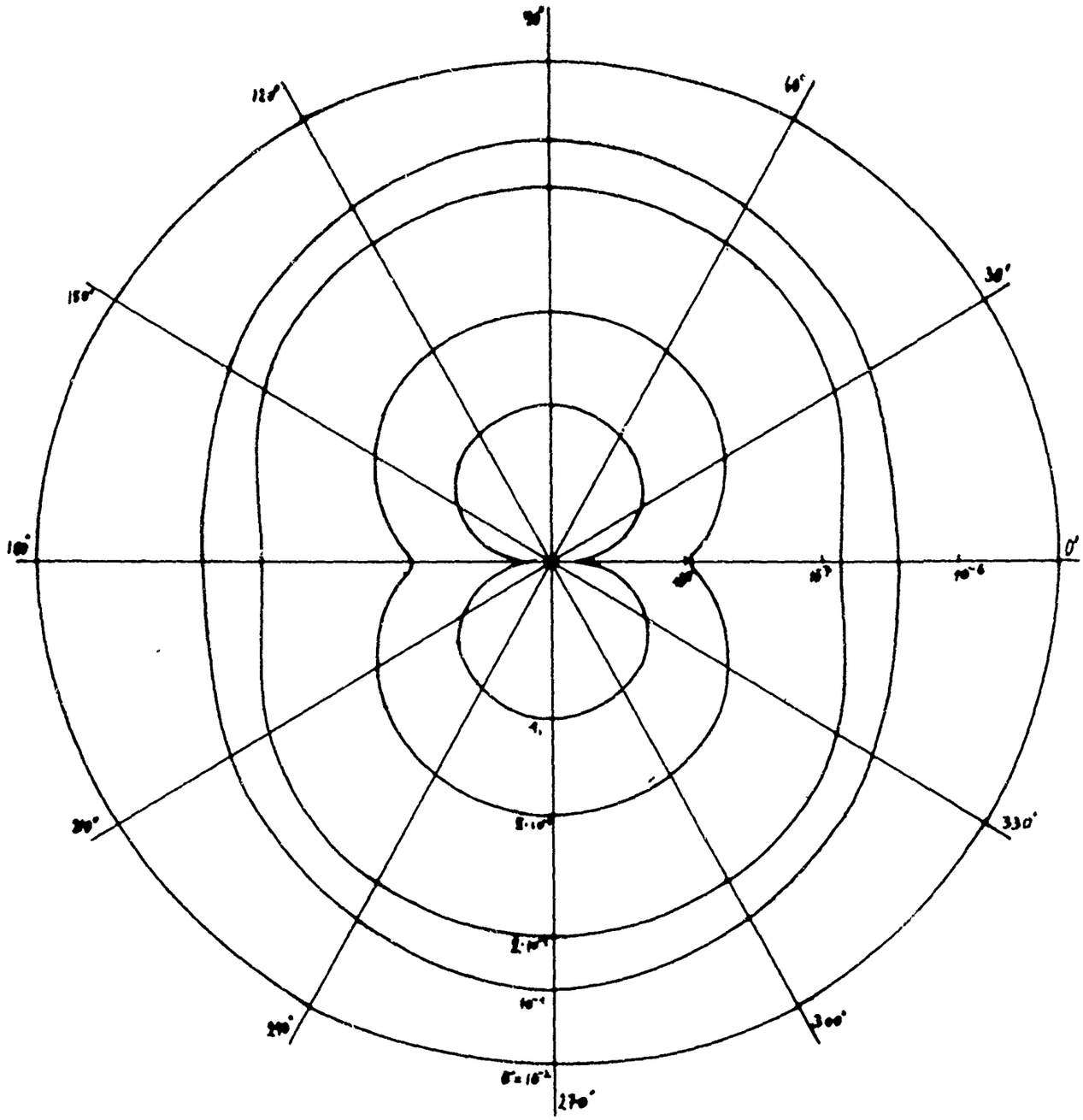

$k(x, \vartheta, \Delta)$
$f = 3\,kc$; $r = 100\,m$

Fig. 1,9

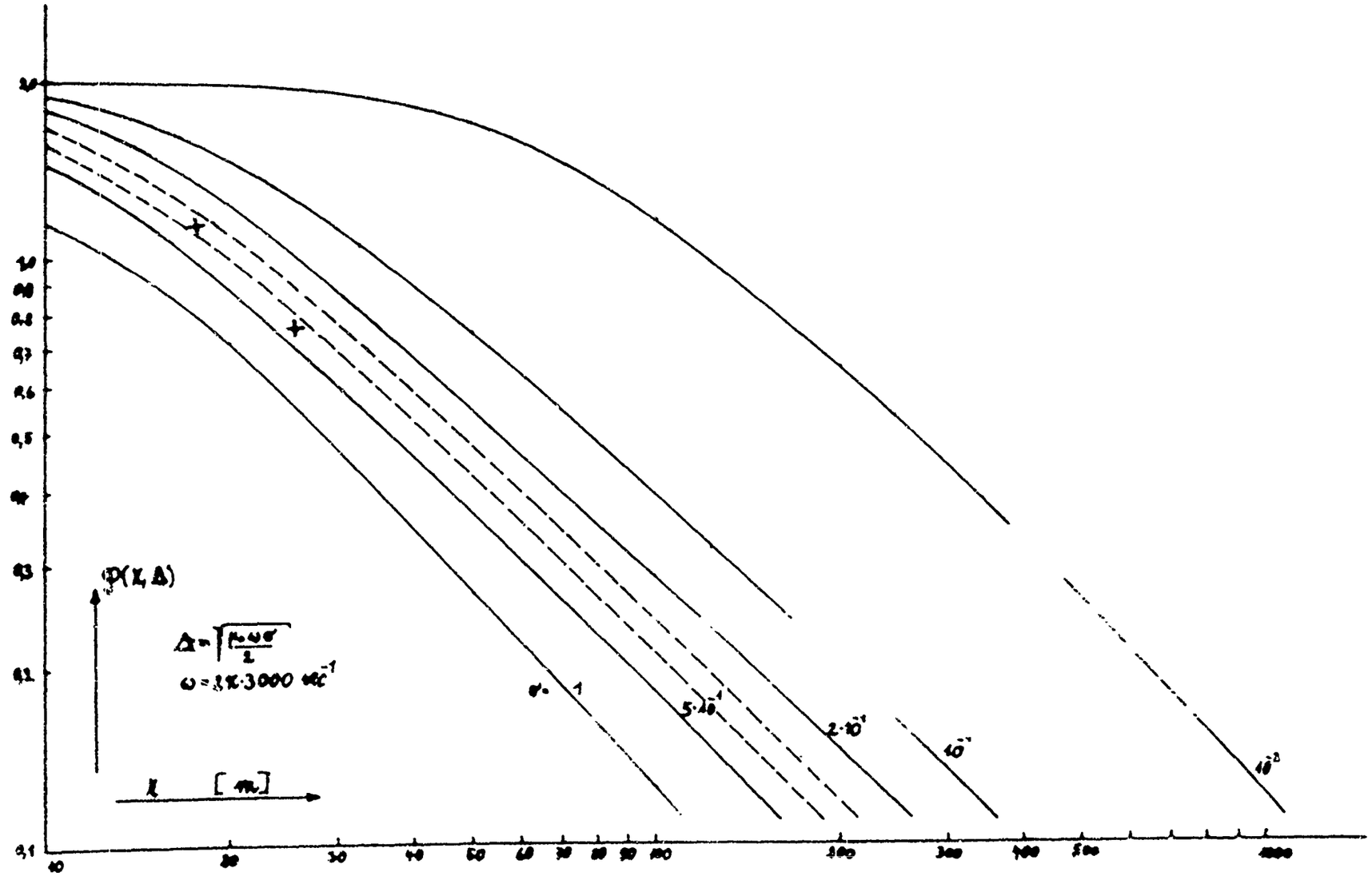
P(X, Δ)
Δ = √(n·ω²/2)
ω = 3π·3000 sec⁻¹
X [m]
1
5·10⁻¹
2·10⁻¹
10⁻¹
10⁻²
INTERPOLATED CURVES

FIG.1,10

variety of flat strata formed by repeated flooding by the sea. The exploitable iron ore field of the Upper Jurassic is accompanied by zones of marly limestone. The rock on top of the mine has an average height of 1000 m, the inclination of the deposit to the horizon being 22°. The concentration of this oolitic ore is approximately 30%, the average size of the individual brown iron grains is 0.5 mm.

Suitable measuring sites with specific conditions in the mine itself were not easy to find. Regions with wires of the mining railway, power cables, or even iron formwork had to be avoided. Two short drifts 18 and 25 m long in the 1000m bed seemed to be most suitable. Despite the short distance between transmitter and receiver, characteristic antenna patterns could be measured owing to the high conductivity of the ore body - a d-c measurement yielded $\sigma \approx 2 \cdot 10^{-1} (\Omega^{-1} m^{-1})$. The working method for finding these diagrams had already been described in detail in the above annual report. The measurements with the receiving antenna were conducted such that the antenna is revolved 360° about its vertical axis at a constant angle ϑ. This rotation corresponds to a change in angle ψ between the dipole axis of the receiving antenna and the field direction. The angle ϑ is the angle between the direction of the dipole axis of the transmitter antenna and the direction to the receiving point. The measured values obtained by this method are given under U_e in Tables III and IV. Column $\bar{U}_e$ was obtained from these values by averaging the measured values belonging to ψ, $\psi+180°$, $\psi \pm 90°$. The mean values thus obtained are shown in Figs. 1,11 and 1,12. The third column gives the mean values $\bar{U}_e$ calculated by the method of least squares, with allowance for the dependence $U_e = U_{e_o} \cdot \cos\psi$. According to Figs. 1,11 and 1,12, this dependence on the angle ψ obviously does not occur, since the minimum of the

curve does not assume the value zero, but decreases only down to a certain fraction of the maximum value (see above). In this case, the situation is probably more complex than it was shown by the above theory.

The voltage induced in the antenna calculated according to the law of induction is: $|U_{ind}| = \frac{d\Phi}{dt} = \frac{d}{dt}\int B\,df\cdot\cos\psi = \frac{d}{dt}B\cdot F\cdot\cos\psi$ (3).

If B is considered to be a constant vector which in the general case may be looked upon as a resultant of the primary field and a series of secondary fields, then it follows from the above equation that the induced voltage becomes zero for the angle $\psi = 90^\circ$. Hence, no conclusions can be made from the measured deviation to the disturbing effect of secondary fields caused by the boundary of the ore body.

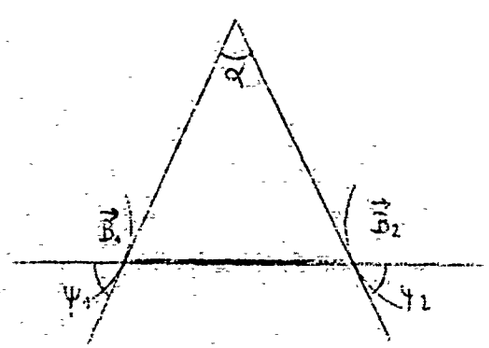

The most obvious assumption that can still explain the measurement is that of a highly inhomogeneous field. In this case, the situation at the receiving antenna can thus be represented.

The induced voltage can be represented by the expression (4). The angles ψ_1 and ψ_2 are different owing to the field inhomogeneity and are interrelated (see diagram) in the following way:

$$U_{ind} \sim \vec{B}_1\cdot\cos\psi_1 + \vec{B}_2\cdot\cos\psi_2 \quad (4); \qquad \psi_1 + \psi_2 + \alpha = 180^\circ \quad (5)$$

This relation can be substituted in (4), α being a measure of the inhomogeneity. From these assumption it follows that the induced voltage need not become zero for whatever value of ψ_1, if the receiving antenna is turned, i.e., if ψ_1 is changed. This is consistent with the actual observation. Here, the effect is explained only qualitatively, not considering the reasons for the great influences on the trans-

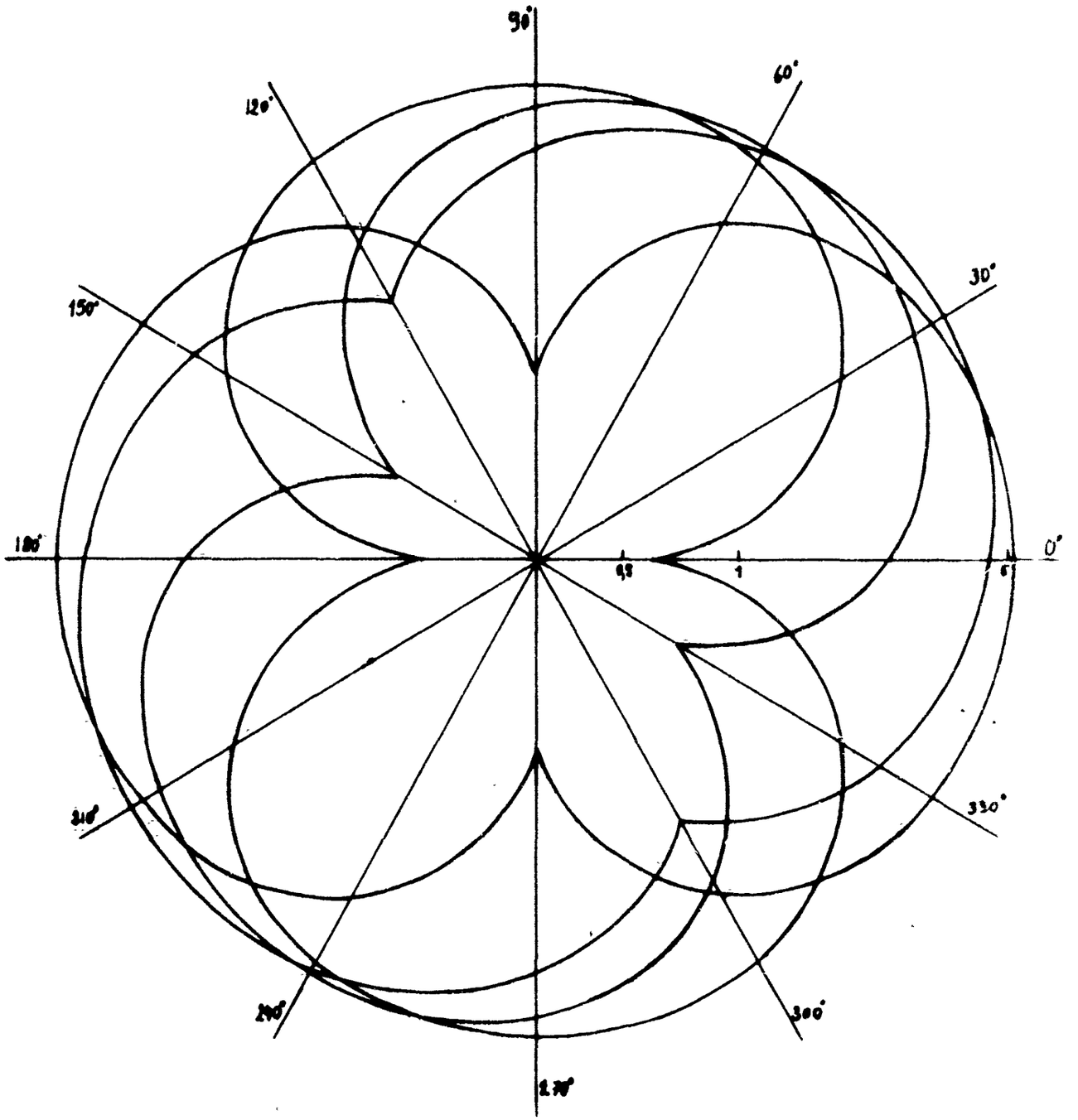

KONRAD I

1. MEASUREMENT

r = 10m f = 3kc

FIG. 1,11

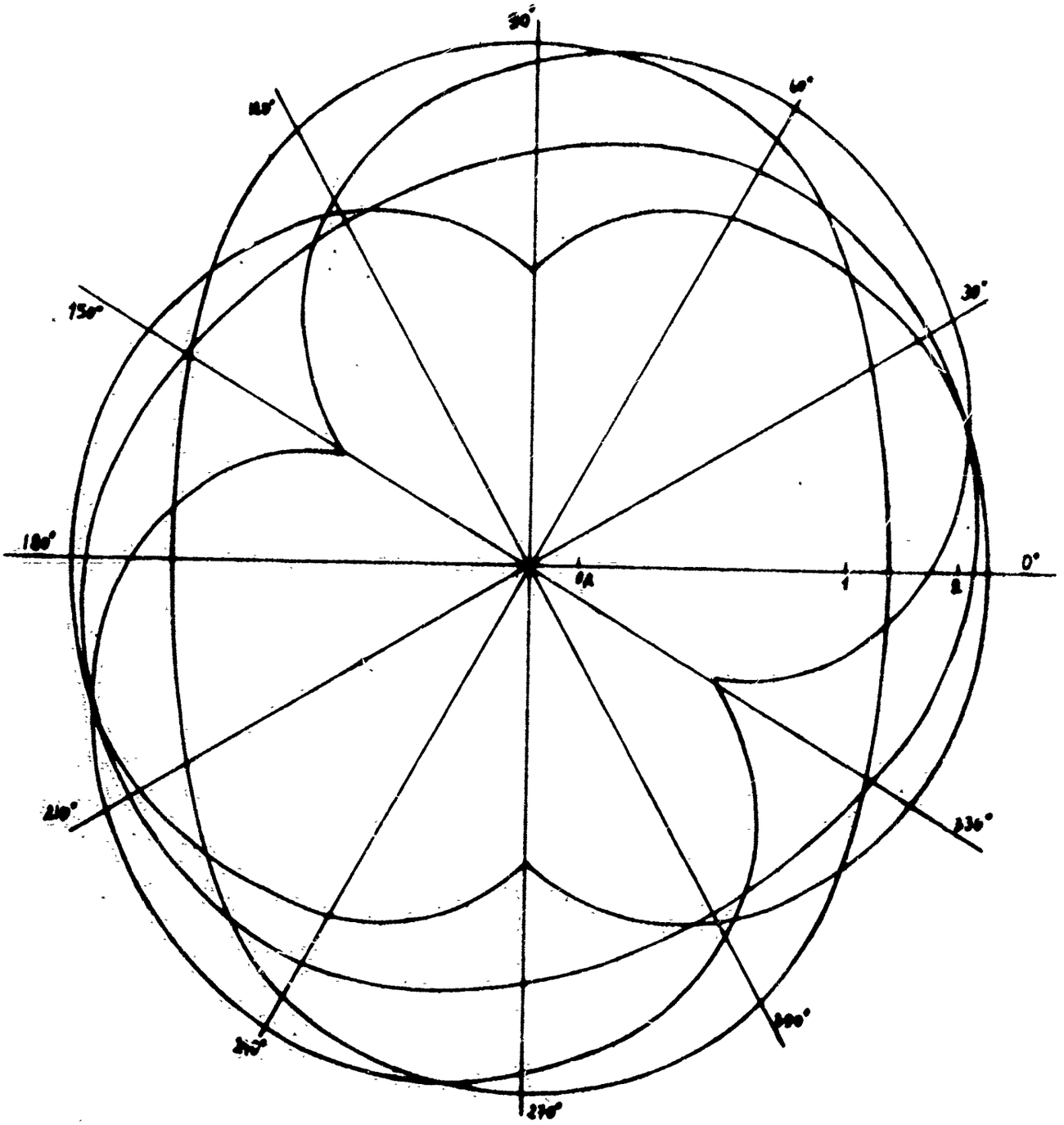

KONRAD I

3. MEASUREMENT

r = 25m f = 3 kc

FIG. 1,12

matter field. The following values of the function $\varphi(r,\Delta)$ for 18 and 25 m are calculated from the two measurements:

$\varphi(r,\Delta)$	r(m)
1.15	18
0.75	25

These values are plotted in Fig. 110. The value obtained with good approximation for the conductivity by interpolation is $\sigma = 3 \cdot 10^{-1} (\Omega^{-1} \cdot m^{-1})$. The error is no more than 25% which considering the small distance is very good. Furthermore, this conductivity is also consistent with that measured with direct current: $2 \cdot 10^{-2} (\Omega^{-1} \cdot m^{-1})$.

For a better understanding of Figs. 1,11; 1,12 it must be added that the envelope of all curves gives the field strength diagrams represented in Figs. 1,6 through 1,9. The conducted measurements show that $\varphi(r,\Delta) < 1$ for a distance of 25 m, hence measurements for distances of 50 m in the studied rock are already conducted in the far field. This fact is of special interest, since the conditions in the mines of Schwaz and St. Gertraudi are completely different; here, $\varphi(r,\Delta)$ was found to decrease but slightly even at 1000 m. For this reason, detailed studies with allowance for the upper and lower boundaries of the ore body can be expected to yield interesting results.

1,6 Potassium mine Hansa III, Empelde near Hannover (Germany)

In Konrad I, the conductivity of rock was generally three orders of magnitude higher than in the mines examined so far, in the mine Hansa III, however, measurements were made in a medium whose conductivity is so low that it can approximately be considered as

an insulator. The measurements were made in a large salt block, under conditions which, owing to the low humidity, suggested the results to be similar to those measured in air.
The bottom of a bed 1000 m below ground was chosen as measuring site, because it contained no rails and no cables; furthermore, we used a number of gangways far away from power cables.
Despite the favorable measuring conditions, a number of unexpected interferences occurred.

(1) Owing to the poor damping in salt bodies, considerable interferences by the underground railways in higher gangways were observed.

(2) The salt is being poured through inclined shafts. Owing to the low content of humidity, it gets electrostatically charged. Continuous discharges, however, cause considerable and irregular fluctuations in deflection of the measuring instrument, making exact measurements very difficult.

For the planned measurements, the transmitter was set up at PP 107 (see Fig. 1,13) the antenna being aligned such that the angular deflections for the individual points of measurement remained as small as possible. Table V gives the measured values for the individual points. The different ϑ values were not taken into account in the graphical representation of Fig. 1,2..

The magnetic field strength is plotted in arbitrary units so that a larger number of measurements of several mines can be represented in one figure. Furthermore, the individual curves were shifted upward or downward in parallel; hence, conclusions from the position of two curves must not be made.

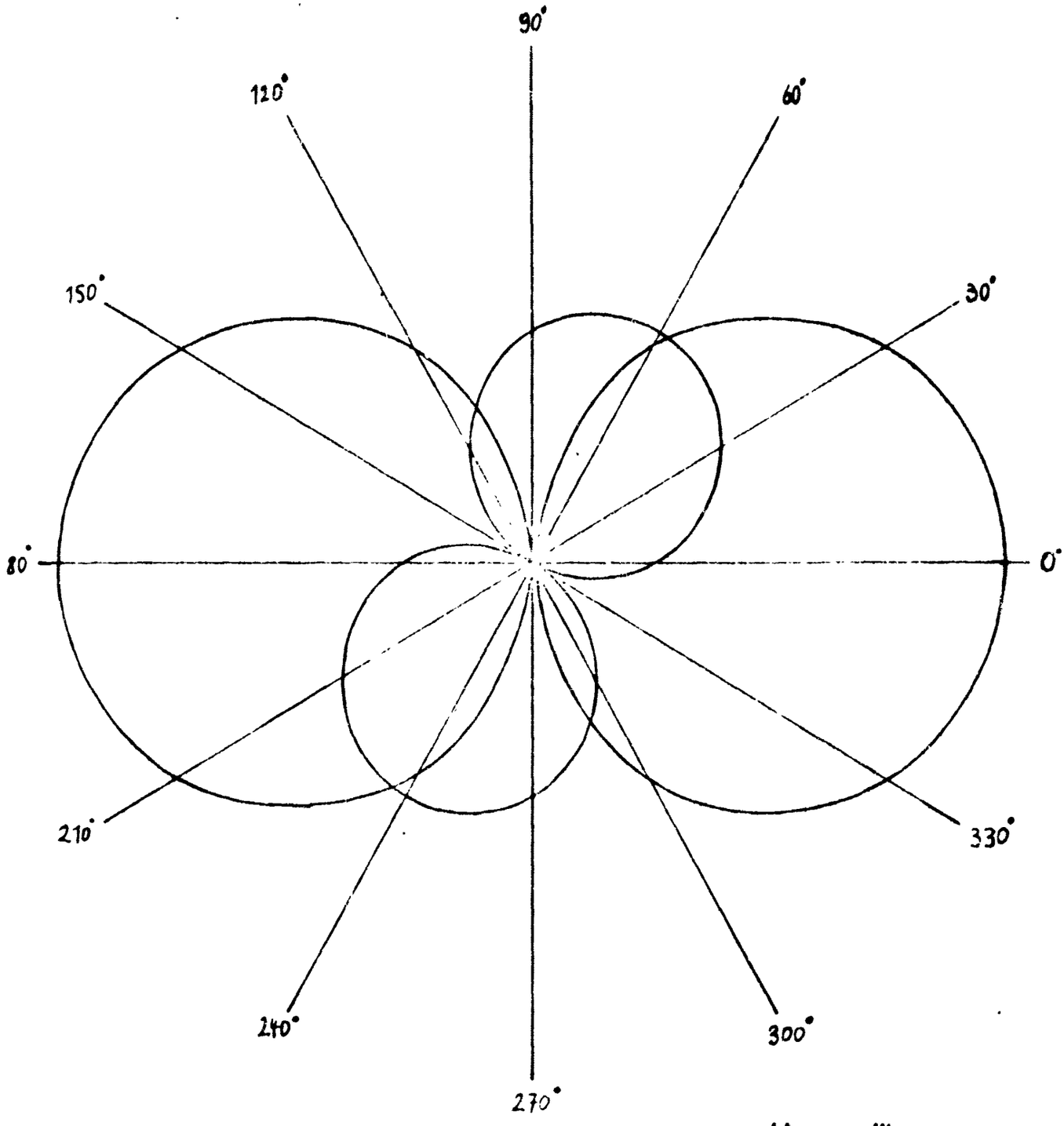

FIG. 1.14

The dependence $h(r,\vartheta,\psi)$ is given in Table IV and Fig. 1,14 with the angles ϑ and ψ being changed at a constant distance of 240 m. From this measurement the value of $\varphi(r,\Delta)$ was determined and found to be approximately 2. This result also suggests that the conductivity of the medium is low.
Although damping in the salt body was poor, the transmitter GBR which is very strong above ground could not be received anywhere in the mine. Reception measurements were conducted 200 - 1000 m below ground. There are probably two reasons for this negative result of the measurements:

(1) There is a layer of ground water at a depth of approximately 180 m which contains much salt and thus screens signals from above ground completely, no matter whether they come from VLF transmitters or atmospherics.

(2) The propagation mechanism of VLF signals is such that there exists a considerable difference whether the wave penetrates the earth's surface vertically or horizontally. The second viewpoint is supported by a number of measurements in other German mines where there is certainly no groundwater layer that contains salt, and also by good receiving conditions in the mines of Schwaz, Lafatsch, and Gertraudi, where the receiving conditions were very good in similar or greater depths.

1,7 Ore mines of Fuesseberg and Georg (Siegerland - Germany)

The conditions in these two mines were similar to those in the mines of Schwaz and Gertraudi. Iron ore (siderite) which is mined there, occurs in the form of a steep plate, approximately 10 m thick. In Fuesseberg it is straight, whereas in the Georg mine it is shaped like a horseshoe (see Figs. 1,15 and 1,17)

The measuring sites were chosen in such a way that most of the line connecting transmitter and receiver passed through ore, or such that the points of measurement were in front of or behind the plate. This arrangement made it possible that the effect of an inhomogeneous medium on the propagation of VLF waves could be studied. The curves that belong to Table VII and Table VIII are shown in Fig. 1,20. On the whole, these curves have the same course as those of our measurements in Schwaz [1] which indicates similar conductivity of the rock. Conductivity measurements with direct current which still have to be discussed show that the dead rock and the ore in the two mines are of almost equal resistivity. Hence, a small difference between the measurements in front of and behind the ore plate is observed. Tables IX and X give the values of another measurement made under the following conditions:

The transmitter was placed at S_2 in a gangway 100 m higher, the axis of the transmitter antenna being horizontal so that approximately equal angles ϑ are obtained for all points of measurement. Then, the field strength was measured at the given points, the receiving antenna having a position that corresponds to $\psi = 0^\circ$ (i.e. maximum input voltage). This measurement could not be represented graphically, as the measured values depend on two independent quantities, the distance r and the angle ϑ. The measurements given in the present report are mainly to be used for comparing the experimental with the theoretical values of a dipole at a certain depth below the earth's surface [7]. Owing to the complicated arrangement, the evaluations have not been completed as yet. In the discussed case, the distance between transmitter and the earth's surface was approximately equal to

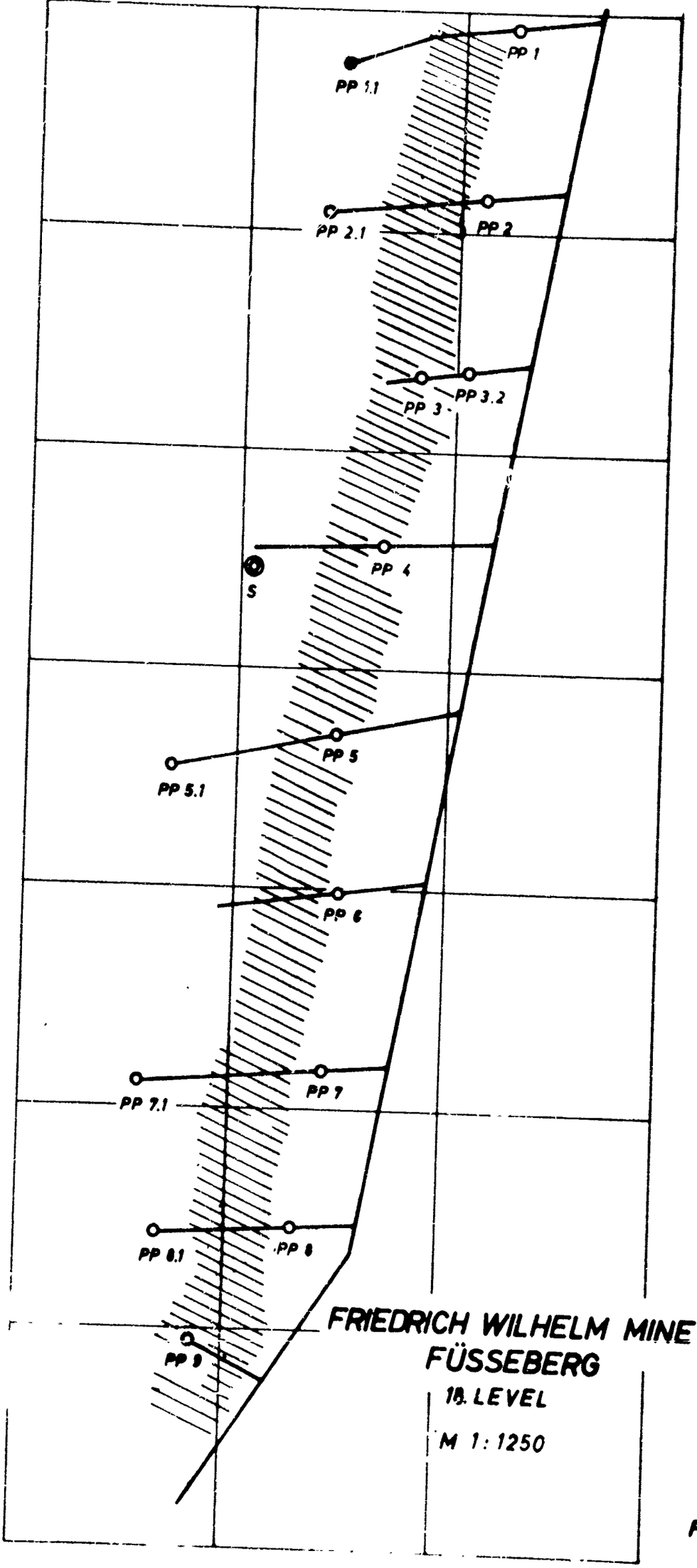
PP 1
PP 1.1
PP 2.1
PP 2
PP 3
PP 3.2
PP 4
S
PP 5
PP 5.1
PP 6
PP 7
PP 7.1
PP 8.1
PP 8
PP 9
FRIEDRICH WILHELM MINE
FÜSSEBERG
18. LEVEL
M 1: 1250

FIG. 1.15

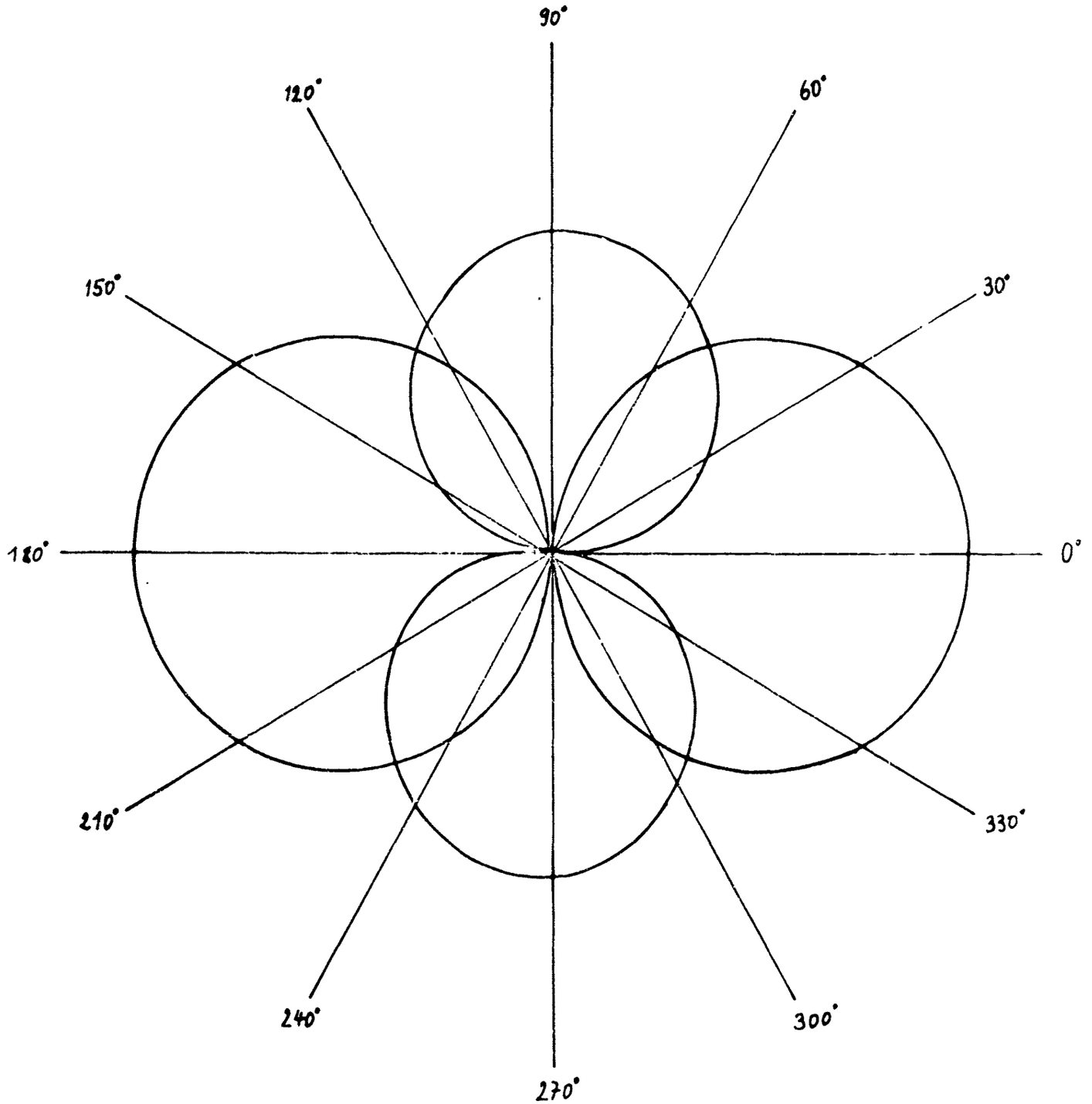

Füsseberg

PP5,1

r = 262m, f = 3kc

FIG. 1.16

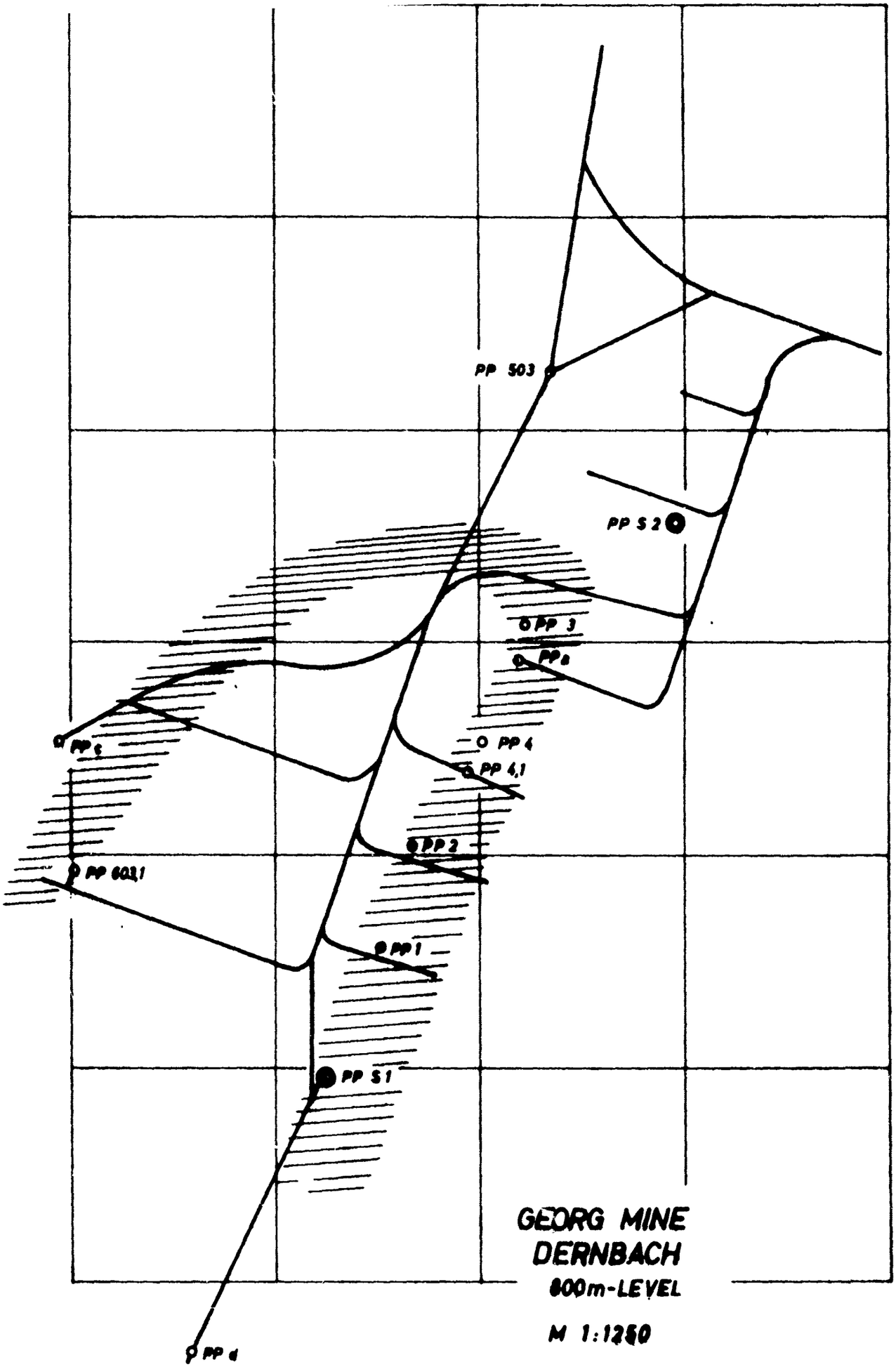
PP 503
PP S 2
PP 3
PP 5
PP 4
PP 4,1
PP 2
PP 603,1
PP 1
PP S 1
PP 6
GEORG MINE
DERNBACH
800m-LEVEL
M 1:1250

FIG.1.17

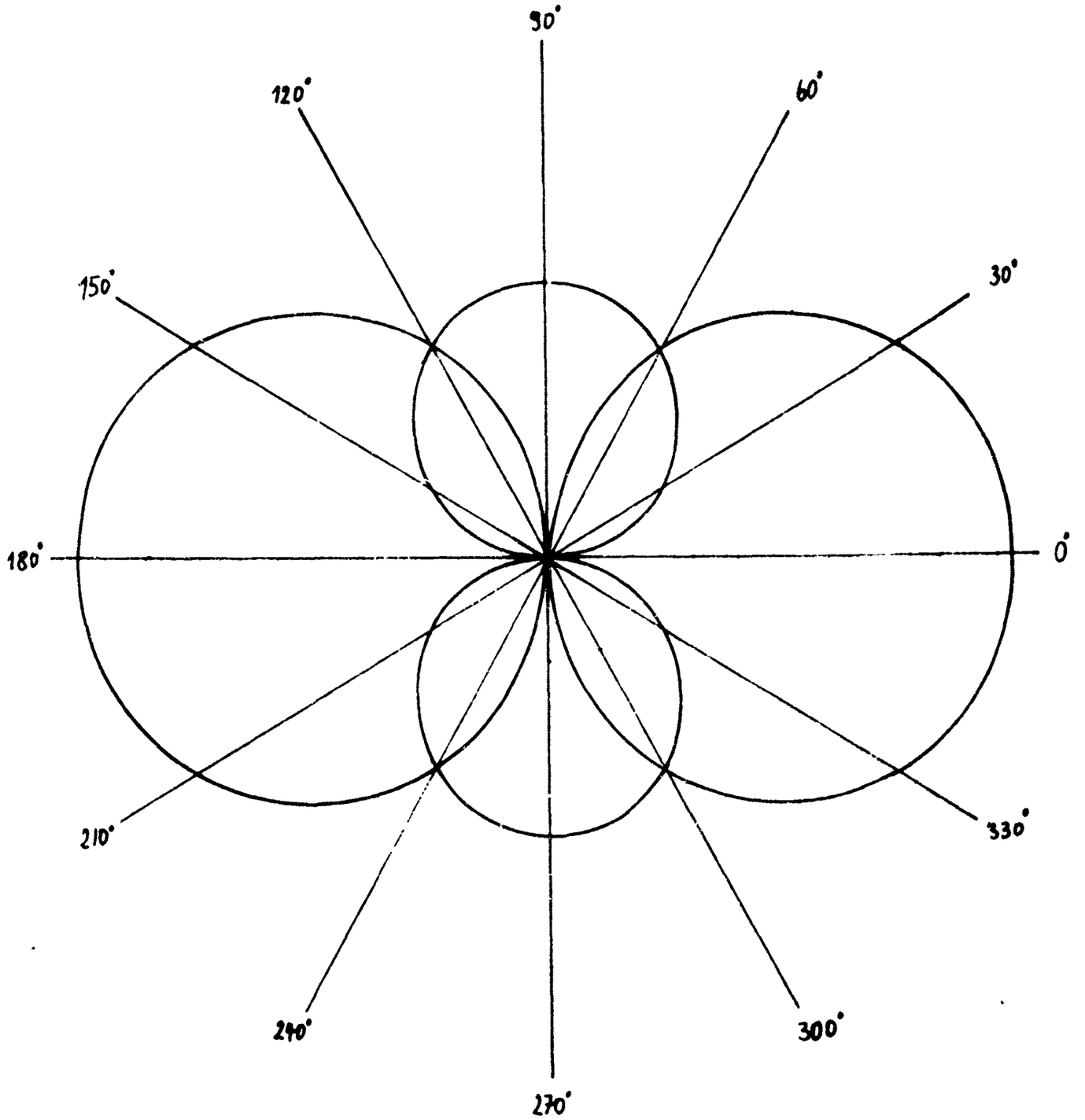

Georg
PP 1.
r = 35 m, f = 3kc

FIG. 1.18

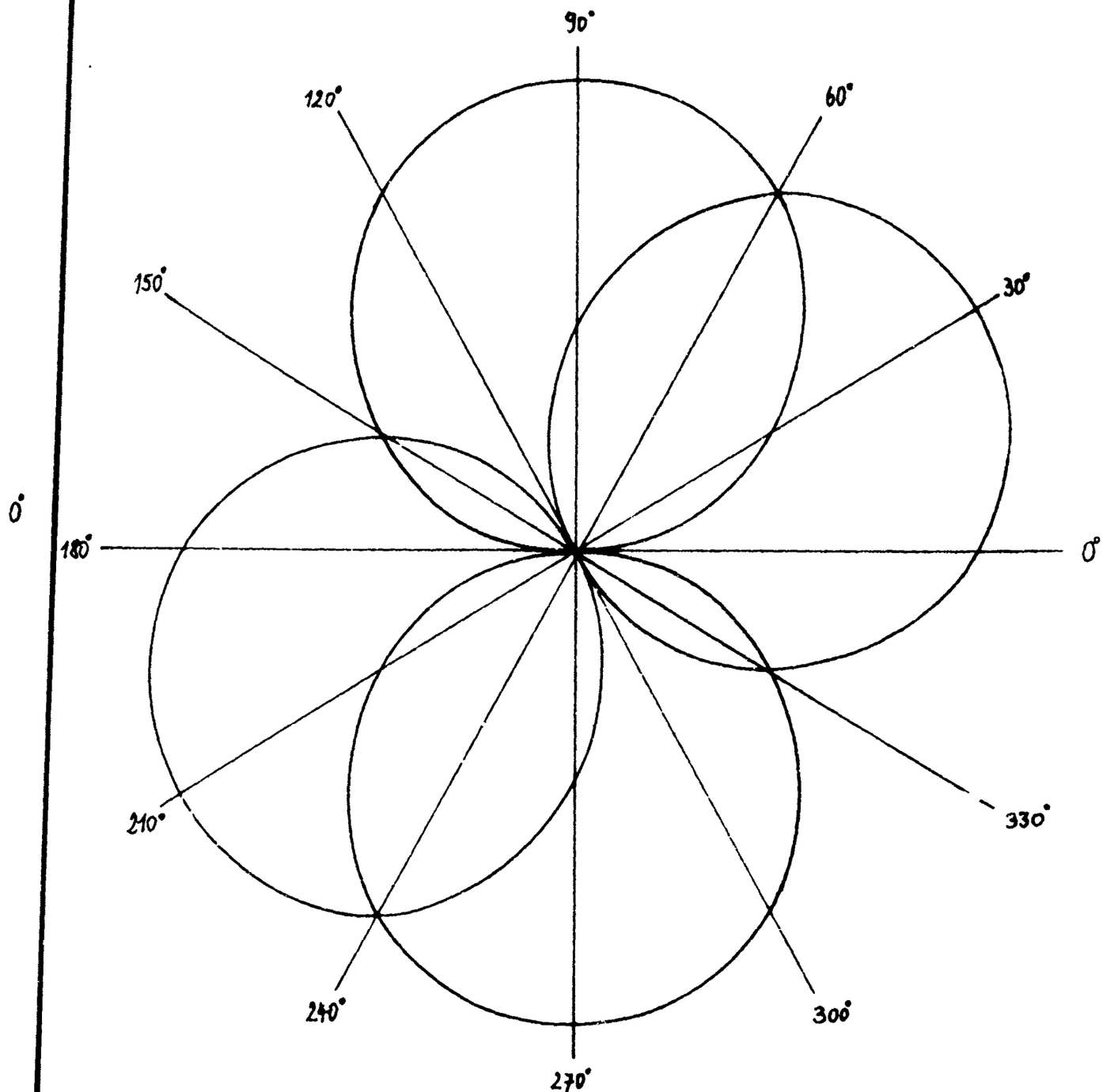

Georg

PP4.1

r=130m, f=3kc

FIG. 1.19

the distance between transmitter and receiver so that a noticeable deviation of the measured value from the theoretical value of a dipole in an unbounded medium was to be expected according to [7].

As in the case of Konrad I, the directivity patterns could be plotted for several distances for both mines. Different from the measurements in Konrad I, the curves here show a clear minimum (see Tables XI - XIII, column U_e). The effect of the bounds of the ore plate is very small, because the electrical properties of the two media differed but slightly. The graphical representation of the measurements is given in Figs. 1,16; 1,18; 1,19 the balanced values $\bar{U}_e$ being plotted radially in linear scale.

1,8 Oranje Nassau mine in Heerlen, Holland

"Nassau III" offered us the only possibility of measuring in a coal mine. Owing to the way the coal is deposited there, we had to measure in the direction of a seam approximately 2 m thick. The management of the mine had ordered that timber-propped galleries were driven into the rock so that there was no iron in the immediate neighborhood of transmitter and receiver. The two receiving sites were placed at a distance of 300 and 500 m from the transmitter. The transmitter antenna had an angle of $\varphi = 0^\circ$ and $\vartheta = 90^\circ$ with respect to the receiving point. We were surprised to find that our conductivity measurements with direct current showed the coal to be of poor conductivity, whereas the rock above and below it is highly conductive. The next chapter will give the values of d-c measurements which show a great difference between coal and dead rock. Hence,

propagation in this case took place along a thin layer of poor conductivity, bounded by two media of high conductivity.

A geometrical arrangement of this type which in principle is found in every coal mine, seems to be suitable for the propagation of VLF waves according to the results of the measurements. We have therefore planned theoretical calculations for studying the propagation in a "sandwich". Unfortunately, these problems could not be sufficiently studied on the spot, but the following factors seem to be of special importance for the propagation along a coal seam:

(1) Thickness of the seam as compared to the total distance between the transmitter and receiver. The conductivities of the different rock layers are assumed to play a decisive part, since the wave length in the medium is more reduced at higher conductivity. The ratio between wave length and dimensions will also be decisive.

(2) The measurements suggest that the antenna alignment with respect to the coal seam and to the transmitter - receiver direction is important. This means that optimum propagation is reached in a given direction for a certain angle δ which must be other than 0^{o} or 90^{o}.

Some measurements have shown that damping in the adjacent rock is extremely high so that signals above ground are practically screened off at depths of no more than 250 m.
The measured values of field strength for distances of 225, 375, and 500 m are given in Table XIV and Fig. 1,20. By repeating the measurement at $\delta = 0^{o}$ and $\delta = 90^{o}$, the value 0,22 was determined for the function $p(r,\Delta)$ defined in [8]. This

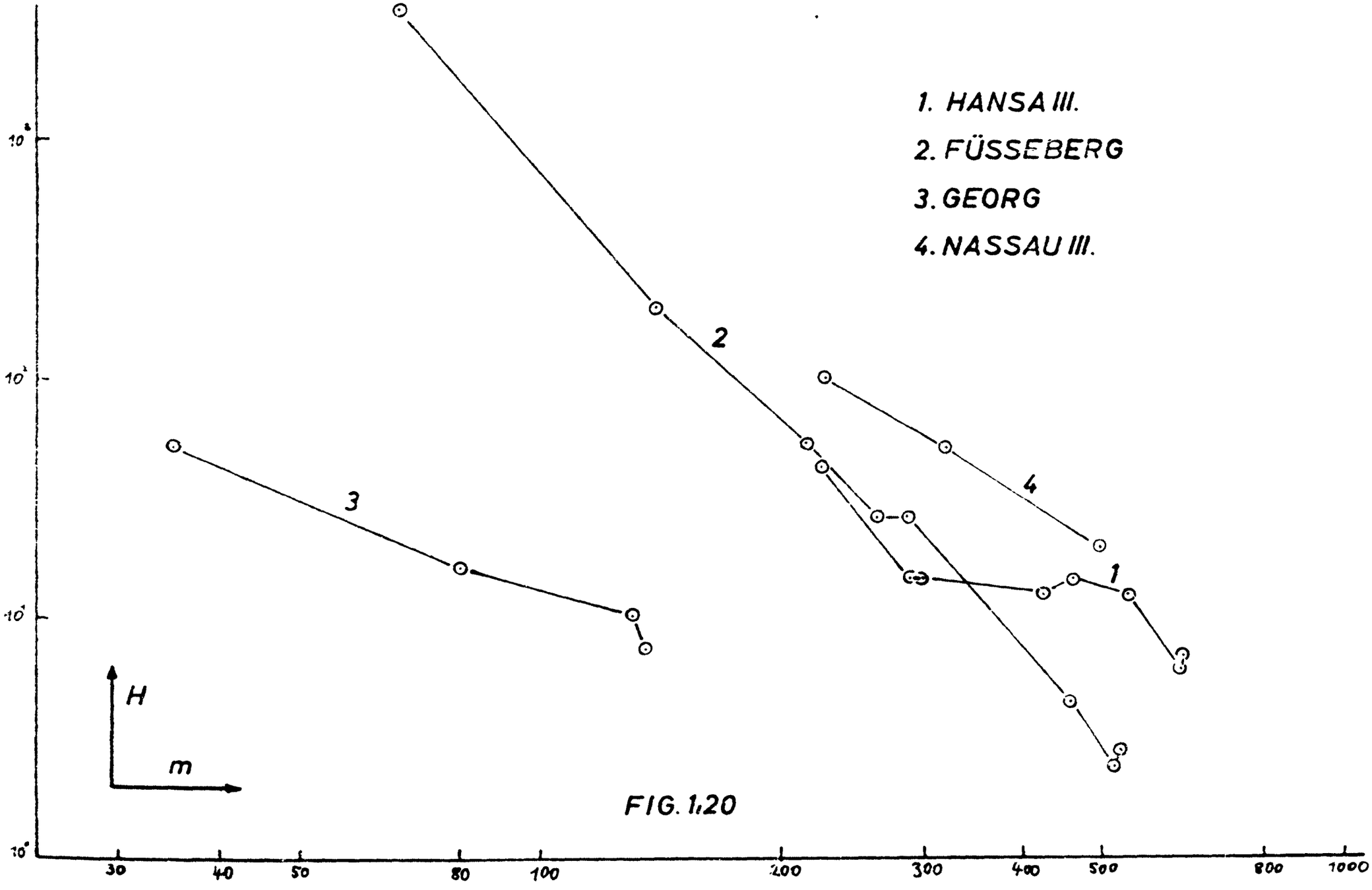
1. HANSA III.
2. FÜSSEBERG
3. GEORG
4. NASSAU III.
1
2
3
4
H
m
30
40
50
80
100
200
300
400
500
800
1000

FIG. 1.20

corresponds to an average conductivity of $\sigma = 10^{-3}$ Ohm^{-1} m^{-1} at a frequency of 3 kc/sec. Considering the highly heterogeneous medium, this value is to be looked upon as a pure mean value. This can also be seen from the values of d-c measurements determined at several limited points.

1,9 St. Gertraudi mine

Besides our measurements in German mines, we also conducted detailed studies in nearby Tyrolese mines. The geological conditions are well known (as far as they influence the propagation of VLF waves), and we therefore concentrated on measuring over very large distances.

For this purpose, the 1 kw transmitter mentioned above was set up. Being a mains-supplied instrument with a power consumption of almost 3 kw when in full operation, it had to be set up permanently in the mine. The position of the laboratory was chosen so that the distances accessible for measurements in the St. Gertraudi mine are as large as possible. Fig. 1,21 shows that the maximum distance is approximately 1.5 km. The region is especially suitable, because it contains no rails or other equipment.

The advantage of a powerful but stationary transmitter, however, also entailed the drawback of the transmitter antenna having to be fixed in a system of galleries in order to utilize the whole output power. The antenna thus cannot be rotated. The fixed SAVIII transmitter antenna has been used for most of the measurements in St. Gertraudi. The problems discussed in part III made measurements over distances larger than 1500 m necessary. For

this purpose, a number of measurements had to be made at ground level, i.e. at zero depth. How far these measurements are meaningful will also be discussed in chapter III.

Let us now discuss a measurement made at a frequency ν = 3kc/sec (as in the last annual report). The range of distances was approximately 100 m - 3.3 km (Fig. 1,21), the measurements on the western drift being continued on the earth's surface from a distance of 15 km onwards. The SAVIII fixed frame was used as transmitter antenna. The accuracy of measurement was considerably increased by repeating the measurement and by using several receiving antennas. The antennas EA IV, EA VI, and the calibration coil ESP described in [1] were used as receiving antennas. The received voltage had to be reduced to the calibration coil in order to make comparisons possible, because the three antennas have different sensitivities. These values are given in Table XV column $\tilde{U}_e$ and plotted in Fig. 3,1. When measuring with the fixed frame, a correction of the ϑ values, i.e. reduction of the measured values to the angle $\vartheta = 0^o$ proved impossible and the measured points plotted in Fig. 3,1 show certain deviations. The present transmitter antenna, which cannot make full use of the new amplifier, cannot be used for measurements over distances greater than 4 km. There are therefore plans to build a much larger frame in the near future which will make possible measurements over a distance at least three times as large. It will then be possible to conduct transmission and reception experiments between the Schwaz and St. Gertraudi mines, which are 10 km apart. Since the sensitivity of the receiving antenna may also be improved (very promising experiments have already been made), we may expect to reach much greater distances still.

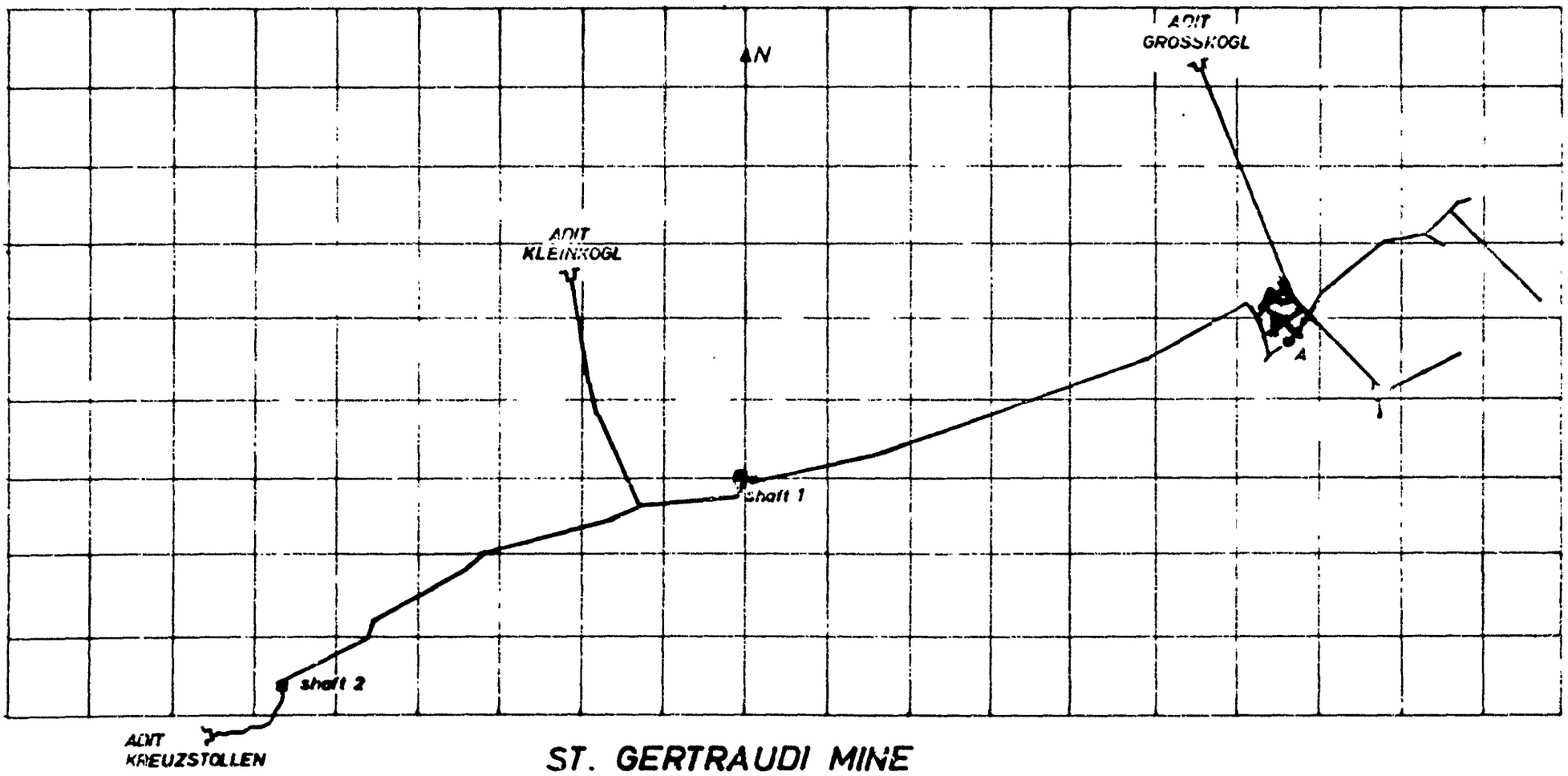

ST. GERTRAUDI MINE

M 1:7500

FIG. 1. 21

The favorable position of the mines in the Tyrol, the maximum distances between the individual mines being 10 km, proved very advantageous.

1,10 Determination of the electrical conductivity of rock

A four-electrode configuration (usually the Wenner configuration) was used for determining the conductivity of various parts of rock (mainly in mines). Only direct current was used for this purpose. It was the purpose of this examination to determine the conductivity of those regions in which the propagation of VLF waves was measured.

1. Theoretical considerations:

According to the analogy between an electrostatic field and a steady electromagnetic field, a point electrode in a homogeneous body with the conductivity σ produces a potential given by $\varphi = \frac{I}{4\pi\sigma r}$ in the receiving point P. If there is a second electrode with the current (- I) in this medium, the potential difference between the points S_1 and S_2 (Fig. 1,22) is calculated as follows:

$$\Delta\varphi = U = \frac{I}{4\pi\sigma} \cdot k \qquad k = \left(\frac{1}{R_1} - \frac{1}{R_2} - \frac{1}{r_1} + \frac{1}{r_2}\right)$$

or

$$\sigma = \frac{I}{4\pi U} \cdot k \qquad (1)$$

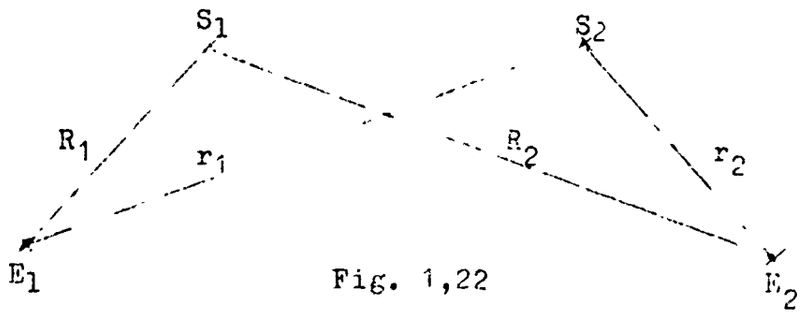

Fig. 1,22

If the electrodes are not in a full space, but on the surface of an unbounded homogeneous semispace, equation (1) goes over into

$$U = \frac{I}{2\pi\sigma} \cdot k$$

or

$$\sigma = \frac{I}{2\pi U} \cdot k \qquad (2)$$

If the electrodes E_1 and E_2 as well as the probes S_1 and S_2 are arranged along a straight line at the distance a (Wenner configuration), k becomes 1/a.

2. Measuring arrangement (Fig. 1,23 and Fig. V)

External circuit:

Two 6-v lead accumulators connected in series feed a motor-generator whose secondary circuit provides a smooth direct voltage of 250 v. This voltage is aprlied to the electrodes E_1 and E_2 via an ammeter having several ranges of measurement. If the conductivity of the rock to be studied is high, the 12 v of the accumulators instead of the 250 v generator voltage can be applied to the electrodes via the instrument by means of a change-over switch.

Voltage measurement

The voltage U between the probes S_1 and S_2 has to be measured with a compensation circuit in order to eliminate the high contact resistance (50 - 500 kohms) of the electrodes and probes. A stabilizing circuit equipped with two transistors AC 125 and a Zener diode OAZ 203 provides a constant voltage of 10 or 1 v across a 50 kohms helical potentiometer (type Spektrol 860). The compensation voltage on the slider of the potentiometer is lead to the probe S_2 via a 100 µA zero indicator connected with a transistorized d-c amplifier. Before the input of the amplifier there is a second compensation circuit for compensating the

contact voltage and polarization voltage of the probes with the electrode current being switched off. The 2 kohms potentiometer with central tapping has a logarithmic characteristic so that the small values occurring frequently can be adjusted accurately.

The amplification factor of the d-c amplifier is 20. Thus, a value of $5 \cdot 10^{-8}$ A can easily be read on the instrument. If an extreme resistance of 1 Mohm is assumed between the probes, a voltage change of $5 \cdot 10^{-2}$ v is necessary to produce a sufficient deflection of the zero instrument. Frequently, however, an accuracy in voltage measurement of $5 \cdot 10^{-3}$ v can be reached owing to the use of a built-in key and owing to the frequently small resistance between the probes.

3. Measuring accuracy:

If the quantities J, U, R_2, r_1, and r_2 have errors μ_I, μ_U, μ_R the error of σ will be

$$\mu_\sigma = \sqrt{\left(\frac{\partial \sigma}{\partial I}\right)^2 \mu_I^2 + \left(\frac{\partial \sigma}{\partial U}\right)^2 \mu_U^2 + \left(\frac{\partial \sigma}{\partial R_1}\right)^2 \mu_{R_1}^2 + \ldots\ldots} \qquad (3)$$

If the errors are substituted in (3) and if the measuring error of the unit distance μ_e is substituted for the error μ_r of the distance measured according to $\mu_r = \mu_e \sqrt{r}$, we obtain

$$\mu_\sigma = \sqrt{\frac{c^2}{U^2}\mu_I^2 + \frac{c^2 I^2}{U^4}\mu^2 + \frac{I^2}{4\pi^2 U^2}\mu_e^2 \left(\frac{1}{r_1^3} + \frac{1}{r_2^3} + \frac{1}{R_1^3} + \frac{1}{R_2^3}\right)}$$

The error for the Wenner configuration will thus be

$$\mu = \sigma \sqrt{\left(\frac{\mu_I}{I}\right)^2 + \left(\frac{\mu_U}{U}\right)^2 + \mu_e^2 \cdot \frac{9}{4} \cdot \frac{1}{a}} \qquad (4)$$

$(R_1 = r_2 = a,\ r_1 = R_2 = 2a)$.

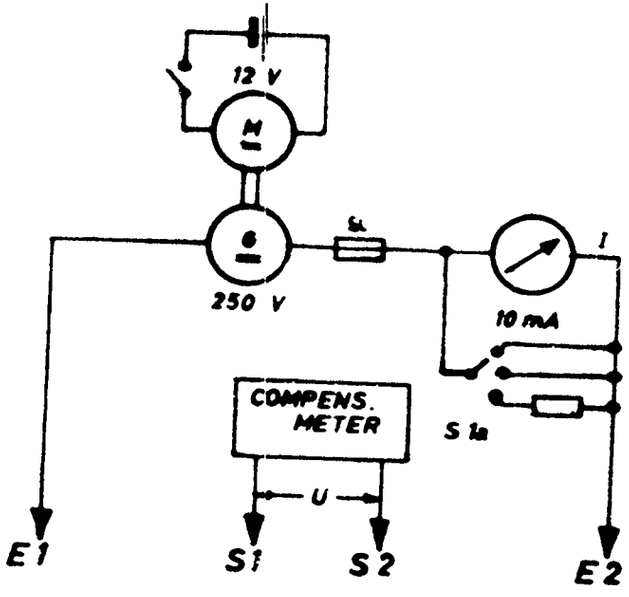

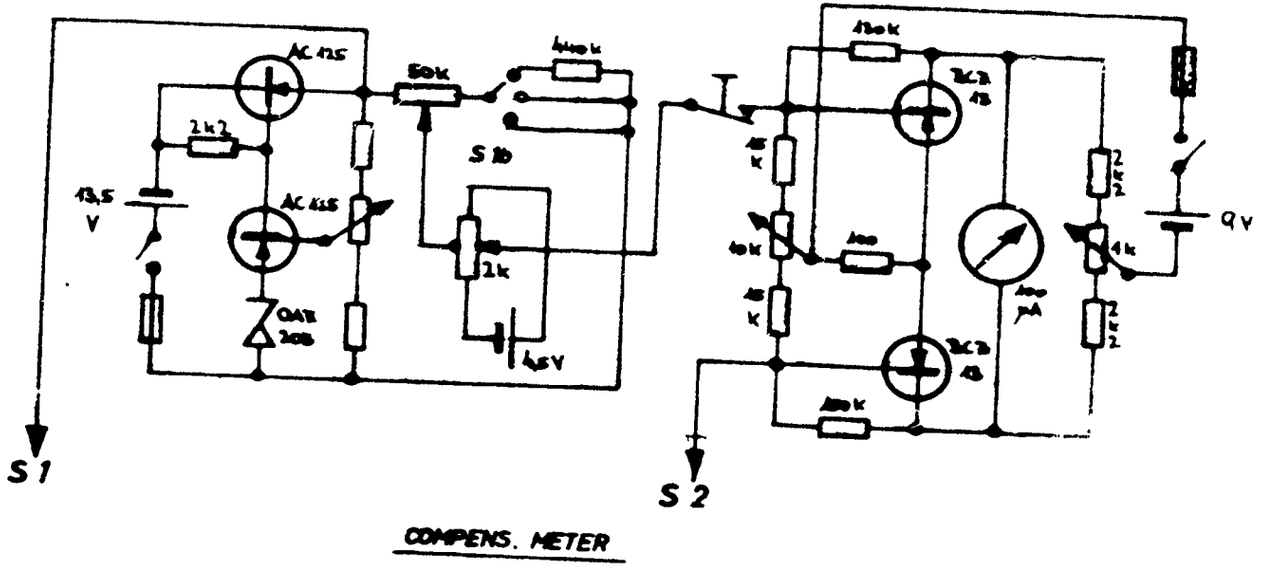

COMPENS. METER

DC CONDUCTIVITY METER

FIG. 123

For the conducted measurements, the following maximum values are to be substituted:

$$\frac{\mu_I}{I} = 0{,}02 \qquad \frac{\mu_U}{U} = 0{,}05 \qquad \mu_e = 0{,}02 \qquad a = 0{,}5$$

With these values, the relative error is 0.07. Thus, the measurements in the most unfavorable case will have an error of 7%.

4. Measurements:

Electrodes and probes:

For electrodes as well as for probes, holes were made into the rock by means of a spudding bit fed by an accumulator, which filled with cotton wool soaked in a salt solution. Then, steel studs were driven into the cotton wool to fasten the wires for the measuring device. Although this method of contacting yields very low contact resistances, the production of electrodes for a large number of measuring points would have consumed too much time. Commercial bolt setting guns (Hilti DX 100) were used to set steel nails into the rock for the below measurements. This, however, was only possible in small cracks in the rock. Two suitable sites were chosen for installing two Wenner configurations at a vertical distance of approximately 10 cm in order to study whether the results of the measurements are affected by a possible difference in conductivity in the cracks filled with wet dust (Fig. 1,24).

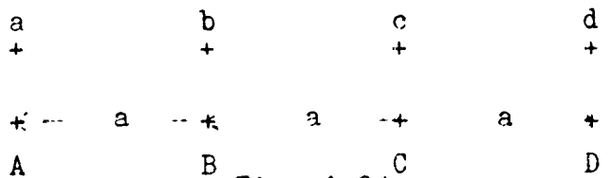

Fig. 1,24

The studs a, b, c, and d were placed into cracks, whereas the studs A, B, C, and D were set into solid rock, their combination being varied during the measurement. The effect of the cracks carrying the electrodes was assumed to be negligible, as the deviation from the mean value is $< 3\%$.

The first measurement was made to determine the conductivity over a large distance by means of the four-electrode method. For this purpose, the configuration was chosen such that it seemed justified that the expression for the full space should be applied. A map is given in Fig. 1,25.

Measurements were conducted with probes on the ceiling and on the walls of the gallery. The electrodes were made different, measurements on these electrodes were repeated several times after periods of some weeks, as the water level in the gaps of this mine changes considerably. The below mean value of 32 measurements was obtained for the apparent specific conductivity on this measuring line.

$$\sigma_s = 1.62 \cdot 10^{-4} \text{ mho/m}$$

the deviation from this mean value being $<8\%$. It has still to be found out (by changing the distances of the configuration) whether this value represents the actual d-c conductivity. For this purpose, similar measurements over smaller distances were also made.

First, studies were necessary to find out whether the measuring results are affected by a difference in conductivity of the often thick and damp layer of dust and the rock below. For this purpose, the theory of the stratified medium with a simplification for only one layer was used. The results are shown in Fig. 1,26.

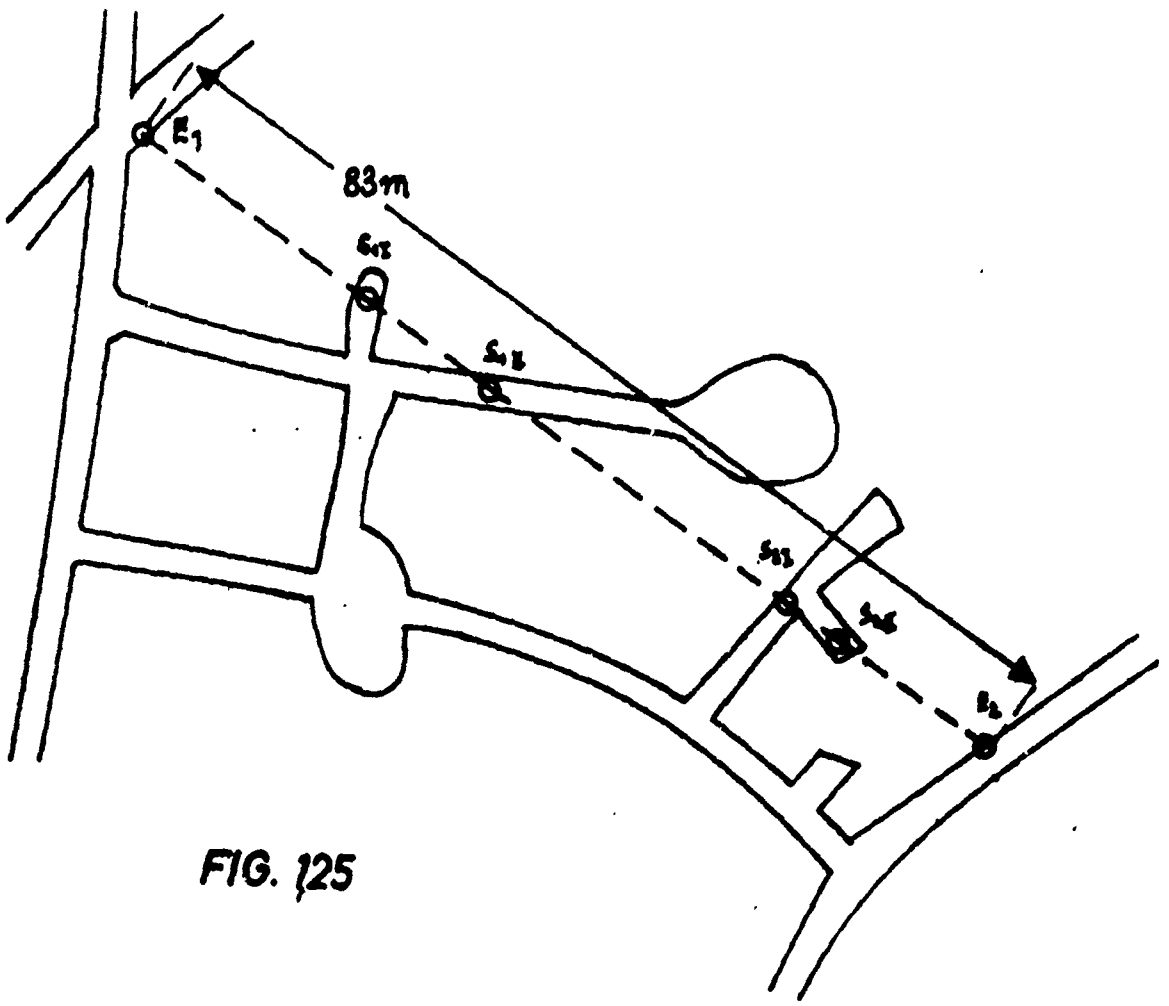

FIG. 125

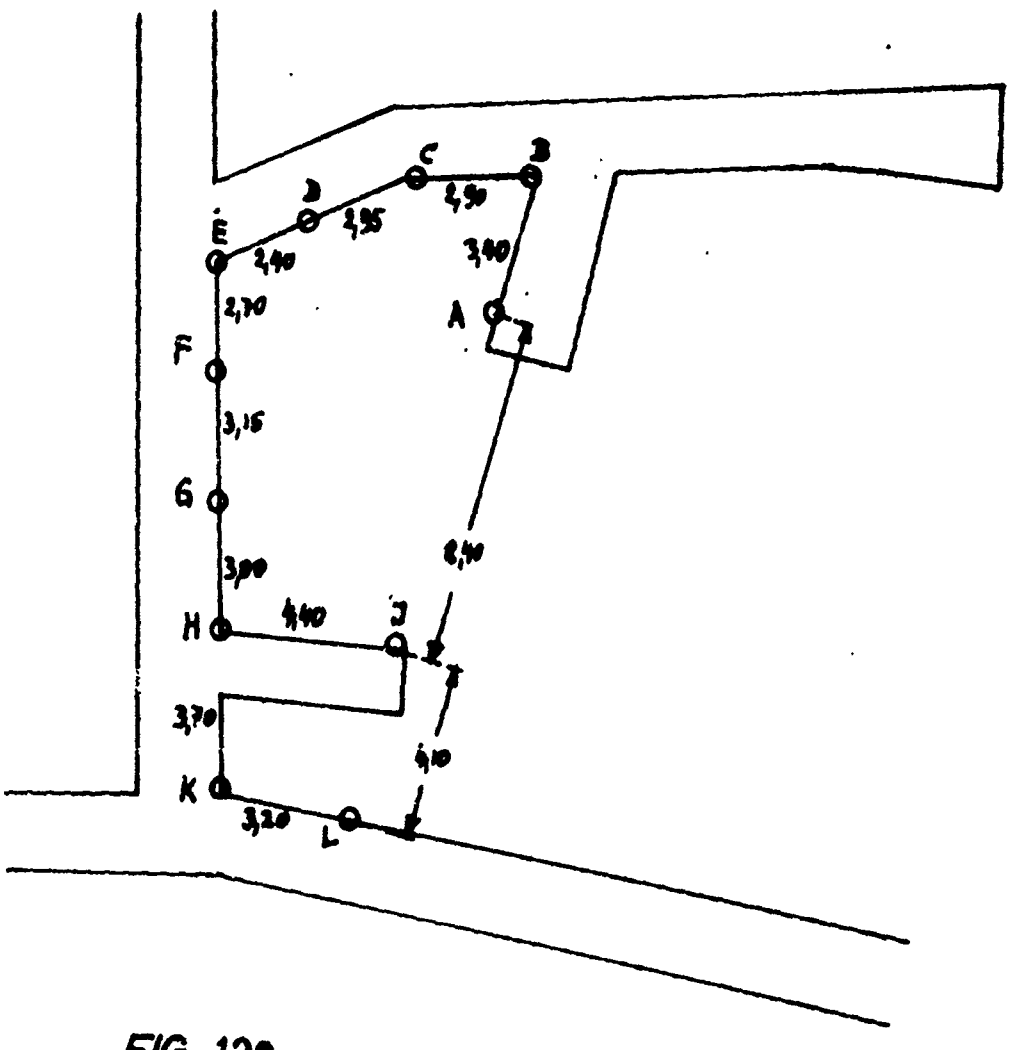

FIG. 128

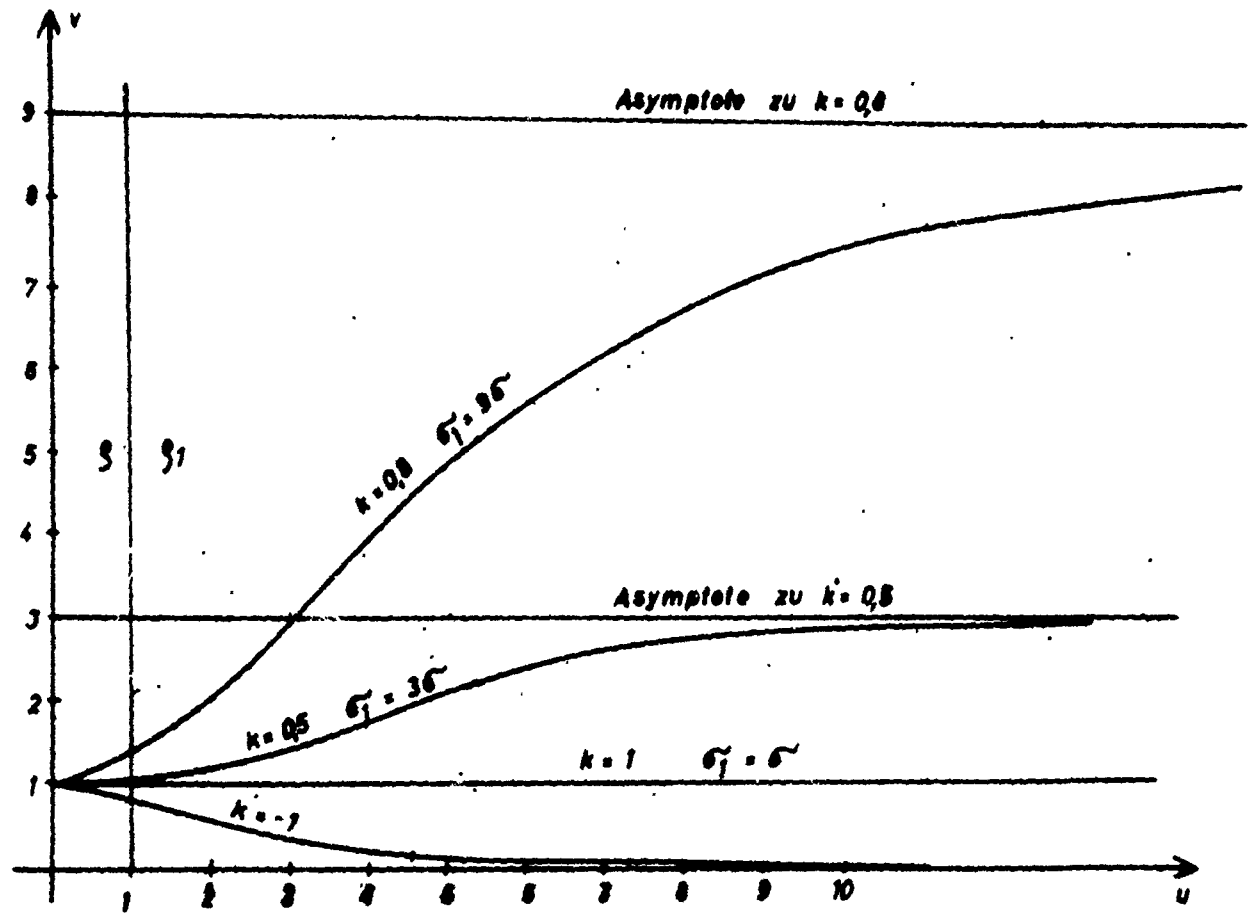

FIG. 1,26

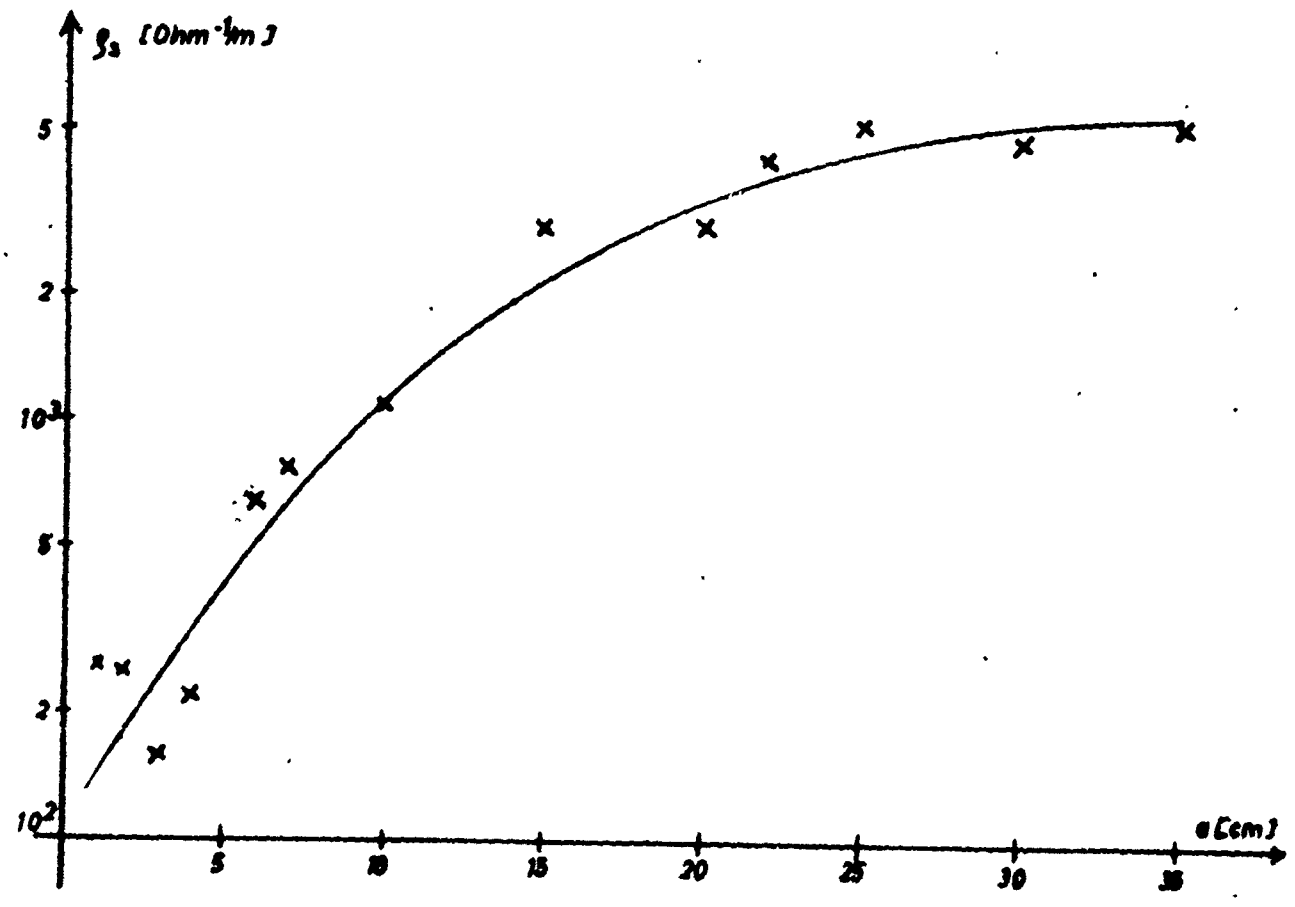

FIG. 1,27

The symbols have the following meaning:

$$k = \frac{\sigma - \sigma_1}{\sigma + \sigma_1}; \quad u = \frac{a}{h}; \quad v = \frac{\rho_s}{\rho}$$

ρ = resistivity of covering layer

ρ_1 = resistivity of bottom

ρ_s = apparent resistivity measured

1 cm was used as the smallest value of a. Studs mounted to a pertinax rod and pressed toward the rock by springs were used as electrodes and probes. Fig. 1,27 gives the result of one measurement. The ordinate, however, gives ρ_s instead of v and the abscissa gives a instead of u.

Hence, a thin surface layer actually has a higher conductivity, which is ineffective already at a = 0.30 m. We only conducted measurements with larger a.

The neighborhood of the electrodes S_2 and E_2 was studied in detail. Fig. 1,28 shows a diagram of the used electrodes. Various combinations of the electrodes were used as four-electrode configurations, and the corresponding apparent conductivity was determined. Table XVI shows the results.

These values differ considerably from each other, the smallest value being $0.74 \cdot 10^{-4}$ mho/m and the largest value being $3.00 \cdot 10^{-4}$ mho/m. The derived error of measurement was checked by repeated measurements showing the results to be well reproducible. For equal electrodes, however, the values on the whole increase if the probes are placed subsequently at FG, FH, and HI. Owing to this regularity, the apparent conductivity is assumed to have different values for two reasons:

(1) There are differences in the actual specific conductivity of the rock.

(2) The differences are due to the effect of the gallery, which with a cross section of approximately 2 m by 2 m is equally large as the distances of the used configuration.

Some other measurements prove the two conclusions to be correct. Four holes at a distance of two meters each (depth 2 m) were drilled into the wall of a larger mine. The Wenner configuration was used for determining σ_s at different distances of the electrodes and probes from the surface. If σ_s is always calculated with the expression of a semispace regardless of the depth, it has to increase with the depth provided the rock is homogeneous. The result (given in Table XVII), however, at this point is independent of the depth, i.e., the actual conductivity increases with the depth. This is confirmed by a measurement in which Wenner configurations above this point were shifted, with the distance a being constant (a = 0.5, 1, 1.5, 2, and 2.5 m). The expected increase in σ_s with a is shown in Fig. 1,29. Every value is plotted in the diagram at the point M which is the center of the configuration. Hence, the conductivity σ changes irregularly within the above limits already at small distances, vertical to the configuration as well as along it. Similar results were found also at other measuring sites.

The measurement below shows that the effect of the gallery cannot always be neglected. Each of the two side walls of a gallery was provided with a Wenner configuration having a = 1.5 m. The site was chosen such that σ_s was the same on either side (Fig. 1,30). The value obtained for σ_s is different, if the probes and electrodes are placed at different sides of the gallery. Table XVIII shows an example of measurement, all values being

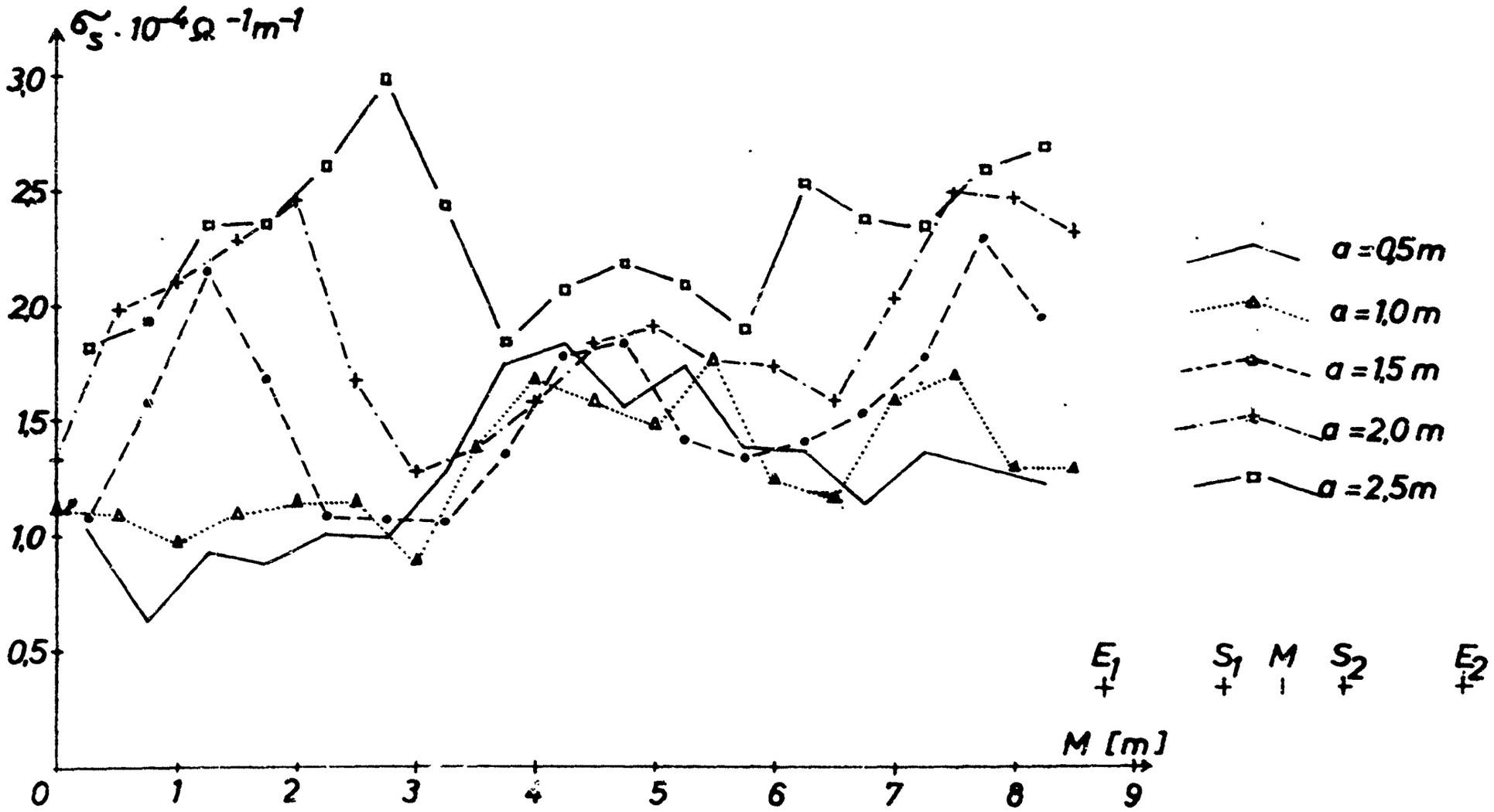
$\tilde{\sigma}_s \cdot 10^{-4} \Omega^{-1} m^{-1}$
3,0
2,5
2,0
1,5
1,0
0,5
0
1
2
3
4
5
6
7
8
9
M [m]
E_1
S_1
M
S_2
E_2
a = 0,5 m
a = 1,0 m
a = 1,5 m
a = 2,0 m
a = 2,5 m

FIG. 129

calculated from the expression (1).

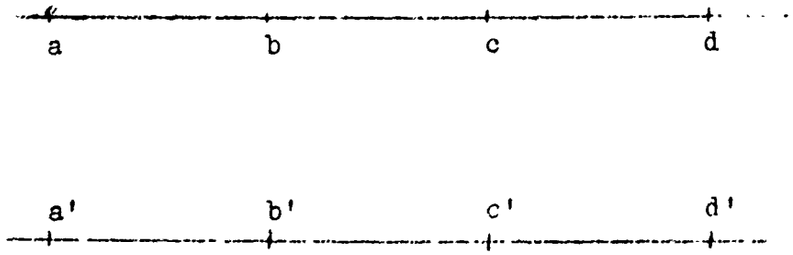

Fig. 1,30

The analogous values for a = 5 m coincide much better. Because of the inhomogeneity of rock, this measurement was conducted for several points by shifting the configuration always by 5 m. Fig. 1,31 shows the result. The difference in the deviation of the corresponding points of measurement is probably due to an asymmetry in homogeneity with respect to the gallery. The values measured at the same site with a = 10 m are in sufficient agreement with allowance for the error limits plotted in one of the curves (Fig. 1,32). This is assumed to show that, under the given conditions, the effect of the space of the gallery from this a-value onward can be neglected and that the expression (1) yields the correct values for the conductivity in homogeneous rock. In order to get a better idea of the restrictions that are to be observed for determining the conductivity in mines by the Wenner configuration it is desirable, that a general relation among the three parameters cross section of the galleries, a and σ be derived. This is planned to be done in the continuation of this study.

After measuring in various parts of the mine with allowance for the above experience, we may now say that the d-c conductivity

changes within the values $0.5 \cdot 10^{-4}$ and $3.0 \cdot 10^{-4}$ mho/m given above, the homogeneous ranges being but small.

5. Furthermore, the results of measurements in German and Dutch mines which we visited in summer 1963, shall be summarized.

(1) Salzgitter, mine Konrad

A highly homogeneous ore body whose conductivity is $3.1 \cdot 10^{-1}$ mho/m. At the edge of this body where it is mixed with dead rock, the conductivity decreases to $1.2 \cdot 10^{-1}$ mho/m, in dead rock (in the 1200 m gallery) to $3.0 \cdot 10^{-2}$ mho/m.

(2) Hannover, potash mine Hansa III-Empelde

Measurements with the available device were impossible because of the high resistivity. In any case, the conductivity is smaller than $1 \cdot 10^{-9}$ mho/m.

(3) Siegerland, ore mines Fuesseberg and Willroth

The ore of both mines is highly inhomogeneous and mixed with dead rock. The results in ore and also in dead rock lie between $2 \cdot 10^{-4}$ mho/m and $8 \cdot 10^{-3}$ mho/m.

(4) Heerlen, coal mine Oranje - Nassau III

Coal showed a clear difference between the results in the direction of the seam and those vertical to the seam.

Result: in direction of the seam $\sigma = 8.0 \cdot 10^{-8}$ mho/m

vertical to the seam $\sigma = 1.5 \cdot 10^{-7}$ mho/m

The possibility of measuring in dead rock was restricted because of the iron props; the few measured values lie between $3.3 \cdot 10^{-3}$ and $1.1 \cdot 10^{-2}$ mho/m.

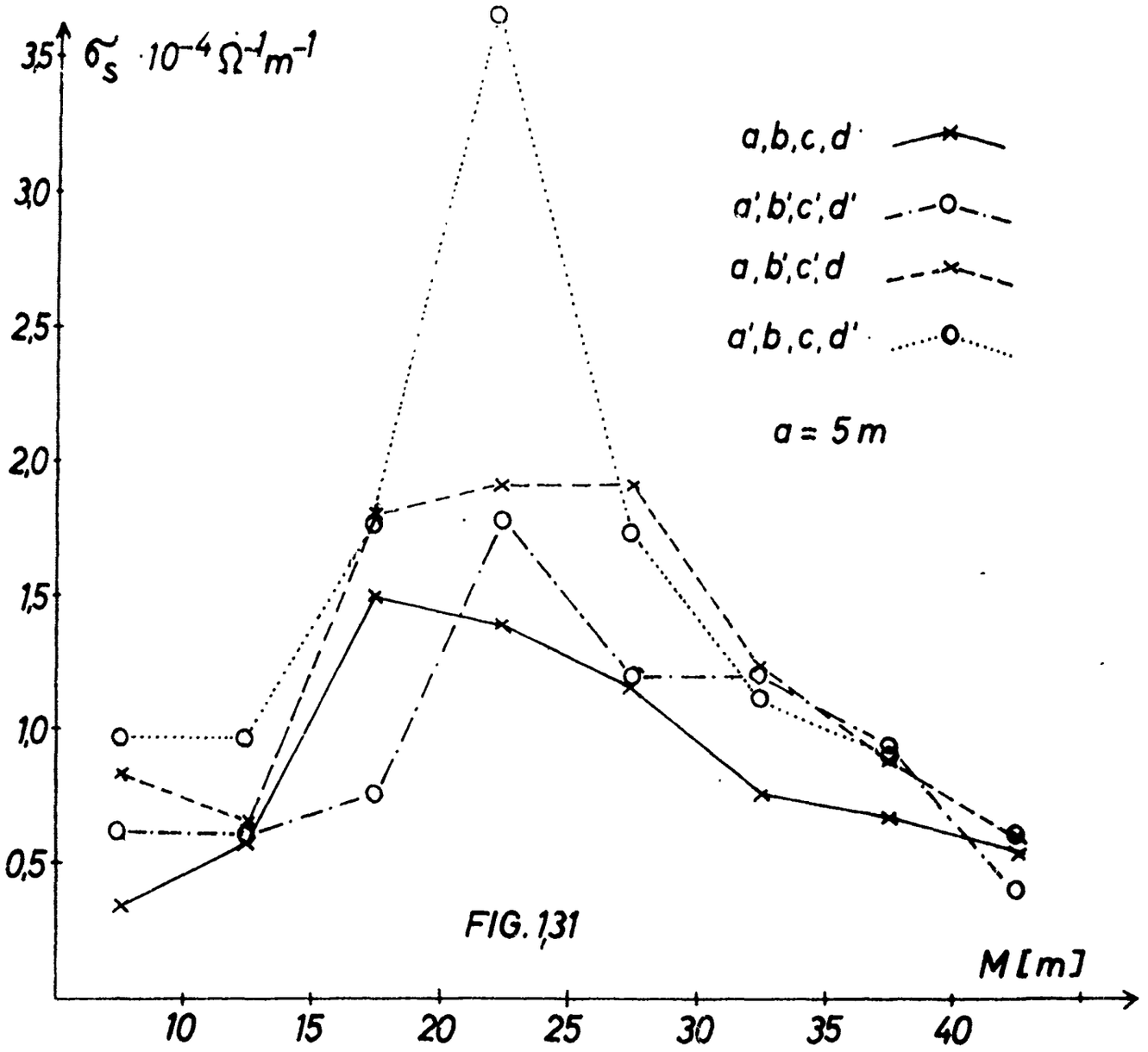

FIG. 1,31

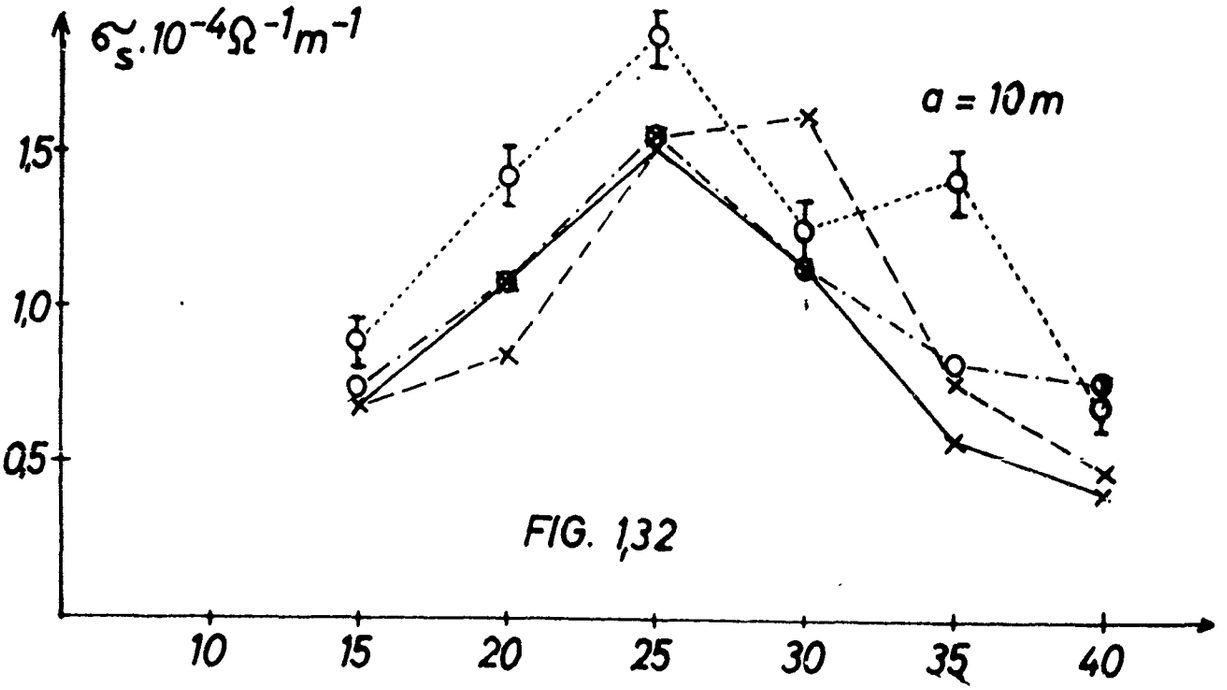

FIG. 1,32

6. Specimen measurements, frequency dependence.

So far, the frequency dependence has only been measured for specimens. For making the specimens, a cylinder with a diameter of 5 cm was bored out of a larger piece of rock (Fig. VI) and was then cut into disks 0.2 - 1.0 cm thick with a stone saw (Fig. VII). The loss factor and the capacitance of the samples were measured in a measuring capacitor (Fig. VIII) built for this purpose by a capacitance bridge (General Radio, type 716 - C) under different conditions. From these values, σ and ε were calculated. The humidity and the porosity of the specimens were determined from the difference in weight before and after drying at 125°C for 24 hours.

In the present report we only want to discuss a few results in brief, namely the values obtained for two specimens (D_1 and D_2) from the St. Gertraudi mine, two ore specimens (S_1 and S_2) from the Salzgitter ore mine, and two specimens (G_1 and G_2) from the Willroth mine. The two specimens are always chosen from a large number of specimens being nearly equal with respect to their electrical properties. D_1 and D_2 consist of dolomite of low porosity (pore volume approximately 0.12% of the total volume), S_1 and S_2 are of oolitic ore of much greater porosity (pore volume approximately 14%), and G_1 and G_2 are ore specimens mixed with dead rock, whose porosity is somewhat higher than that of dolomite differing considerably in various specimens - in contrast to the specimens D and S. The electrical properties were first measured immediately after cutting the specimens, i.e. in a largely natural state. The specimens were then dried and the measurements were repeated. The third measurements were made

with the specimens saturated in distilled water. The values of ε and σ are given in Table XIX and Figs. 1,33 and 1,34

The values for σ are all several powers of ten smaller than those measured with direct current in outcrops. Thus it seems that boring and cutting the specimens changes their electrical properties considerably, and hence that the frequency curves for the conductivity measured for the specimens are completely different from the d-c values measured in outcrops. On the other hand, since the factor between the values at 100 cps and 10 kc/sec is two powers of ten at least, it seems necessary that the frequency dependence should also be measured at the outcrop. For this purpose, a second transmitter was set up in the St. Gertraudi mine lab (besides the Savage amplifier used for propagation experiments) which also had an output power of 1 kw and was suitable as a voltage source. However, our work on the measurement of the frequency dependence of conductivity in the outcrop has not progressed far enough for the results to be discussed in the present report.

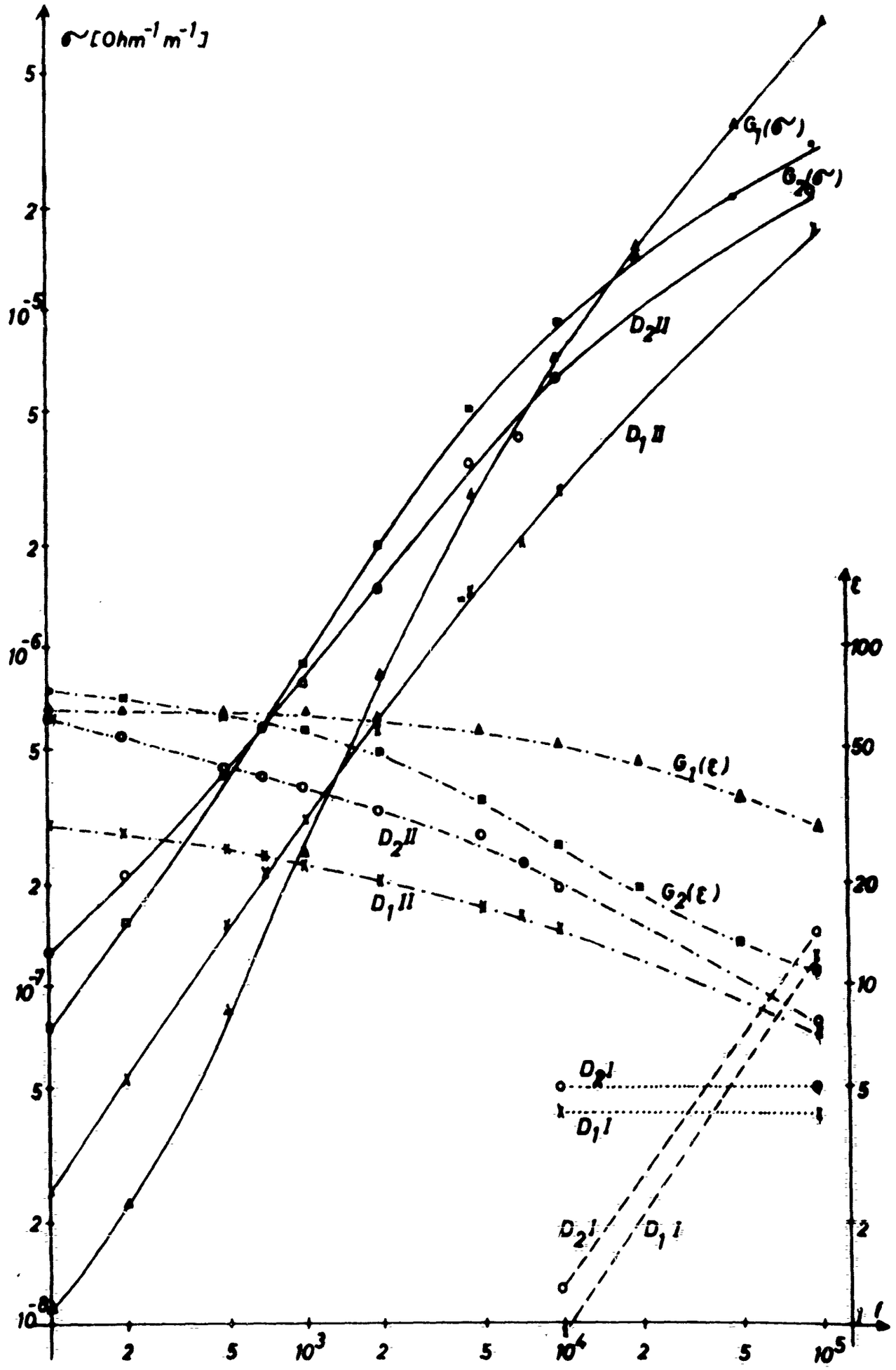
σ~[Ohm⁻¹ m⁻¹]
G₁(σ~)
G₂(σ~)
D₂II
D₁II
G₁(ℓ)
G₂(ℓ)
D₂II
D₁II
D₂I
D₁I
D₂I
D₁I
ℓ
100
50
20
10
5
2
1
l
5
2
10⁻⁵
5
2
10⁻⁶
5
2
10⁻⁷
5
2
10⁻⁸
2
5
10³
2
5
10⁴
2
5
10⁵

FIG. 133

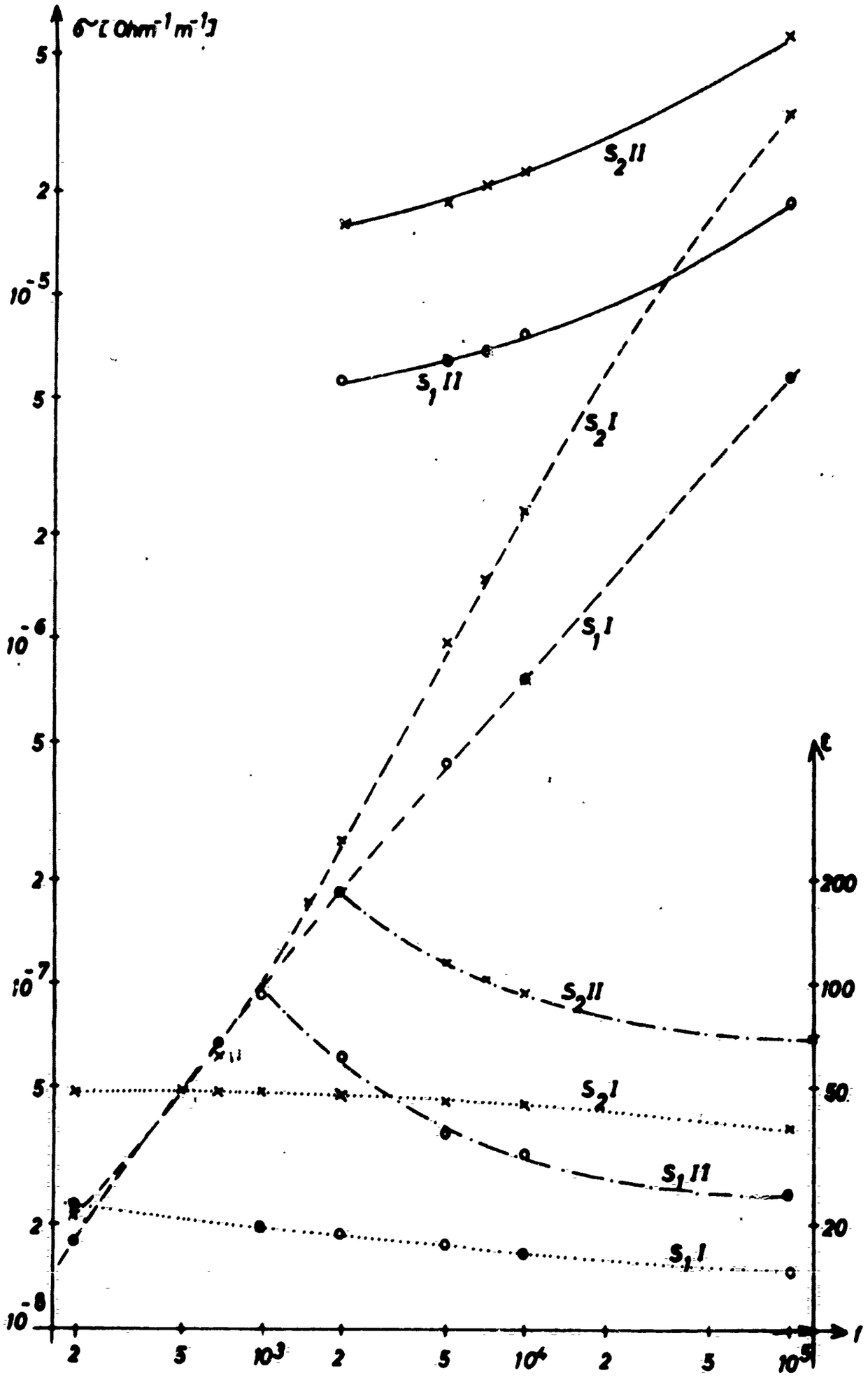
σ~[Ohm⁻¹m⁻¹]
5
2
10⁻⁵
5
2
10⁻⁶
5
2
10⁻⁷
5
2
10⁻⁸
S₂II
S₁II
S₂I
S₁I
S₂II
S₂I
S₁II
S₁I
ε
200
100
50
20
2
5
10³
2
5
10⁴
2
5
10⁵
f

FIG. 1,34

TABLE I

Calculation of the function

$$h(r,\vartheta,\Delta) = \frac{\exp(-\Delta r)}{r}\left\{\frac{4\cos^2\vartheta}{r^2}\left(\frac{1}{r^2}+\frac{2\Delta}{r^2}+2\Delta^2\right)+\sin^2\vartheta\left(\frac{1}{r^4}+\frac{2\Delta}{r^3}+\frac{2\Delta^2}{r^2}+\frac{4\Delta^2}{r}+4\Delta^2\right)\right\}^{1/2}$$

$$\Delta=\sqrt{\frac{\mu_0\omega\sigma}{2}}$$

f = 3 kc/sec

r	ϑ	Δ = $1.085\cdot10^{-2}$ σ = 10^{-2} ($^{-1}m^{-1}$)	$3.45\cdot10^{-2}$ 10^{-1}	$4.86\cdot10^{-2}$ $2\cdot10^{-1}$	$7.7\cdot10^{-2}$ $5\cdot10^{-1}$	$1.09\cdot10^{-1}$ 1
10 m	0	$2\ .10^{-3}$	$1.97.10^{-3}$	$1.9\ .10^{-3}$	$1.79.10^{-3}$	$1.58.10^{-3}$
	30	$1.8\ .10^{-3}$	$1.79.10^{-3}$	$1.73.10^{-3}$	$1.66.10^{-3}$	$1.54.10^{-3}$
	60	$1.31.10^{-3}$	$1.34.10^{-3}$	$1.33.10^{-3}$	$1.38.10^{-3}$	$1.41.10^{-3}$
	90	$9.9\ .10^{-4}$	$1.04.10^{-3}$	$1.\ 8.10$	$1.22.10^{-3}$	$1.36.10^{-3}$
20 m	0	$2.5\ .10^{-4}$	$2.28.10^{-4}$	$2.08.10^{-4}$	$1.59.10^{-4}$	$1.23.10^{-4}$
	30	$2.26.10^{-4}$	$2.13.10^{-4}$	$2.00.10^{-4}$	$1.65.10^{-4}$	$1.36.10^{-4}$
	60	$1.67.10^{-4}$	$1.78.10^{-4}$	$1.77.10^{-4}$	$1.76.10^{-4}$	$1.6\ .10^{-4}$
	90	$1.27.10^{-4}$	$1.58.10^{-4}$	$1.65.10^{-4}$	$1.81.10^{-4}$	$1.7\ .10^{-4}$
50 m	0	$1.52.10^{-5}$	$9.25.10^{-6}$	$5.6.10^{-6}$	$2.1.10^{-6}$	$6.1\ .10^{-7}$
	30	$1.39.10^{-5}$	$1.01.10^{-5}$	$7.20.10^{-6}$	$3.39.10^{-6}$	$1.31.10^{-6}$
	60	$1.08.10^{-5}$	$1.16.10^{-5}$	$9.60.10^{-5}$	$5.05.10^{-6}$	$2.05.10^{-6}$
	90	$8.90.10^{-6}$	$1.23.10^{-5}$	$1.04.10^{-5}$	$5.70.10^{-6}$	$2.33.10^{-6}$
100 m	0	$1.58.10^{-6}$	$3.56.10^{-7}$	$1.22.10^{-7}$	$1.04.10^{-8}$	$1.55.10^{-9}$
	30	$1.51.10^{-6}$	$5.50.10^{-7}$	$2.38.10^{-7}$	$3.10.10^{-8}$	$6.35.10^{-8}$
	60	$1.42.10^{-6}$	$8.10.10^{-7}$	$3.70.10^{-7}$	$4.94.10^{-8}$	$1.07.10^{-8}$
	90	$1.36.10^{-6}$	$9.66.10^{-7}$	$4.20.10^{-7}$	$5.70.10^{-8}$	$1.24.10^{-8}$
200 m	0	$1.15.10^{-7}$	$2.62.10^{-9}$	$2.17.10^{-10}$	$5.85.10^{-11}$	
	30	$1.37.10^{-7}$	$6.90.10^{-9}$	$7.75.10^{-10}$	$3.32.10^{-10}$	
	60	$1.64.10^{-7}$	$1.13.10^{-8}$	$1.30.10^{-9}$	$5.70.10^{-10}$	
	90	$1.78.10^{-7}$	$1.30.10^{-8}$	$1.50.10^{-9}$	$6.55.10^{-10}$	
500 m	0	$6.06.10^{-10}$	$1.49.10^{-14}$	$1.89.10^{-17}$		
	30	$1.27.10^{-9}$	$9.25.10^{-14}$	$1.60.10^{-16}$		
	60	$2.03.10^{-9}$	$1.59.10^{-13}$	$2.78.10^{-16}$		
	90	$2.32.10^{-9}$	$1.84.10^{-13}$	$3.20.10^{-16}$		

TABLE II

Function $\varphi(r, \Delta)$

r \ Δ	10^{-2}	10^{-1}	$2 \cdot 10^{-1}$	$5 \cdot 10^{-1}$	1
10	2.02	1.93	1.83	1.47	1.16
20	1.97	1.44	1.26	0.88	0.72
50	1.71	0.75	0.54	0.37	0.266
100	1.16	0.37	0.29	0.182	0.125
200	0.65	0.2	0.145	0.09	-
500	0.26	0.081	0.059	-	-

TABLE III

Measurement I

r=18 m

$\vartheta = 0^\circ$

Ψ	U_e	$\bar{U}_e$	$\bar{\bar{U}}_e$
0°	5.3	5.3	5.37
30°	4.5	4.6	4.65
60°	2.5	2.8	2.68
90°	0.85	0.9	0
120°	3.0	2.8	2.68
150°	4.8	4.6	4.65
180°	5.4	5.3	5.37
330°	4.8	4.6	4.65
300°	3.0	2.8	2.68
270°	1.0	0.9	0
240°	2.5	2.8	2.68
210°	4.5	4.6	4.65
0°	5.3	5.3	5.37

$\vartheta = 30^\circ$

Ψ	U_e	$\bar{U}_e$	$\bar{\bar{U}}_e$
30°	5	5	5.16
60°	4.8	4.5	4.46
90°	2.5	3.2	2.58
120°	1.7	1.7	0
150°	2.3	3.2	2.58
180°	4.3	4.5	4.46
210°	5.2	[illegible]	5.16
0°	4.2	4.5	4.46
330°	2.4	3.2	2.58

$\vartheta = 60^\circ$

Ψ	U_e	$\bar{U}_e$	$\bar{\bar{U}}_e$
60°	4.7	4.7	4.72
30°	4.2	4.1	4.16
0°	2.7	2.5	2.41
330°	0.8	0.8	0
300°	2.1	2.5	2.41
270°	4.0	4.1	4.16
90°	4.0	4.1	4.16
120°	2.4	2.5	2.41
150°	0.8	0.8	0
180°	2.6	2.5	2.41

$\vartheta = 90^\circ$

Ψ	U_e	$\bar{U}_e$	$\bar{\bar{U}}_e$
270°	4.6	4.6	4.75
60°	4.3	4.3	4.12
30°	2.7	2.5	2.38
90°	4.6	4.6	4.75
120°	4.0	4.3	4.12
150°	2.0	2.5	2.38
180°	0.63	0.6	0
210°	2.7	2.5	2.38
240°	4.3	4.3	4.12

TABLE IV

Measurement II

r = 25 m

$\varphi = 0^\circ$

ψ	U_e	$\bar{U}_e$	$\bar{\bar{U}}_e$
0°	2.4	2.4	2.5
30°	2.0	2.2	2.16
60°	1.3	1.6	1.25
90°	0.85	0.85	0
120°	1.6	1.6	1.25
150°	2.2	2.2	2.16
180°	2.4	2.4	2.5
330°	2.2	2.2	2.16
300°	1.55	1.6	1.25
270°	0.85	0.85	0

$\varphi = 30^\circ$

ψ	U_e	$\bar{U}_e$	$\bar{\bar{U}}_e$
0°	2.2	2.2	2.34
30°	2.4	2.4	2.7
60°	2.3	2.2	2.34
90°	1.8	1.7	1.35
120°	1.5	1.5	0
150°	1.7	1.7	1.35
180°	2.2	2.2	2.34
330°	1.7	1.7	1.35
300°	1.5	1.5	0

$\varphi = 60^\circ$

ψ	U_e	$\bar{U}_e$	$\bar{\bar{U}}_e$
60°	3.4	3.4	3.3
90°	2.8	2.8	2.85
120°	1.7	1.7	1.65
150°	0.55	0.55	0
180°	1.6	1.7	1.65
210°	2.8	2.8	2.85
30°	2.8	2.8	2.85
0°	1.75	1.7	1.65

$\varphi = 90^\circ$

ψ	U_e	$\bar{U}_e$	$\bar{\bar{U}}_e$
90°	3.2	3.2	3.18
60°	2.7	2.7	2.74
30°	1.75	1.6	1.59
0°	1.35	1.3	0
120°	2.7	2.7	2.74
150°	1.6	1.6	1.59
180°	1.3	1.3	0
210°	1.6	1.6	1.59
240°	2.7	2.7	2.74

Table V

transmitter at PP107
f = 3 kHz; I = 0.75 a; SAVI

PP	m	ϑ	U_e [μV]
51	435	13°	1.5
64	538	42°	1.3
99	630	48°	1.1
10	420	52°	1.3
52	290	15°	1.5
93	240	0°	43
100	627	6°	1.0
103	300	10°	1.5

Table VII

measurement 1; transmitter PP9;
f = 3 kc; I = 3.5 a; SAVI;
receiving antenna EAVI

PP	m	ϑ	U_e [μV]
8	67	40°	3500
7	140	25°	200
6	213	15°	55
5	285	5°	27
5.1	262	0°	26.5
3.2	460	10°	4.5
2	535	10°	2.8
2.1	520	0°	2.4

Table VI

transmitter at PP107: f = 3 kc; r = 240 m, receiver PP93

ϑ = 0°			ϑ = 60°		
ψ°	U_e [μV]	$\overline{U}_e$ [μV]	ψ°	U_e [μV]	$\overline{U}_e$ [μV]
0	4	4.10	270	2.0	1.92
30	3.6	3.54	300	1.4	1.11
60	1.9	2.05	330	0.4	0
90	0.3	0	0	1.0	1.11
120	2.1	2.05	30	1.9	1.92
150	3.6	3.54	60	2.3	2.22
330	3.6	3.54	240	2.2	2.22
300	2.0	2.05	210	1.7	1.92
270	0.3	0	340	0.4	0

Table VIII

measurement 1: transmitter S_1

f = 3 kc; I = 0.4 a, SAVI

PP	m	$\bar{U}_e$ [μV]
1	35	52.7
603.1	80	16.5
4.1	130	10
4	135	9.2

Table X

measurement 2: transmitter S_2

f = 3 kc; I = 0.7 a, SAVI

PP	m	ϑ^o	U_e [μV]
503	60	57	210
c	160	58	60
603.1	164	46	33
d	222	19	26
S_1	156	22	42
1	125	28	60
4.1	81	37	130

Table IX

measurement 2: transmitter S_2; f = 3 kc; SAVI; I = 3.5 a; receiving antennas EAIV and EAVI

PP	m	ϑ^o	U_e(EAVI)	U_e(EAIV)	$\bar{U}_e$ [μV]
1	170	43	6	30	6.05
1.1	119	42	11	45	10.1
2	141	53	11	53	10.9
2.1	166	52	15	67	14.3
3.2	122	68	70	450	81
4	107	86	100	550	106
5	110	71	37	170	36
5.2	109	67	20	100	20.2
6	126	54	17	80	16.7
7.1	153	42	11	52	10.8
7	150	43	13	55	12.1
8	180	34	8	-	8
8.1	182	34	7	35	7.1
9	202	30	4.6	25	4.9

Table XI

$\vartheta = 0°$			r = 262 m	$\vartheta = 90°$	
$\psi°$	$U_e[\mu V]$	$\overline{U}_e[\mu V]$	$\psi°$	$U_e[\mu V]$	$\overline{U}_e[\mu V]$
0	24	24.1	265	18	17.8
330	21.5	20.8	240	16.5	16.1
300	14	12	210	11.5	10.4
270	0.5	0	175	0	0
240	10.5	12	180	3.3	1.55
210	10	12	300	14.2	14.6
180	24	24.1	330	7	7.52
30	20	20.8	0	3	1.55
60	11	12	30	11	10.4
90	0.5	0	60	16.5	16.1
120	14	12	90	17.5	17.6
150	21.5	20.8	150	6.4	7.52

Table XII

transmitter PPS_1, r = 35 m, f = 3kc

$\vartheta = 0°$			$\vartheta = 90°$		
$\psi°$	$U_e[\mu V]$	$\overline{U}_e[\mu V]$	$\psi°$	$U_e[\mu V]$	$\overline{U}_e[\mu V]$
180	53	52.7	270	30	30
150	47	45.5	240	27	26
120	28	26.4	210	16	15
90	1	0	180	2	0
60	23.5	26.4	150	14	15
30	45	45.5	120	25	26
210	45	45.5	90	30	30
240	24	26.4			
270	1	0			
300	27	26.4			

Table XIII

r = 130 m, transmitter PPS_1

ψ°	$U_e[\mu V]$	$\bar{U}_e[\mu V]$	ψ°	$U_e[\mu V]$	$\bar{\bar{U}}_e[\mu V]$
210	10.5	10.15	270	10	10
180	9	8.8	240	8.6	8.65
150	4.3	5.07	210	5.0	5.0
120	0.2	0	180	0.8	0
90	4.8	5.07	150	4.6	5.0
240	8.8	8.8	120	8.4	8.65
270	5.0	5.07	90	9.6	10
300	0.2	0	300	8.6	8.65

Table XIV

transmitter: f = 3 kc,
I = 1a, SAVI

r	ϑ°	$U_e[\mu V]$
225	0	1
225	90	0.5
375	0	0.5
375	90	2.3
500	0	0.2

Table XV

transmitter: f = 3kc, I = 25a, SAVIII

m	ϑ°	$\bar{U}_e[\mu V] \pm 10\%$
185	39	72.5
280	33	21.84
380	21	9.3
475	30	4.94
580	30	2.74
680	30	1.71
720	30	1.215
840	30	0.85
840	30	0.71
960	30	0.545
1040	30	0.45
1100	28	0.445
1200	28	0.33
1270	27	0.344
1320	27	0.262
1550	23	0.348
1800	0	0.151
2000	27	0.088
2200	24	0.197
3000	36	0.058
3500	4	0.0197

Table XVI

electrodes	probes	k	J	U	$\sigma \cdot 10^{-4}$ mho/m
D - K	F - G	0.246	1.75	0.17	2.02
	F - H	0.425	1.60	0.25	2.17
	F - I	0.351	1.55	0.21	2.06
	G - I	0.105	1.55	0.06	2.16
	G - H	0.179	1.60	0.10	2.29
	I - H	0.074	1.45	0.05	1.71
F - K	G - H	0.275	1.15	0.12	2.10
	G - I	0.222	1.20	0.11	1.93
	I - H	0.053	1.25	0.032	1.65
G - K	H - I	0.063	1.10	0.075	0.74
D - H	F - G	0.379	3.40	0.60	1.71
E - I	F - G	0.253	6.60	0.67	1.99
	F - H	0.356	6.70	0.86	2.21
	G - H	0.103	6.60	0.18	3.00
E - L	F - G	0.232	3.50	0.32	2.02
	F - H	0.350	3.70	0.44	2.35
	F - I	0.423	3.70	0.52	2.40
	H - I	0.073	3.60	0.08	2.62
	G - I	0.101	3.65	0.19	2.92
F - L	G - H	0.214	2.60	0.20	2.21
	G - I	0.308	2.60	0.28	2.28
	H - I	0.094	2.60	0.09	2.16
	B - I	0.162	2.40	0.14	2.21
G - L	H - I	0.210	2.60	0.29	1.50
B - L	F - I	0.176	3.50	0.225	2.18
	A - I	0.373	3.40	0.43	2.35

Table XVII

Depth of configuration	0	0.5	1.0	1.5	2.0
$\sigma_s \cdot 10^{-4}$	2.02	2.12	2.27	2.05	2.01

Table XVIII

Electrodes	Probes	k	J	U	$\sigma_s \cdot 10^{-4}$
a - d	b - c	0.667	1.62	0.321	2,68
a'-d'	b'-c'	0.667	6.15	1.245	2.62
a - d	b'-c'	0.349	1.62	0.050	9.03
a'-d'	b - c	0.349	6.15	0.192	8.87

Table XIX

A. Dried specimens

1)

f[kcps]	D_1 (Fig. 1,33; D_1I) ε	D_1 (Fig. 1,33; D_1I) σ	D_2 (Fig. 1,33; D_2I) ε	D_2 (Fig. 1,33; D_2I) σ
10	4.11	$9.25 \cdot 10^{-9}$	4.92	$1.25 \cdot 10^{-8}$
100	4.09	$1.22 \cdot 10^{-7}$	4.88	$1.42 \cdot 10^{-7}$

2)

f[kcps]	S_1 (Fig. 1,34; S_1I) ε	S_1 (Fig. 1,34; S_1I) σ	S_2 (Fig. 1,34; S_2I) ε	S_2 (Fig. 1,34; S_2I) σ
0.1	23.7	$8.4 \cdot 10^{-9}$	50.0	$9.70 \cdot 10^{-9}$
0.2	22.1	$1.83 \cdot 10^{-8}$	49.7	$2.16 \cdot 10^{-8}$
0.7	20.2	$6.90 \cdot 10^{-8}$	48.8	$6.06 \cdot 10^{-8}$
1	19.7	$1.00 \cdot 10^{-7}$	48.6	$1.01 \cdot 10^{-7}$
2	18.7	$1.87 \cdot 10^{-7}$	48.0	$2.60 \cdot 10^{-7}$
5	17.4	$4.35 \cdot 10^{-7}$	46.3	$9.80 \cdot 10^{-7}$
7	17.0	$5.56 \cdot 10^{-7}$	45.6	$1.50 \cdot 10^{-6}$
10	16.7	$7.57 \cdot 10^{-7}$	44.7	$2.34 \cdot 10^{-6}$
100	14.8	$5.96 \cdot 10^{-6}$	38.1	$3.33 \cdot 10^{-5}$

Table XIX

B. Specimens saturated with distilled water

1)

f [kcps]	D_1 (Fig. 1,33; D_1II) ε	σ	D_2 (Fig. 1,33; D_2II) ε	σ
0.1	30.0	$2.45 \cdot 10^{-8}$	65.0	$1.23 \cdot 10^{-7}$
0.2	28.4	$5.13 \cdot 10^{-8}$	53.8	$2.10 \cdot 10^{-7}$
0.5	25.2	$1.51 \cdot 10^{-7}$	43.8	$4.38 \cdot 10^{-7}$
0.7	24.0	$2.15 \cdot 10^{-7}$	41.2	$5.81 \cdot 10^{-7}$
1	22.6	$3.06 \cdot 10^{-7}$	38.5	$7.99 \cdot 10^{-7}$
2	20.1	$5.74 \cdot 10^{-7}$	33.0	$1.47 \cdot 10^{-6}$
5	16.9	$1.45 \cdot 10^{-6}$	27.9	$3.46 \cdot 10^{-6}$
7	15.8	$2.02 \cdot 10^{-6}$	22.8	$4.61 \cdot 10^{-6}$
10	14.4	$2.88 \cdot 10^{-6}$	19.4	$6.28 \cdot 10^{-6}$
100	7.2	$1.71 \cdot 10^{-5}$	7.8	$2.42 \cdot 10^{-5}$

2)

f [kcps]	S_1 (Fig. 1,34; S_1II) ε	σ	S_2 (Fig. 1,34; S_2II) ε	σ
1	92.5	$< 4.72 \cdot 10^{-6}$	---	$< 9.62 \cdot 10^{-6}$
2	60.6	$5.53 \cdot 10^{-6}$	186.0	$1.55 \cdot 10^{-5}$
5	37.9	$6.37 \cdot 10^{-6}$	115.7	$1.87 \cdot 10^{-5}$
7	34.0	$6.85 \cdot 10^{-6}$	103.5	$2.04 \cdot 10^{-5}$
10	31.0	$7.75 \cdot 10^{-6}$	94.8	$2.30 \cdot 10^{-5}$
100	23.4	$1.85 \cdot 10^{-6}$	69.8	$5.64 \cdot 10^{-5}$

3)

f [kcps]	G_1 (Fig. 1,33) ε [G_1]	σ [G_1]	G_2 (Fig. 1,33) ε [G_2]	σ [G_2]
0.1	66.0	$1.12 \cdot 10^{-8}$	74.9	$7.63 \cdot 10^{-8}$
0.2	65.4	$2.26 \cdot 10^{-8}$	70.1	$1.52 \cdot 10^{-7}$
0.5	64.1	$8.47 \cdot 10^{-8}$	62.3	$4.12 \cdot 10^{-7}$
1	63.2	$2.42 \cdot 10^{-7}$	56.7	$8.93 \cdot 10^{-7}$
2	61.8	$8.06 \cdot 10^{-7}$	48.6	$2.00 \cdot 10^{-6}$
5	57.2	$2.81 \cdot 10^{-6}$	35.3	$5.02 \cdot 10^{-6}$
10	51.9	$7.04 \cdot 10^{-6}$	26.4	$9.08 \cdot 10^{-6}$
20	45.7	$1.53 \cdot 10^{-5}$	19.6	$1.40 \cdot 10^{-5}$
50	35.7	$3.54 \cdot 10^{-5}$	13.4	$2.11 \cdot 10^{-5}$
100	29.2	$7.04 \cdot 10^{-5}$	11.2	$3.03 \cdot 10^{-5}$

Fig. I

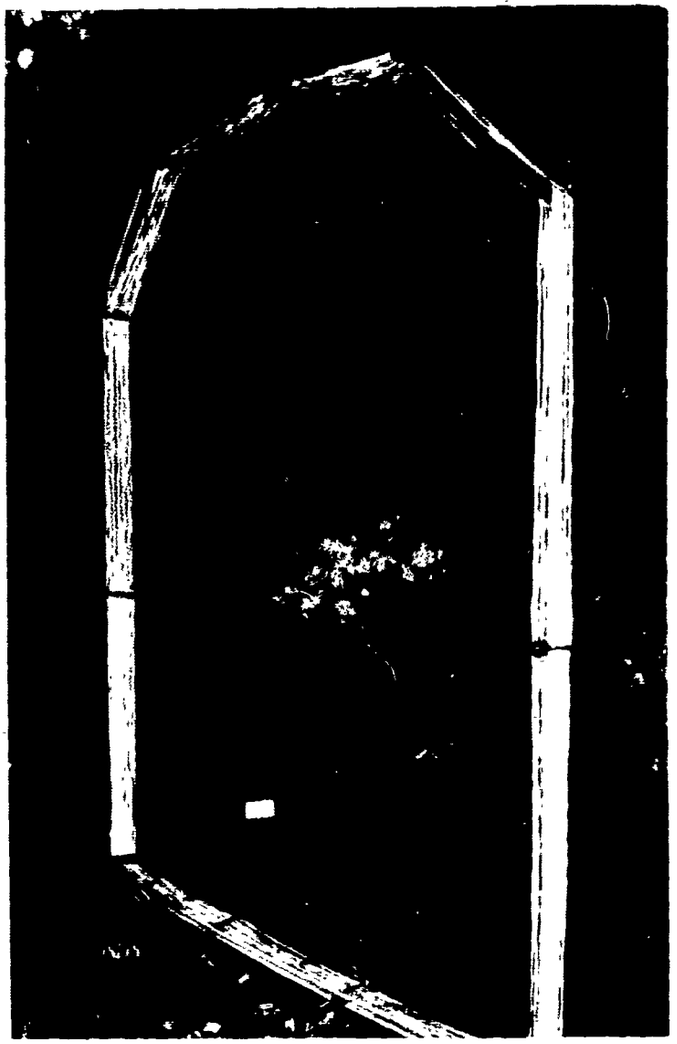

Fig. II

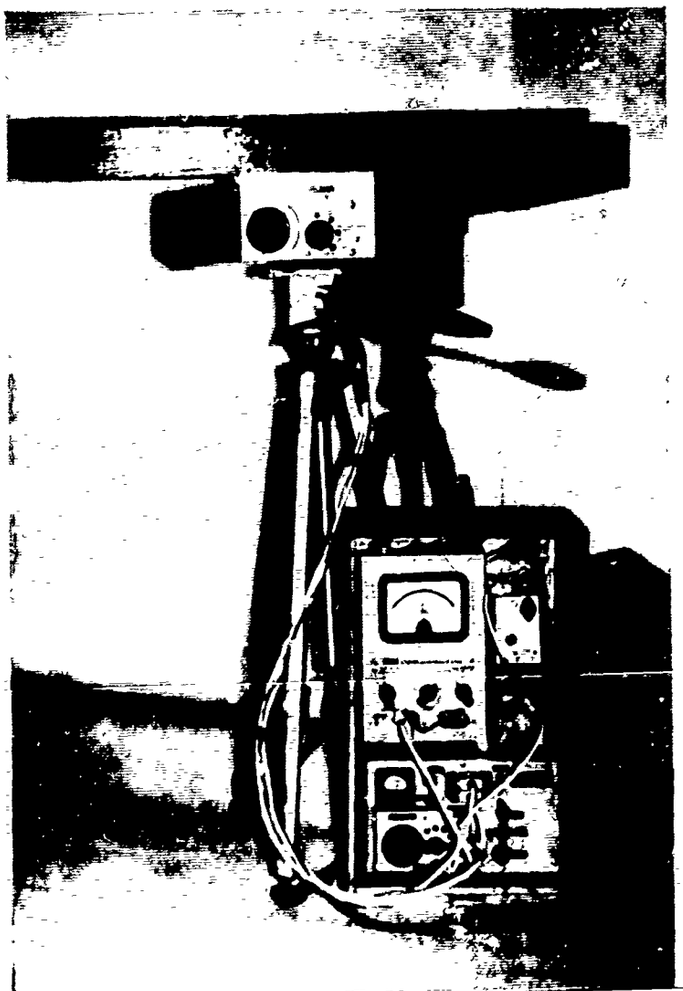

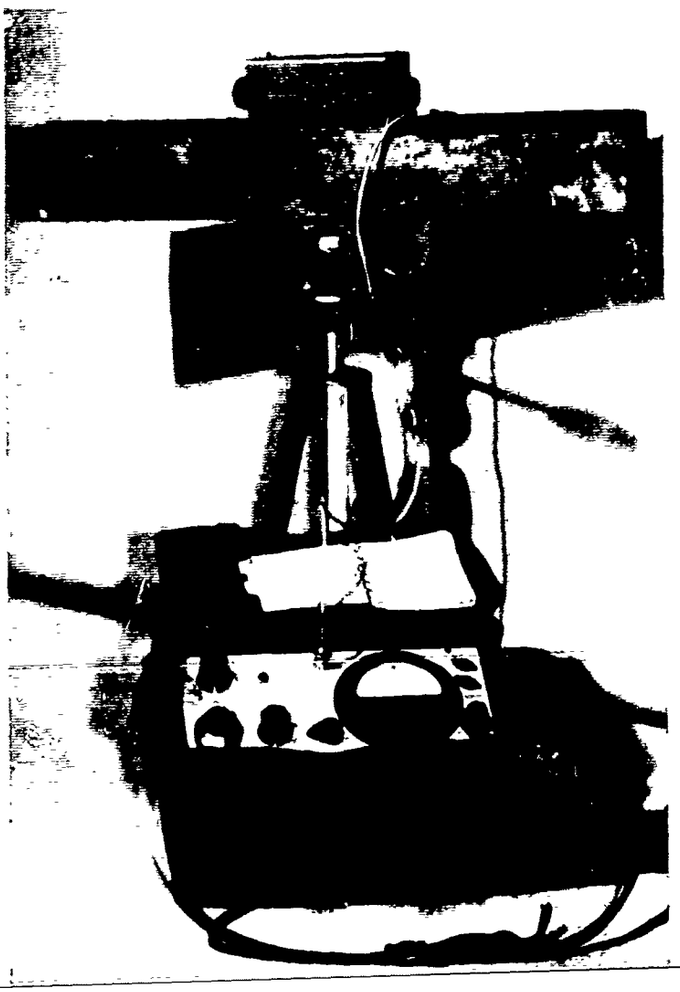

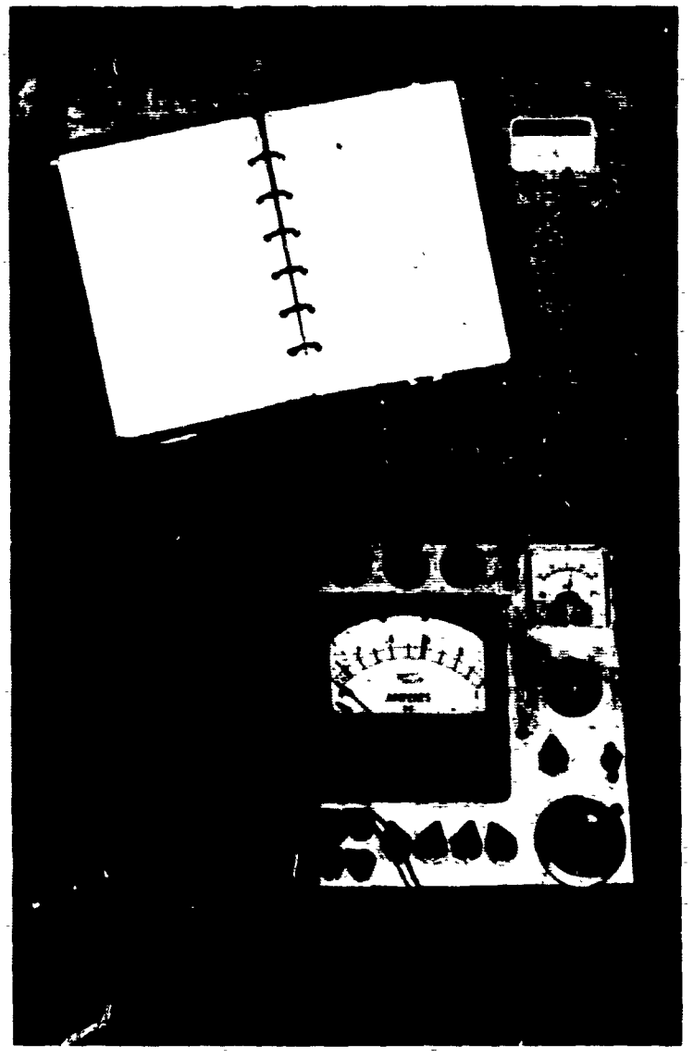

Fig. V

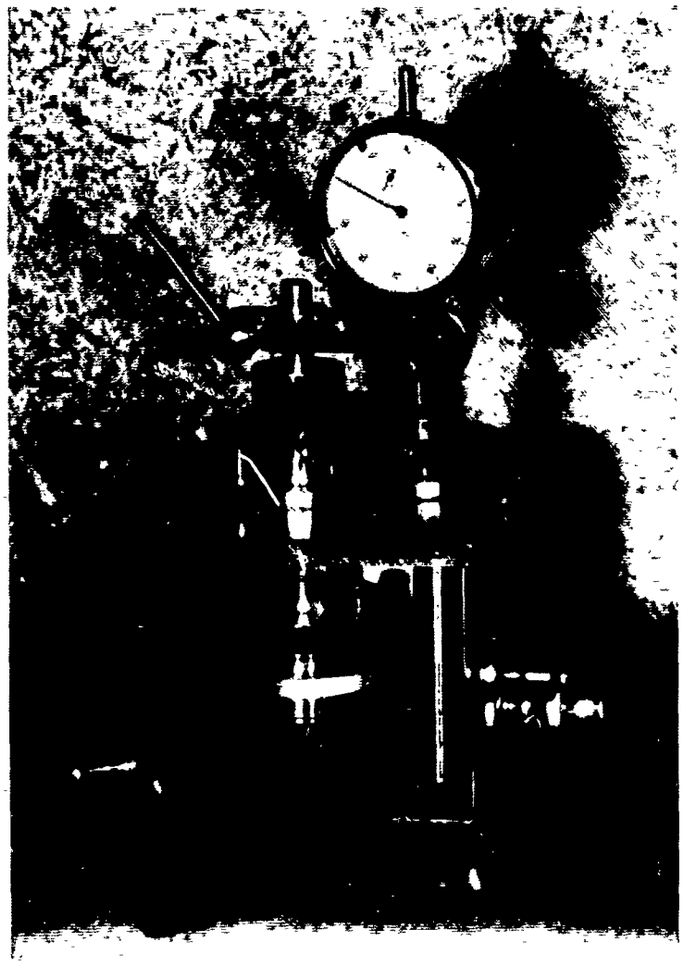

Fig. VI

II. Theoretical part

2,1 Effect of quadrupole radiation

The following expression was obtained in [1] for the field strength H^Q of a quadrupole (p. 17, expressions (56) - (59)):

$$H_r(r,\vartheta) = 3a_o(3\cos^2\vartheta-1)\exp(-ik_E r)\left\{-\frac{k_E^2}{r^2}+\frac{3ik_E}{r^3}+\frac{3}{r^4}\right\}$$

$$H_\vartheta(r,\vartheta) = a_o\frac{3}{2}\sin 2\vartheta\exp(-ik_E r)\left\{-\frac{ik_E^3}{r}-\frac{3k_E^2}{r^2}+\frac{6ik_E}{r}+\frac{6}{r^4}\right\}$$

In order to examine what effect these terms have on the dipole field, we take the square of the whole field

$$|H^D + H^Q|^2 = |H^D|^2 + \Omega^2$$

where Ω is the corrective function to be estimated, which is calculated as follows:

$$\Omega^2 = |H_r^D|^2(\Omega_r^2+\bar{\Omega}_r^2) + |H_\vartheta^D|^2(\Omega_\vartheta^2+\bar{\Omega}^2)$$

$$\Omega_\vartheta^2 = \frac{a_o^2}{m^2}\cos^2\vartheta\,\Omega_{1\vartheta}^2 \qquad \Omega_r^2 = \frac{a_o^2}{m^2}\frac{(3\cos^2\vartheta-1)^2}{\cos^2\vartheta}\Omega_{1r}^2$$

$$\bar{\Omega}_\vartheta^2 = -\frac{a_o}{m}\cos\vartheta\,\bar{\Omega}_{1\vartheta}^2 \qquad \bar{\Omega}_r^2 = \frac{a_o}{m}\frac{3\cos^2\vartheta-1}{\cos\vartheta}\bar{\Omega}_{1r}$$

The functions $\Omega_{1\vartheta}^2$, $\bar{\Omega}_{1\vartheta}^2$, Ω_{1r}^2, $\bar{\Omega}_{1r}^2$ were numerically computed for f = 3 Mc/sec and $\Delta = \sqrt{\frac{\omega\mu_o\sigma}{2}} = 7.69\cdot10^{-4}$, $2.43\cdot10^{-3}$, and $2.43\cdot10^{-2}$ (see Table 2,1)

Table 2,1

Δ	$7.69\cdot10^{-4}$	$2.43\cdot10^{-3}$	$2.43\cdot10^{-2}$	r[m]
Ω^2_{1r}	0.20	0.20	0.20	10
	0.002	0.002	0.0039	100
	$2.2\cdot10^{-5}$	$9.2\cdot10^{-5}$	$2.6\cdot10^{-3}$	1000
$\Omega^2_{1\vartheta}$	3.24	3.24	3.24	10
	0.03	0.03	0.04	100
	$2.56\cdot10^{-6}$	$2.25\cdot10^{-4}$	$7.3\cdot10^{-3}$	1000
$\bar{\Omega}^2_{1r}$	0.9	0.9	0.9	10
	0.09	0.09	0.138	100
	0.009	0.015	0.081	1000
$\bar{\Omega}^2_{1\vartheta}$	-3.6	-3.6	-3.6	10
	-0.36	-0.45	-1.98	100
	-0.12	-0.19	-1.73	1000

Substitution of the values for r = 100 m, $\sigma = 5\cdot10^{-4}$ [mhos/m] and f = 3 kc/sec yields

$$\Omega^2 = 0.37\,|H^D|^2 \qquad \vartheta = 0^\circ$$

$$\Omega^2 = 0.008\,|H^D|^2 \qquad \vartheta = 90^\circ$$

under the arbitrary assumption that $a_o/m = 1$.

Owing to this result, the quadrupole terms are assumed to be negligible from a distance of 100 m onward, since the assumption $a_o/m = 1$ certainly describes the maximum effect of the quadrupole

2,2 Effect of cavity

In our last annual report [1], the effect of the cavity in the form of an influencing secondary field in the surrounding medium has been dealt with. This theory which in the considered parameter range yields no measurable effect, was examined critically and the result has again been confirmed. We now want to give a brief survey of these detailed considerations:

From the solution of the wave equation

$$k^2 \vec{A}_1 + \Delta \vec{A}_1 = 0$$

we obtained

$$A_{Ir} = \left(A_o \frac{\exp(-ik_I r)}{r} + B \frac{\sin k_I r}{k_I r}\right) \cos\vartheta$$

$$A_{IIr} = C \frac{\exp(-ik_{II} r)}{r} \cos\vartheta$$

$$A_{I\vartheta} = -\left(A_o \frac{\exp(-ik_I r)}{r} + B \frac{\sin k_I r}{k_I r}\right) \sin\vartheta$$

$$A_{II\vartheta} = C \frac{\exp(-ik_{II} r)}{r} \sin\vartheta$$

where k_I = wave number of the medium in the cavity and k_{II} = wave number of the surrounding medium. The conditions of continuity are used to eliminate B. For C and A_o an equation is obtained which gives the effect of the cavity in the form of the change in C with respect to A. From [1] (p. 19), we obtain

$$E = \sin(k_I r_o)/k_I r_o - \cos(k_I r_o) \qquad k_I r_o = x \ll 1$$

yielding

$$\frac{r\partial E}{E\partial r} = (x \sin x)/(\sin x/x - \cos x) =$$

$$= \frac{\frac{x^2}{1!} - \frac{x^4}{3!} \pm \cdots}{1 - \frac{x^2}{3!} + \frac{x^4}{5!} \cdots - 1 + \frac{x^2}{2!} - \frac{x^4}{4!} \pm \cdots} = \frac{x^2 \cdot 3!}{-x^2 + 3x^2} = 3$$

which is valid to $k_I r_o < 2 \cdot 10^{-1}$. Thus, we obtain

$$A_o \exp(-ik_I r_o)(k_I^2 r_o^2 - 3ik_I r_o - 3) = C \exp(-ik_{II} r_o)(k_{II}^2 r_o^2 - 3ik_o r_o - 3)$$

$$C = A \frac{(3 + 3ik_I r_o - k_I^2 r_o^2)}{(3 + 3ik_{II} r_o - k_{II}^2 r_o^2)} \exp(i(k_{II} - k_I) r_o)$$

Since $k_I r_o \ll 1$, $k_{II} r_o \ll 1$, quadratic terms are negligibly small with respect to unity (at an accuracy of 1%). Hence,

$$\mathfrak{G} = A \left(\frac{1 + ik_I r_o + \cdots}{1 + ik_{II} r_o + \cdots} \right) \left(1 + \frac{i(k_{II} - k_I) r_o}{1!} + \cdots \right) =$$

$$= A \left(1 + \frac{k_{II}^2 r_o^2 - k_I k_{II} r_o^2 + \cdots}{1 + ik_{II} r_o + \cdots} \right)$$

Only terms of the second order yield a correcting contribution. for $k_I r_o \ll 10^{-1}$ and $k_{II} r_o \ll 10^{-2}$, i.e. $f < 100$ kc/sec and $r < 300$ m this correction is smaller than 1% and thus far below the reachable accuracy of measurement.

2,3 Maximum moment of magnetic antennas

As the strength of the excitation of electromagnetic waves in any point $\vec{r}$ is proportional to the antenna moment, we studied what maximum change can be reached by filling the antenna coil with an iron core or a similar material of high permeability.

From the well-known relation

$$m = \frac{\mu}{1 + (\mu - 1)N} m_o$$

where N is the demagnetizing factor and $m_o = \frac{\mu_o In}{l}$ is the moment of the unfilled antenna, it follows by a limiting process

$$\lim_{\mu \to \infty} m = \frac{m_o}{N}$$

i.e. that no more than the 1/N-fold of m_o can be reached by increasing the permeability. As m_o depends on I as well as on the geometrical dimensions of the coil, every coil filled with material can be replaced by an air antenna with the same moment, if the dimensions and number of turns are chosen adequately.

2,4 Sub-scale tests

The possibility of sub-scale tests in the laboratory was taken into consideration as the theory studied so far requires certain conditions as to the geometry of the range of measurement and its physical properties (e.g. unbounded space, homogeneity, etc) which are difficult to fulfill in practice. In our case, however, such experiments proved impossible mainly because of the required high conductivity of the model and its frequency dependence. A survey of the references in this connection has been given in TN 1 [2].

2,5 Determination of rock conductivity from VLF-propagation measurements

In the propagation of VLF waves the conductivity of the earth plays an important role for the attenuation of these waves. The conductivity was determined by extensive calculations for a large range of all variables (conductivity $\sigma = 10^{-4} - 5 \cdot 10^{-7}\ \Omega^{-1} m^{-1}$

frequency $\nu = 1$ cps - 100 kcps

distance $r = 100 - 20\,000$ m)

The formulas used were derived with the aid of a Hertz potential for a dipole in the dissipative medium. (Exact derivation see [1])

$$|\vec{H}| \sim cB \sim f(r, \nu, \sigma) = e^{-\sqrt{\frac{\mu_o \alpha}{2}}\, r} \left\{ \frac{1}{r^6} + \frac{2\sqrt{\frac{\mu_o \alpha}{2}}}{r^5} + \frac{\mu_o \alpha}{r^4} \right\}^{1/2}$$

$$\alpha = \omega \cdot \sigma = 2\pi\nu \cdot \sigma$$

For purposes of clarity some of the values calculated are compiled in Fig. 2,1. The conductivity of the medium is to be concluded from the value of the attenuation. In order to separate two values of σ, the corresponding value of B must have a difference of at least 5% because of the $\sim 5\%$ measurement inaccuracy. Only thus approximately safe conductivity values can be obtained. Fig. 2,1 shows that only at $r > 1000$ m a differentiation of the field strength received can be expected. At a frequency of 1000 cps, only from $\sim 10\,000$ m upwards a conductivity up to $\sim 5 \cdot 10^{-7}$ can be determined from the attenuation.

At higher conductivities, approximately from 10^{-5} upwards, measurements give reasonable results already at 5000 m. At 500 cps, however, and $\sigma = 10^{-4}$ a measurement is expedient only

at a distance of 20000m, i.e. a difference of 5% is observed with respect to neighboring values of about $3 \cdot 10^{-4}$ and $5 \cdot 10^{-5}$. For $\sigma = 5 \cdot 10^{-7}$ a distance of 20 km is necessary. Table 2,2 shows the minimum measurement distances for σ for the ordinary frequencies on the assumption that a change of the conductivity by a factor of 3 results in a change in B by about 5%. At a given measurement inaccuracy of 5% this will probably lead to a reasonable determinability of the σ.

Table 2,2

frequency ν	minimum distance for $\sigma = 10^{-3}$	$\sigma = 10^{-4}$	$\sigma = 10^{-5}$	$\sigma = 5 \cdot 10^{-7}$
500 cps	1500 m	2000 m	10 000 m	20 km
1000 cps	1200 m	1500 m	5 000 m	10 km
3000 cps	800 m	1000 m	3 000 m	8 km
10kcps	300 m	500 m	1 500 m	5000 m
100 kcps	100 m	150 m	500 m	1500 m

The measurements have hitherto been made [1] at distances below 1000 m (in exceptional cases up to 1300 m) at 3000 cps. Since the conductivity is very likely below 10^{-4} no definite conductivity can be expected from these measurements according to Table 2,2. To confirm this theory various measurement series from [1] with widely differing σ are interpreted.

In order to compare the theoretical values ($f(r,\alpha)$) with the experimental results (B) the mean value of the $C(\alpha)$ is calculated for different α (different σ) from

$$C(\alpha) \cdot f(r\alpha) = B(r)$$

for constant α and the corresponding curves are compared.

This comparison is limited, however, to the slope of the curves. No absolute comparison was made. The relative deviation of the $C(\alpha)$ from the mean value $\overline{C}(\alpha)$ is the measure for the goodness of the approximation. For measurement values B see [1]

Table 2,3

Measurement Gertraudi

σ	10^{-6}	10^{-5}	$5\cdot10^{-5}$	10^{-4}	$8\cdot10^{-4}$	$8\cdot10^{-10}$
$\Delta C/\overline{C}$	0.7	0.25	1.2	> 4	> 4	0.7

Measurement Gertraudi

σ	10^{-6}	10^{-5}	$5\cdot10^{-5}$	10^{-4}
$\Delta C/\overline{C}$	0.5	0.5	0.5	0.5

Measurement Lafatsch

σ	10^{-7}	10^{-6}	10^{-5}	10^{-4}	$8\cdot10^{-4}$
$\Delta C/\overline{C}$	0.6	0.8	0.7	0.6	>3

Measurement Schwaz

σ	$8\cdot10^{-10}$	10^{-6}	10^{-5}	10^{-4}	$8\cdot10^{-4}$
$\Delta C/\overline{C}$	0.8	1.1	1.0	> 3.5	> 4

This clearly indicates that the conductivity cannot be determined from these measurements. High conductivities above 10^{-4} can be excluded definitely which is in agreement with the data in Table 2,1

Effect of the displacement current:

(for exact theory see [1]) For a conducting medium the wave-number becomes complex $k_3 = k_1 - ik_2$. With the measurements hitherto made a conductivity of $< 5\cdot10^{-5}\,\Omega^{-1}m^{-1}$ is likely.

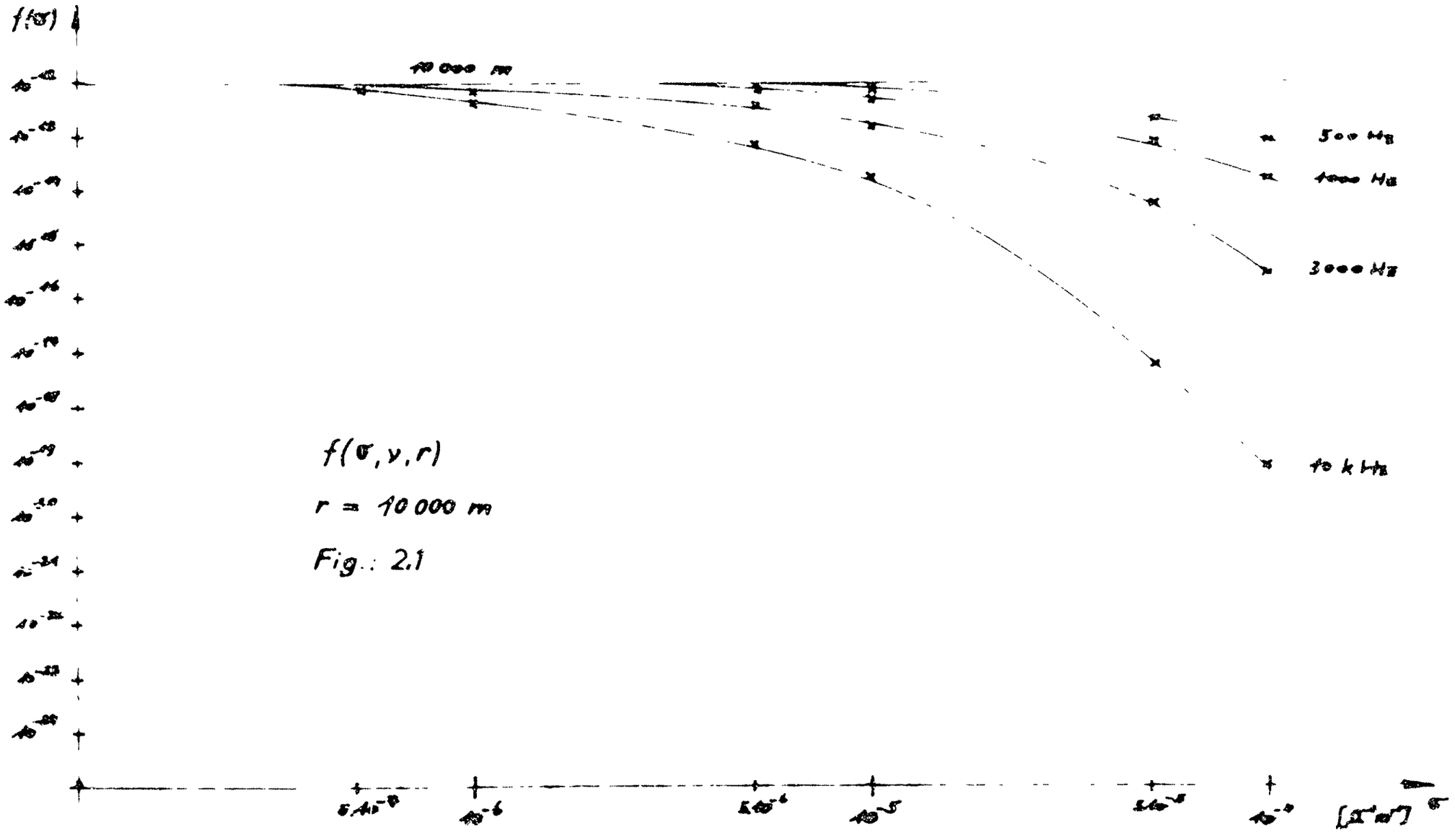

Fig.: 2.1

Table 2,4 gives a survey on the error arising due to the neglection of the displacement current, at $\sigma = 10^{-5}$.

Table 2,4

frequency	minimum distance	difference between k_3 and $k_1; k_2$	difference in B and f
5 kcps	2 km	1 %	< 1 %
10 kcps	1.5 km	2 %	1 %
50 kcps	1 km	5 %	2.5%
100 kcps	500 m	20 %	10 %

k_1 and k_2 give the exact values of the wave number with displacement current, for k_3 the displacement current was neglected. Since also the measurement distance enters the error, the error becomes larger for smaller σ and correspondingly smaller for higher conductivities because the measurement distances required become larger or smaller.
Since the measurement inaccuracy is at about 5% it is justified - because of the very short measurement distances available - to make the measurements at 10 to 50 kcps above 1300 m without taking account of the displacement current in order to be able to determine the order of magnitude of the conductivity.

2,6 Horizontal magnetic dipole at the depth h under the earth's surface – Calculation of the radiation field by the integral method

1) The radiation field of electric and magnetic dipoles in vertical and horizontal position on the earth's surface and an expansion of the field strengths in powers of the numerical distance was given by Sommerfeld [9] [10]. In a similar manner, Ott [11] calculated the Hertzian vector $\vec{\pi}$ of a vertical electric dipole located in a non-conducting but optically denser medium. By a proper path of integration he succeeded in separating the excitation into a main wave and a secondary wave called flanking wave.

In the present paper, Ott's method is used to calculate the radiation field of a horizontal magnetic dipole within conducting earth under a plane earth's surface. Ott's separation into main and secondary waves was shown to be feasible.

2) The vector and the boundary conditions:

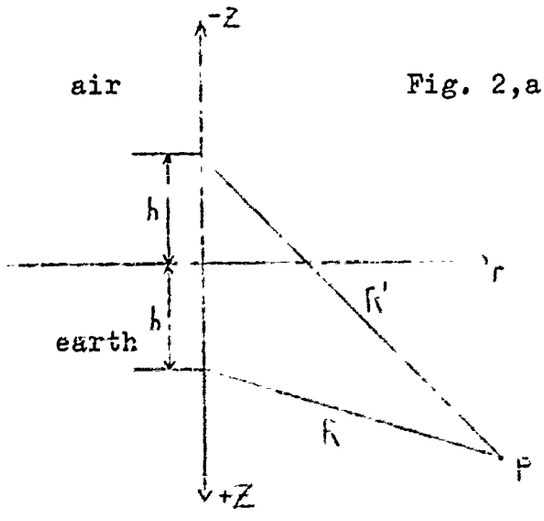

Fig. 2,a

A horizontal magnetic dipole be at the depth h under the interface earth-air. The electric properties of the earth are characterized by the conductivity σ, the dielectric constant ϵ, the permeability $\mu = \mu_0$ and the wavenumber k_E.

Let the conductivity of air be zero, its wavenumber $k = \omega/c$.

the following is to hold:

$$k = k_E n \qquad |n| < 1$$

For a time dependence $\exp[-i\omega t]$

$$k_E^2 = \frac{\omega^2}{c^2}\left[\varepsilon + i\frac{\sigma}{\omega\varepsilon_o}\right] = \frac{k^2}{n^2} \qquad n^2 = \frac{\varepsilon - i\frac{\sigma}{\omega\varepsilon_o}}{\varepsilon^2 + \frac{\sigma^2}{\omega^2\varepsilon_o^2}}$$

ω angular velocity, c light velocity, $\varepsilon_o = 8.859 \cdot 10^{-12}$[As/Vm]

k_E and n are mostly used in the following form:

$$k_E = |k_E|\, e^{i\varphi} \qquad n = |n|\, e^{-i\varphi}$$

The electric and magnetic fields are obtained from a two-component Hertzian vector $\vec{\Pi} = (\Pi_x, 0, \Pi_z)$ (cf. Sommerfeld [9]). By suppressing a optional constant and the time dependence here and in the following:

$$\vec{H}_E = k_E^2 \vec{\Pi}_E + \text{grad div } \vec{\Pi}_E \qquad z > 0$$

$$\vec{H} = k^2 \vec{\Pi} + \text{grad div } \vec{\Pi} \qquad z < 0$$

At the interface z = 0, Π must satisfy the following four conditions:

$$\begin{aligned} \vec{\Pi}_{Ex} &= n^2 \Pi_x & \frac{\partial \Pi_{Ex}}{\partial z} &= \frac{\partial \Pi_x}{\partial z} \\ \vec{\Pi}_{Ez} &= \Pi_z & \frac{\partial \Pi_{Ex}}{\partial x} - \frac{\partial \Pi_x}{\partial x} &= \frac{\partial \Pi_z}{\partial z} - \frac{\partial \Pi_{Ez}}{\partial z} \end{aligned} \qquad (1)$$

3) The x-component of the excitation:

Π_{Ex} is composed of a primary excitation Π_o and the reflected wave Π_g. No primary excitation is assumed to exist in the air. Thus, Π_x is equal to the refracted wave Π_g

$$\Pi_{Ex} = \Pi_o + \Pi_r$$

$$\Pi_x = \Pi_g$$

$\Pi_o = \frac{e^{ik_E R}}{R}$ can be represented in the cylindrical coordinates

r, z, φ as a superposition of plane waves in integral form:

$$\Pi_o = \frac{ik_E}{2\pi} \int\int e^{ik_E(r \sin\vartheta \cos(\varphi'-\varphi) \pm (z+h)\cos\vartheta)} \sin\vartheta \, d\vartheta \, d\varphi' \qquad (2)$$

In the exponent, the plus sign holds for $z > h$, the minus sign for $z < h$. The integration with respect to φ' is carried out from 0 to 2π. The integration with respect to ϑ, is conducted along the curve C' in the complex ϑ-plane (Fig. 2,b). Likewise, the reflected and the refracted wave can be represented in integralform:

$$\Pi_r = \frac{ik_E}{2\pi} \int\int e^{ik_E[r \sin\vartheta \cos(\varphi'-\varphi) + (z-h_1)\cos\vartheta]} f(\vartheta)\sin\vartheta \, d\vartheta \, d\varphi'$$

$$\Pi_s = \frac{ik_E}{2\pi} \int\int e^{ik_E[r \sin\vartheta_2 \cos(\varphi'-\varphi) - (z-h_2)\cos\vartheta_2]} g(\vartheta)\sin\vartheta \, d\vartheta \, d\varphi' \qquad (3)$$

The amplitude functions $f(\vartheta)$ and $g(\vartheta)$ are determined from the boundary conditions (1)

$$f(\vartheta) = -1 + n^2 g(\vartheta) \qquad g(\vartheta) = \frac{2\cos\vartheta}{n^2\cos\vartheta + (n^2 - \sin^2\vartheta)^{1/2}}$$

$$f(\vartheta) = \frac{n^2\cos\vartheta - (n^2 - \sin^2\vartheta)^{1/2}}{n^2\cos\vartheta + (n^2 - \sin^2\vartheta)^{1/2}}$$

For this we find

$$k_E h \cos\vartheta = -k_E h_1 \cos\vartheta = k h_2 \cos\vartheta_2$$

and the law of refraction

$$k_E \sin\vartheta = k \sin\vartheta_2$$

Integration in (2) and (3) with respect to φ' gives the Bessel function $J_o(k_E r \sin\vartheta)$ under the integral sign. Finally, the following is obtained for the x-component of $\vec{\Pi}$ using the relations

$$J_o = \frac{1}{2}(H_o^1 + H_o^2) \quad \text{and} \quad H_o^2(-x) = H_o^1(x)$$

$$\Pi_{xE} = \frac{e^{ik_E R}}{R} + \frac{ik_E}{2} \int_C H_o^1(k_E r \sin\vartheta) \, e^{ik_E(z+h)\cos\vartheta} f(\vartheta)\sin\vartheta \, d\vartheta \qquad (4)$$

$$\Pi_x = \frac{ik_E}{} \int_C H_o^1(k_E r \sin\vartheta)\, e^{-ik_E z(n^2-\sin^2\vartheta)^{1/2} + ik_E h\cos\vartheta}\, g(\vartheta)\sin\vartheta\, d\vartheta \quad (4)$$

The curve C is shown in Fig. 2,b.

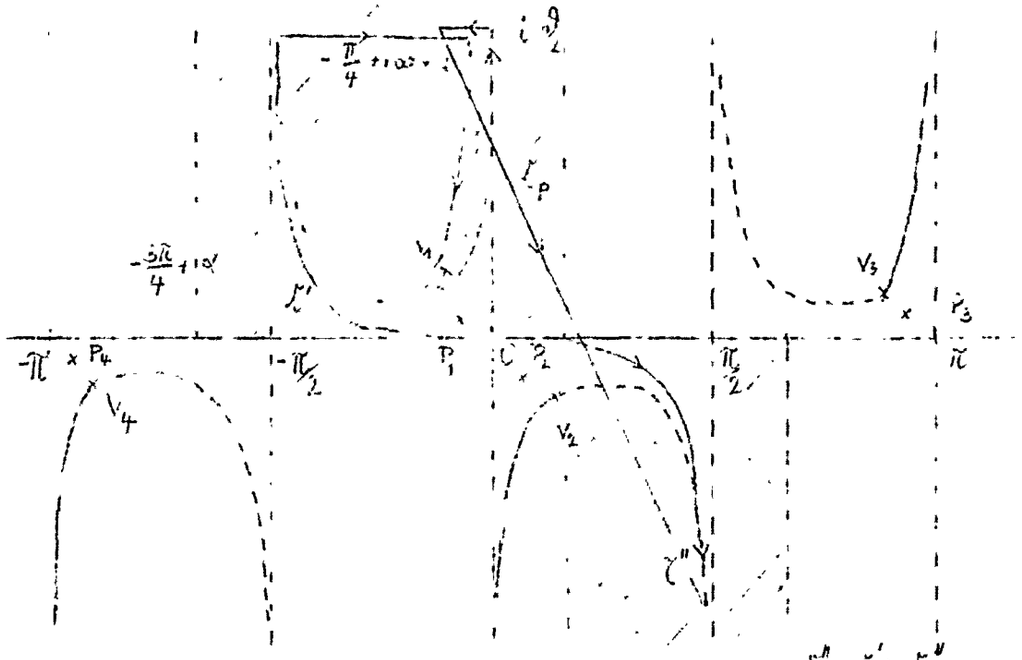

$\zeta = \zeta' + \zeta''$ Fig. 2,b

4) The z-component of the excitation:

Here, Π_{zE} also has no primary excitation. The boundary conditions demand a slightly modified formulation (cf. Sommerfeld [9])

$$\Pi_{zE} = \cos\varphi \frac{ik_E}{2}\frac{\partial}{\partial r}\int_C H_o^1(k_E r \sin\vartheta)\, e^{ik_E(z+h)\cos\vartheta}\, s(\vartheta)\sin\vartheta\, d\vartheta \quad (5)$$

$$\Pi_z = \cos\varphi \frac{ik_E}{2}\frac{\partial}{\partial r}\int_C H_o^1(k_E r\sin\vartheta) e^{-ik_E z(n^2-\sin^2\vartheta)^{1/2}+ik_E h\cos\vartheta}\, s(\vartheta)\sin\vartheta\, d\vartheta$$

$$s(\vartheta) = \frac{2\cos\vartheta\, i(n^2-1)}{k_E[n^2\cos\vartheta + (n^2-\sin^2\vartheta)^{1/2}][\cos\vartheta + (n^2-\sin^2\vartheta)^{1/2}]}$$

5) Calculation of the integrals by the saddle-point method:

The root $w = (n^2 - \sin^2\vartheta)^{1/2}$ is contained in the functions $f(\vartheta)$ and $s(\vartheta)$. To obtain w as a unique function, we choose the real axis of the w-plane as branch cut and image it in the ϑ-plane. Branching points appear in the periodic interval $[-\pi, \pi]$ at $\sin\vartheta = \pm n$ and $\sin(\pi-\vartheta) = \pm n$ (Fig. 2,b). The equation for the branch

cut Im(w) = 0 reads

$$\sin 2\vartheta_1 \sinh 2\vartheta_2 = -2|n^2| \sin 2\varphi = \text{const.}$$

It describes a curve through the branch point; its solid part in Fig. 2,b renders the axis Im(w) = 0 and its dash-lined part the axis Re(w) = 0.

$f(\vartheta)$ and $g(\vartheta)$ have poles for $\cos\vartheta_p = -w_p/n^2$, with the solution

$$\sin\vartheta_p = \pm(n^2/1 + n^2)^{1/2}$$

In the pole, the root has the form $w_p = \pm n^2/(1 + n^2)^{1/2}$. With $1 + n^2 = |1 + n^2| e^{-i2\mu}$ w_p reads $w_p = \pm|n^2/(1+n^2)^{1/2}|e^{-i(2\varphi-\mu)}$ where $2\varphi - \mu > 0$. This shows that in the upper Riemann sheet (Im(w) > 0) the negative sign must be chosen for w_p. Thus,

$$\cos\vartheta_p = \cos\vartheta_1 \cosh\vartheta_2 - i \sin\vartheta_1 \sinh\vartheta_2 = |1/(1+n^2)^{1/2}|e^{i\mu}$$

This gives

$$P_1: \quad \vartheta_2 > 0 \qquad -\frac{\pi}{2} \leqslant \vartheta_1 \leqslant 0$$

$$P_2: \quad \vartheta_2 < 0 \qquad 0 \leqslant \vartheta_1 \leqslant \frac{\pi}{2}$$

in the upper sheet. In the lower sheet (Im(w) < 0), the following is found analogously:

$$P_3: \quad \vartheta_2 > 0 \qquad -\frac{\pi}{2} \leqslant \vartheta_1 \leqslant \pi$$

$$P_4: \quad \vartheta_2 > 0 \qquad -\pi \leqslant \vartheta_1 \leqslant -\frac{\pi}{2}$$

Besides it can be shown that the poles always lie between the real axis and the curves given by $\sin 2\vartheta_1 \sinh 2\vartheta_2 = \text{const.}$ (Fig. 2,b). In the 0 point of the upper sheet w_p has the form $w_p = \pm n = \pm|n|e^{-i\varphi}$. As in the upper sheet Im(w) > 0, the negative sign is applied. Thus, w_p has a positive real and imaginary component before the branch cut, the signs only changing beyond the cut.

In Π_{Ex} we replace $f(\vartheta)$ by $-1 + n^2 g(\vartheta)$. The contribution of the summand -1 can be immediately found, and we obtain

$$\Pi_{Ex} = \frac{e^{ik_E R}}{R} \cdot \frac{e^{ik_E R'}}{R'} + I_1$$

$$I_1 = \frac{ik_E n^2}{2} \int_C H_o^1(k_E r \sin\vartheta) e^{ik_E(z+h)\cos\vartheta} g(\vartheta)\sin\vartheta \, d\vartheta$$

To calculate I_1 we lead C, the path of the integration, somewhat out of zero and first replace $H_o^1(k_E r\sin\vartheta)$ by its assymptotic value

$$H_o^1(k_E r \sin\vartheta) = \sqrt{\frac{2}{\pi k_E r\sin\vartheta}}\, e^{i(k_E r\sin\vartheta - \frac{\pi}{4})}$$

The eligible exponent is now

$$i[k_E r \sin\vartheta + k_E(z+h)\cos\vartheta]$$

or, after introducing polar coordinates α, R' in the r,z-plane

$$r = R'\sin\alpha \qquad z+h = R'\cos\alpha$$

$$i[k_E R' \sin\alpha \sin\vartheta + k_E R' \cos\alpha \cos\vartheta = ik_E R' \cos(\alpha-\vartheta)$$

The real component of the exponent becomes <0 for

$$-\pi + \frac{\pi}{4} + \alpha < \vartheta_1 < \frac{\pi}{4} + \alpha \qquad \vartheta_2 > 0$$

$$\alpha < \delta_1 < \frac{\pi}{2} + \alpha \qquad \vartheta_2 < 0$$

The path of integration may run in the hatched part of Fig. 2,b. Since $ik_E R' \sin(\alpha-\vartheta) = 0$ for $\alpha = \vartheta$, the saddle point lies on the real axis. The falling line $\mathrm{Im}(\cos(\alpha-\vartheta)) = \text{const.}$ runs near the real axis from the pass $\vartheta = \alpha$ under 135° toward $\pm(\frac{\pi}{4} - i\infty) + \alpha$. At a greater distance from the pass its gradient deviates from the value -1 but the pass road is no longer forcing there. When we transfer the path of integration into the falling line, the branch cut disturbs us in the second quadrant for $\alpha > \alpha_o = \arcsin n$. From the end point $\frac{\pi}{2} + i\infty$ no direct path leads to the pass. Therefore, we must go round the branch cut and take the following path for this purpose: from $\frac{\pi}{2} + i\infty$ on the upper sheet to $+i\infty$, from there along the branch cut to its origin V_1 and on the other side back to $+i\infty$, from there on the lower sheet to the

end point of the pass road $-\frac{\pi}{4} + \alpha + i\infty$ and from there over the pass $\vartheta = \alpha$ to the old end point $\frac{\pi}{2} - i\infty$ (Fig. 2,b, curve C_p). As the integrand on the approaching paths vanishes at infinity the integral I_1 is split up into two parts I_1' and I_1''. I_1' represents the saddle value I_1'' the integral along the branch cut. In I_1' we replace $g(\vartheta)$ by the saddle value $g(\alpha)$, which is permitted for $\alpha \neq \frac{\pi}{2}$, and draw this factor out before the integral. If we use the original value instead of the asymptotic one for the Hankel function under the integral sign, we obtain:

$$I_1' = \frac{ik_E n^2 g(\alpha)}{2} \int_{C_p} H_o^1(k_E r \sin\vartheta)\, e^{ik_E(z+h)\cos\vartheta} \sin\vartheta\, d\vartheta = n^2 g(\alpha)\, \frac{e^{ik_E R'}}{R'}$$

or, according to (4)

$$\Pi_{Ex} = \frac{e^{ik_E R}}{R} + f(\alpha)\, \frac{e^{ik_E R'}}{R'} + I_1''$$

Analogously we obtain

$$\Pi_{Ez} = \cos\varphi\, \frac{\partial}{\partial r} \left[s(\alpha)\, \frac{e^{ik_E R'}}{R'} + I_2'' \right]$$

with a corresponding definition of I_2''.

Near $\alpha = \frac{\pi}{2}$, where $g(\alpha)$ and $s(\alpha)$ disappear, the approximation becomes useless. We must develop $g(\vartheta)$ and $s(\vartheta)$ in $\vartheta = \alpha$ and take account of further terms. Confining ourselves to the second order term we obtain

$$I_1' = \left[n^2 g(\alpha) - \frac{i n^2 g''(\alpha)}{2k_E R'} \right] \frac{e^{ik_E R'}}{R'}$$

$$I_2' = \cos\varphi\, \frac{\partial}{\partial r} \left[\left(s(\alpha) - \frac{i s''(\alpha)}{2k_E R'} \right) \frac{e^{ik_E R'}}{R'} \right] \qquad \alpha \approx \frac{\pi}{2}$$

This is the separation into main and secondary waves as shown by Ott [11], I_1' and I_2' are the corresponding quantities in our

expressions. Marking the hitherto calculated integrals by the superscript M we obtain for the main wave in the earth:

$$\Pi^M_{Ex} = \frac{e^{ik_E R}}{R} + f(\alpha)\frac{e^{ik_E R'}}{R'}$$

$$\Pi^M_{Ez} = \cos\varphi \frac{\partial}{\partial r}\left[s(\alpha)\frac{e^{ik_E R'}}{R'}\right]$$

$$\left.\begin{aligned} \Pi^M_{Ex} &= \frac{e^{ik_E R}}{R} - \frac{e^{ik_E R'}}{R'} + \left[n^2 g(\alpha) - \frac{in^2 g''(\alpha)}{2k_E R'}\right]\frac{e^{ik_E R'}}{R'} \\ \Pi^M_{Ez} &= \cos\varphi \frac{\partial}{\partial r}\left[\left(s(\alpha) - \frac{is''(\alpha)}{2k_E R'}\right)\frac{e^{ik_E R'}}{R'}\right] \end{aligned}\right\} \quad \alpha \approx \frac{\pi}{2}$$

6) The secondary wave I''_1 and I''_2:

As on the branch cut $(n^2 - \sin^2\varphi)^{1/2} = \pm\tau$, where τ is a real number, we bring I''_1 with the aid of this substitution equation into the form

$$I''_1 = \frac{-ik_E n^2}{2}\int_{-\infty}^{\infty} H_0^1(k_E r\sqrt{n^2-\tau^2})\, e^{ik_E(z+h)\sqrt{1-n^2+\tau^2}}\, \frac{2\tau\, d\tau}{\tau+n^2\sqrt{1-n^2+\tau^2}}$$

and for the integration we again pass over to the complex τ-plane. Branch points lie at $\tau = \pm n$ and $\tau = \pm i(1-n^2)^{1/2}$. If we again choose the real axis of $w_1 = (n^2-\tau^2)^{1/2}$, the equation for the branch cut reads

$$\tau_2 = \pm\frac{|n^2|\sin 2\varphi}{\tau_1}$$

The poles are given by $\tau_p = \pm|n^2/(1+n^2)^{1/2}|e^{-i(2\varphi-\mu)}$ i.e. they lie in the second and fortl quadrants of the τ-plane and do not disturb us when we transfer the path of integration into the pass road.

With use of the asymptotic representation for the Hankel function, the exponent in question becomes

$$ik_E R' \left[\sin\alpha (n^2 - \tau^2)^{1/2} + \cos\alpha (1 - n^2 + \tau^2)^{1/2} \right] = f(\tau)$$

$$\frac{df(\tau)}{d\tau} = 0 \quad \begin{cases} \tau = 0 \\ \tau = (n^2 - \sin^2\alpha)^{1/2} \end{cases}$$

Thus, the saddle point in question lies at $\tau = 0$. The expansion of $f(\tau)$ in $\tau = 0$ reads:

$$f(\tau) = ik_E R' \cos(\alpha - \vartheta_0) - |q| e^{i\beta} \tau^2 + \ldots$$

$$q = \frac{ik_E R' \sin(\alpha - \vartheta_0)}{2 \sin\vartheta_0 \cos\vartheta_0} \qquad \sin\vartheta_0 = n$$

The equation for the passroad is

$$\tau_2 = (c \pm \sqrt{c^2 + 1})\, \tau_1 \qquad c = \operatorname{ctg}\beta$$

and its gradient near $\tau = 0$ is given by

$$\operatorname{tg}\eta = - \operatorname{tg}\frac{\beta}{2} \qquad \beta = \arg[q]$$

$1/N(\tau) = 1/\left[\tau + n^2 (1 - n^2 + \tau^2)^{1/2}\right]$, expanded in $\tau = 0$, gives

$$1/N(\tau) = 1/N(0) - \tau/N(0)^2$$

where only the second term makes a contribution to I_2''. Thus, we obtain

$$I_1'' = \frac{ik_E}{n^2(1-n^2)} \sqrt{\frac{2}{\pi k_E r n}}\, e^{ik_E R' \cos(\alpha - \vartheta_0) - i\frac{\pi}{4}} \int_{-\varepsilon}^{\varepsilon} e^{-|q|\tau^2 e^{i\beta}}\, \tau^2 d\tau$$

and finally

$$\Pi_{Ex}^{s} = \frac{2e^{i\gamma}}{k(1-n^2)} \left| \frac{1}{1 - \operatorname{tg}\vartheta_0 \operatorname{ctg}\alpha} \right|^{3/2} \frac{e^{ik_E\left[nr + (z+h)\sqrt{1-n^2}\right]}}{r^2}$$

$$\gamma = \frac{\pi}{4} + 3\varphi - \frac{3\beta}{2}$$

and analogously

$$\Pi_{Ez}^{S} = \cos\varphi \frac{2\ln|(1-n^4)}{k^2(1-n^2)^{1/2}} \frac{\partial}{\partial r} \left| \frac{1}{1 - \operatorname{tg}\vartheta_0 \operatorname{ctg}\alpha} \right|^{3/2} \frac{e^{ik_E\left[nr + (z+h)\sqrt{1-n^2}\right] - i\gamma_1}}{r^2}$$

$$\gamma_1 = \frac{\pi}{4} + \frac{3\beta}{2} - 2\varphi$$

Thus, the vector π is determined in the earth. We should like to mention, that, in agreement with Ott [11], the secondary wave disappears in the angular space $\alpha < \alpha_o = \arcsin n$ since the branch cut in the fourth quadrant must be also avoided and thereby I_1'' and I_2'' are just eliminated. Besides, this representation is identical to that originally given by Sommerfeld [9] [10]; if $k_E \sin\vartheta$ in (3) is replaced by λ the expressions go over into the Sommerfeld integrals. Integration, however, is different from that in Sommerfeld's paper and does not give rise to any residue waves since the path of integration does not include the poles.

7) <u>The vector $\vec{\pi}$ for $z < 0$:</u>

By means of the transformation $\sin\vartheta = n \sin\xi$ we transform π_x into

$$\frac{ik}{2} \int H_o^1(kr \sin\xi)\, e^{-ikz\cos\xi + ik_E h\sqrt{1-n^2\sin^2\xi}}\, p(\xi) \sin\xi\, d\xi$$

$$p(\xi) = \frac{2n\cos\xi}{n^2\sqrt{1-n^2\sin^2\xi} + n\cos\xi}$$

Calculated analogously to the former integrals and using the polar coordinates

$$r = R_o \sin\beta \qquad -z = R_o \cos\beta$$

this gives for the antenna depth $h = 0$

$$\pi_x^M = p(\beta)\, \frac{e^{ikR_o}}{R_o}$$

$$\pi_x^M = \left(p(\beta) - \frac{ip''(\beta)}{2kR_o}\right) \frac{e^{ikR_o}}{R_o} \qquad \beta \approx \frac{\pi}{2}$$

$$\pi_z^M = \cos\varphi \frac{\partial}{\partial r}\left(s(\beta)\, \frac{e^{ikR_o}}{R_o}\right)$$

$$\pi_z^M = \cos\varphi \frac{\partial}{\partial r}\left[\left(s(\beta) - \frac{is''(\beta)}{2kR_o}\right) \frac{e^{ikR_o}}{R_o}\right] \qquad \beta \approx \frac{\pi}{2}$$

and for the secondary wave:

$$\Pi_x^S = \frac{k_E n^2}{2(1-n^2)} \left(\frac{2}{k_E R_o \sin\beta\, |q_2|^3} \right)^{1/2} e^{ik_E R_o [\sin\beta + \cos\beta \sqrt{n^2-1}] + i\gamma_2} \qquad (9)$$

$$\Pi_z^S = \cos\varphi \frac{n^2+1}{2\sqrt{n^2-1}} \frac{\partial}{\partial r} \left(\frac{2}{k_E R_o \sin\beta\, |q_2|^3} \right)^{1/2} e^{ik_E R_o [\sin\beta - \cos\beta \sqrt{n^2-1}] + i(\gamma_2 - \frac{\pi}{2})}$$

$$\gamma_2 = \frac{\pi}{4} - \frac{3r}{2} \qquad q_2 = \frac{ik_E R_o}{2} \left[\sin\beta - \frac{\cos\beta}{\sqrt{n^2-1}} \right]$$

$$r = \arg[q_2]$$

The formulas (8) and (9) give π for the case $h = 0$. For finite h, this representation may be taken as a good approximation for the following case:

$$k_E h \sqrt{1-n^2\sin^2\xi} \ll k R_o \cos(\xi - \beta)$$

or on the pass

$$h \ll \left| \frac{nR_o}{\sqrt{1-n^2\sin^2\beta}} \right| \qquad (10)$$

As soon as this relation does not hold any longer, the above integrals can be calculated in the same manner for finite h, while the saddle point is shifted by a factor depending on h. Concerning the range of validity for the representation by the saddle point method we should compare the theoretical study in [12], according to which the neglect in an integral of the form $\int F(z) e^{mf(z)} dz$ is of the order $1/m$, which means in our case that the error becomes of the order $|1/k_E R|$. The expression for π can be cimplified if we leave the hitherto observed generality and restrict ourselves to $n \leq 10^{-1}$. In the exponent of (7) the term $(1-n^2\sin^2\xi)^{1/2}$ can be considered constant and the factor $e^{ik_E h}$ can be drawn out before the integral. That means that we have found a representation also for large h, for which relation (10) does not hold. The expression for $h = 0$ has only to be multiplied by the factor $e^{ik_E h}$. Thus the effect of h is characterized by a phase

shift and a damping.

Hence,

$$\Pi_x^M = e^{ik_E h} p(\beta) \frac{e^{ikR_o}}{R_o}$$

$$\Pi_z^M = e^{-ik_E h} \cos\varphi \frac{\partial}{\partial r} \left[s(\beta) \frac{e^{ikR_o}}{R_o} \right]$$

and, analogously, the other formulas.

8) The field strengths:

Although the calculation of field strengths in the earth is a little complicated it does not involve very great difficulties for numerical computation. Since in (6) the first term contains R while the other terms are written in R', we transfer the center of the coordinate system into the mirror point and calculate in the spherical polar coordinates R', α, φ.

Because $R = R' - \partial R'/\partial z = R' - 2h \cos\alpha$

$$1/R = 1/R - \partial 1/R'/\partial z = 1/R'(1 + 2h \cos\alpha/R')$$

we can write

$$e^{ik_E R}/R = e^{ik_E R'}/R'(1 + 2h\cos\alpha/R')e^{-i2k_E h\cos\alpha}$$

The functions $f(\alpha)$ and $s(\alpha)$ can be simplified for $\alpha > 20^\circ$ and $n < 10^{-1}$ to $f(\alpha) = -1$

$$s(\alpha) = -2/k_E \operatorname{ctg}\alpha(\cos\alpha - i \sin\alpha) = s_1(\alpha)/k_E$$

Thus, we obtain the components H_R; H_α; H_φ of the main wave after long intermediate calculations in the following form, where A is an antenna constant:

$$H_R = A \cos\varphi \, e^{i(k_E R' - \omega t)} \sum_{i=1}^{6} \frac{g_i(\alpha,h,k_E)}{R'^i}$$

$$H_\alpha = A \cos\varphi \, e^{i(k_E R' - \omega t)} \sum_{i=1}^{5} \frac{f_i(\alpha,h,k_E)}{R'^i} \qquad (11)$$

$$H_\varphi = -A \sin\varphi \, e^{i(k_E R' - \omega t)} \sum_{i=1}^{6} \frac{h_i(\alpha,h,k_E)}{R'^i}$$

$$g_1 = k_E^2 \, (i \sin\alpha \cos\alpha \, s_1(\alpha) - \sin\alpha)$$

$$g_2 = (-2hk_E^2 \cos\alpha \sin\alpha - ik_E^2 \sin\alpha \, e^{-\xi})$$

$$\xi = ik_E^2 \, h\cos\alpha$$

$$g_3 = \sin\alpha \, e^{-\xi}(-14h \cos\alpha ik_E + 2 - 4h^2 k_E^2 \cos^2\alpha) +$$

$$+ 2is_1(\alpha) \cos\alpha \, (\frac{1}{\sin\alpha} + \sin\alpha + i \cos\alpha)$$

$$g_4 = [\sin\alpha \, e^{-\xi}(-24ik_E h^2 \cos^2\alpha + 18h \cos\alpha)]$$

$$g_5 = [\sin\alpha \, e^{-\xi}(48h^2 \cos^2\alpha - 8h^3 \cos^3\alpha ik_E)]$$

$$g_6 = \sin\alpha \, e^{-\xi} \, 40h^3 \cos^3\alpha$$

$$f_1 = k_E^2[- i \sin^2 s_1(\alpha) + \cos\alpha(e^{-\xi}-1)]$$

$$f_2 = [k_E \cos\alpha \, s_1(\alpha) \, (\frac{1}{\cos\alpha} + i \sin\alpha) + k_E s_1(\alpha) \sin^2\alpha] +$$

$$+ e^{-\xi}[2hk_E^2 \, (\cos^2\alpha - \sin^2\alpha) + ik_E \cos\alpha]$$

$$f_3 = [e^{-\xi}(4hik_E \cos^2\alpha - \cos\alpha - 8k_E^2 h^2 \cos\alpha \sin^2\alpha - 6ik_E h \sin^2\alpha) -$$

$$- \frac{\partial}{\partial\alpha} is_1(\alpha) \cos\alpha \, (\sin\alpha + \frac{1}{\sin\alpha} + i \cos\alpha)$$

$$f_4 = e^{-\xi} \, (4ik_E h^2 \cos^3\alpha - 6h \cos^2\alpha - 8k_E^2 h^3 \cos^2\alpha \sin^2\alpha +$$

$$+ 6h \sin^2\alpha - 20ik_E h^2 \cos\alpha \sin^2\alpha)$$

$$f_5 = e^{-\xi} \, (24h^2 \cos^2\alpha \sin^2\alpha - 24ik_E h^3 \cos^2\alpha \sin^2\alpha - 12h^2 \cos^3\alpha)$$

$$h_1 = k_E^2 \, (e^{-\xi} - 1)$$

$$h_2 = e^{-\xi} \, (2k_E^2 \, h \cos\alpha + ik_E)$$

$$h_3 = e^{-\xi} \, (4h \cos\alpha \, ik_E - 1) - s_1(\alpha) \, \frac{i\cos\alpha}{\sin\alpha} + \sin\alpha + i\cos\alpha)$$

$$h_4 = e^{-\xi} \, (4h^2 ik_E \cos^2\alpha - 6h \cos\alpha)$$

$$h_5 = e^{-\xi} \, (-12h^2 \cos^2\alpha)$$

$$h_6 = e^{-\xi} \, (-8h^3 \cos^3\alpha)$$

The formulas for the earth's surface z = 0 are much simpler. In a polar coordinate system r,ϑ, φ the origin of which is on the surface perpendicular over the dipole, the following holds for $n^2 \ll 1$

$$H_r = A \cos\varphi \frac{2ik_E^2 e^{ik_E h}}{k^3} \frac{e^{ikr}}{r^2} \left(-\frac{4ik}{r} + \frac{6}{r^2} \right)$$

$$H_\vartheta = A \cos\varphi \frac{2ik_E^3 e^{ik_E h}}{k^4} \frac{e^{ikr}}{r^2} \left(-\frac{3ik}{r} + \frac{6}{r^2} \right) \qquad (12)$$

$$H_\varphi = A \sin\varphi \frac{2ik_E^2 e^{ik_E h}}{k^3} \frac{e^{ikr}}{r^2} \left(k^2 + \frac{ik}{r} - \frac{2}{r^2} \right)$$

where the dependence on time has to be included yet.

The results for the secondary wave in the earth are as follows:

$$H_{R'} = \cos\varphi \frac{2Ae^{i\gamma}}{k} \frac{e^{ik_E R' \cos(\alpha-\delta_o)}}{R'^2 \sin^2\alpha} \left[k_E^2 (\sin\alpha - n\cos\alpha - 2n^2 \sin\alpha) - \right.$$

$$\left. - \frac{2ik_E(\cos\alpha + 4n\sin\alpha)}{R'\sin\alpha} + \frac{12}{R'^2 \sin^2\alpha} \right]$$

$$H_\alpha = \cos\varphi \frac{2Ae^{i\gamma}}{k} \frac{e^{ik_E R' \cos(\alpha-\vartheta_o)}}{R'^2 \sin^2\alpha} \left[k_E^2 (\cos\alpha + n\sin\alpha) + \right.$$

$$\left. + \frac{2ik_E \sin\alpha}{R' \sin\alpha} + \frac{12\cos\alpha}{R'^2 \sin^2\alpha} \right]$$

$$H_\varphi = -\sin\varphi \frac{2Ae^{i\gamma}}{k} \frac{e^{ik_E R' \cos(\alpha-\vartheta_o)}}{R'^2 \sin^2\alpha} \left[k_E^2 + \frac{2ik_E n}{R'\sin\alpha} - \frac{4}{R'^2 \sin^2\alpha} \right]$$

$$\sin\vartheta_o = n$$

and on the earth's surface z = 0

$$H_r = \cos\varphi \frac{2iAe^{ik_E h + i\gamma} k_E^2}{k^3} \frac{e^{ikr}}{r^2} \left[-ik^2(1-2n) - \frac{kn^2}{r} - \frac{12in^2}{r^2}\right]$$

$$H_\vartheta = \cos\varphi \frac{2iAe^{ik_E h + i\gamma} k_E^3}{k^4} \frac{e^{ikr}}{r^2} \left[-ik^2 n(2+n) + \frac{6kn^2}{r}\right] \qquad (14)$$

$$H_\varphi = -\sin\varphi \frac{2iAe^{ik_e h + i\gamma} k_E^2}{k^3} \frac{e^{ikr}}{r^2} \left[-ik^2 + \frac{2kn^2}{r} + \frac{4in^2}{r^2}\right]$$

Comparing (14) to (12) one can see that the effect of the secondary wave increases with increasing distance; from a certain minimum distance on - for $k^2 \approx 10^{-5}$ about $8 \cdot 10^2$ m - it will even exceed the main wave. As the phase shift of the secondary wave $\gamma = \frac{\pi}{4} + 3\varphi - \frac{3\beta}{2}$ and $\beta = \arg\left[\frac{ik_E R' \sin(\alpha - \vartheta_o)}{2 \sin\vartheta_o \cos\vartheta_o}\right]$ follows for $k_E = \Delta(i+1)$, (displacement current neglected) for $n < 10^{-1}$, $h = 250$ m and $r > 2.5 \cdot 10^3$ m $\beta = \arg\left[(1-i)\bar{n}\right]$. Thus γ is independent on r. With these restrictions the amplitude of the field strengths at z = 0 is given by:

$$\frac{|H_r|}{A} = \cos\varphi \frac{4\Delta^2}{k^3} e^{-\Delta h} \frac{1}{r^2} \left\{ \left[\frac{k^3}{\Delta} - k^2 + \frac{k^3}{2\Delta^2}\frac{1}{r} + \frac{6}{r^2}\right]^2 + \left[\frac{k^3}{\Delta} + \frac{4k}{r} - \frac{6k^2}{\Delta^2}\frac{1}{r^2}\right]^2 \right\}^{1/2}$$

$$\frac{|H_\vartheta|}{A} = \cos\varphi \frac{4\sqrt{2\Delta^3}}{k^4} e^{-\Delta h} \frac{1}{r^2} \left\{ \left[\frac{k^3}{\Delta} + \frac{3k^3}{\Delta^2 r} - \frac{6}{r^2}\right]^2 + \left[\frac{k^3}{\Delta} + \frac{k^4 - 6k\Delta^2}{2\Delta^2}\frac{1}{r}\right]^2 \right\}^{1/2} \qquad (15)$$

$$\frac{|H_\varphi|}{A} = \sin\varphi \frac{4\Delta^2}{k^3} e^{-\Delta h} \frac{1}{r^2} \left\{ \left[\frac{k^3}{\Delta^2 r} + \frac{2}{r^2}\right]^2 + \left[\frac{k}{r} - \frac{2k^2}{\Delta^2 r^2}\right]^2 \right\}^{1/2}$$

2,7 Calculation of the dipole field using the VLF approximation

The range of validity for field strength formulas based on the saddle point method is somewhat restricted by the fact that some parts of the calculating procedure rest on the assumption of high dimensionless values $k_E R'$ characterizing the distant field of the dipole.

This makes it desirable to employ separate formulas for the range between the remoter parts of the near field and a few wavelengths. Such a separation would make it possible on the one hand to calculate the strength of the field at every distance and on the other hand to compare the ranges of transition as between the near field and the distant field, a comparison which is of particular interest experimentally because the range of the measuring transmitter is limited.

The starting point for these considerations is once again the electrical vector potential π which is related to the field strength $\vec{H}$ in the following way:

$$\vec{H} = k^2 \pi + \text{grad div } \vec{\pi}$$
$$\vec{E} = -j\omega\mu\mu_o \text{ rot } \vec{\pi} \qquad (1)$$

Assuming the same orientation of the dipole as in (2,7) or in [5], $\vec{\pi}$ has two components π_x and π_z which can, in the usual way, be represented as an integral through the eigenfunction $J_n(\lambda\varrho)\cdot\exp \pm \mu z\cdot\cos n\phi$

Earth space:

$$\pi_{xE} = a_E\int_0^\infty e^{\mu(z-h)}J_o(\lambda\varrho)\,\frac{\lambda}{\mu}\,d\lambda + \int_0^\infty f_E(\lambda)e^{-\mu_E z}J_o(\lambda\varrho)d\lambda$$

$$\pi_{zE} = \int_0^\infty g_E(\lambda)e^{-\mu_E z}J_1(\lambda\varrho)d\lambda\cdot\cos\varphi$$

Air Space:

$$\pi_{xo} = \int_0^\infty f_o(\lambda)e^{\mu_o z}J_o(\lambda\varrho)d\lambda$$

$$\pi_{zo} = \int_0^\infty g_o(\lambda)e^{\mu_o z}J_1(\lambda\varrho)d\lambda\cdot\cos\varphi$$

It is more expedient to retain the Sommerfeld formulation, integrating in the λ field. Here

$$\mu_E = \sqrt{\lambda^2 - k_E^2}\,, \qquad \mu_o = \sqrt{\lambda^2 - k_o^2}\,, \qquad \varrho = \sqrt{x^2 + y^2}\,,$$

$$\varphi = \tan^{-1} x/y\,, \qquad a_E = I\,F/4\pi$$

The conditions for the continuity of $\vec{E}$ and $\vec{H}$ in the boundary plane $z = 0$ enable the amplitude functions f and g to be determined as

$$f_E(\lambda) = A \cdot \frac{\lambda}{\mu_E} e^{-\mu_E h} \frac{\mu_E k_o^2 - \mu_o k_E^2}{\mu_o k_E^2 + \mu_E k_o^2}$$

$$f_o(\lambda) = A \cdot \lambda \cdot e^{-\mu_E h} \frac{2k_E^2}{\mu_o k_E^2 + \mu_E k_o^2} \qquad (3)$$

$$g_o(\lambda) = g_E(\lambda) = - A \cdot \lambda^2 e^{-\mu_E h} \frac{k_o^2 - k_E^2}{\mu_o k_E^2 + \mu_E k_o^2} \cdot \frac{2}{\mu_E + \mu_o}$$

If the integrands in (2) are simplified by using what is called the VLF approximation, the four integrals in (2) can be calculated exactly. By contrast with this, the method of calculation explained in (2,6) or in [5] although not neglecting anything contained in the integrands does not lead to closed solutions of the integrals. The approximation consists in neglecting k_o^2 as against k_E^2 in the expressions (3), which is permissible as long as the condition $\frac{\sigma}{\omega \varepsilon_o} \gg 1$ is satisfied, the latter being almost identical with the condition $\left(\frac{\sigma}{\omega \varepsilon_o \varepsilon}\right)^2 \gg 1$ which has to be satisfied if the displacement current is neglected (and which is valid if $\sigma/\omega \gg 10^{-10}$).

The vector potential $\vec{\pi}_E$ in the earth space which is of sole

interest here (the horizontal components of the field strength on the earth's surface being calculable from $\vec{\pi}_E$) then works out as follows using the relationship $\frac{\partial}{\partial x} J_o = -\lambda \cos\varphi \cdot J_1$:

$$\pi_{xE} = a_E \int_0^\infty \left(e^{-\mu_E |z-h|} - e^{-\mu_E (z+h)}\right) \frac{\lambda}{\mu_E} J_o(\lambda\varrho) d\lambda$$

$$\pi_{zE} = -a_E \frac{\partial}{\partial x} \int_0^\infty e^{-\mu_E (z+h)} \frac{2}{\mu_E + \lambda} J_o(\lambda\varrho) d\lambda \qquad (4)$$

The physical situation postulated by this mathematical approximation is to be interpreted simply in the sense that the equations (4) apply only to such fields as are originated by conducted currents, which cannot of course exist in the air space. The theory erected on the basis of the VLF approximation is, therefore, a direct corollary from the calculations made in the second report [1], wherein the displacement current was suppressed. Neglecting the displacement currents immediately restricts the range over which the equations are valid, limiting their application to the distance within which the conducted currents in the earth space are

due mainly to the primary excitation and not to the inductive effect of the displacement currents in the air space, as would be the case if $k_0 R$ were large, i.e. in the distant vacuum field. The resulting expressions for the field strength can, therefore, be applied in the near field up to distances corresponding to a few vacuum wavelengths (λ_0 = 100 km at f = 3 kHz [3000 cps]). They serve to complement the formulas of the saddle point method in the short distance range.

The integrals (4) are referred back, by double integration with regard to z, to the known main integrals

$$\int_0^\infty e^{-\mu_E B} J_0(\lambda\varrho) \frac{\lambda}{\mu_E} d\lambda \quad \text{or} \quad \int_0^\infty e^{-\mu_E B} J_0(\lambda\varrho) \frac{1}{\mu_E} d\lambda$$

which, by elementary calculation, work out as

$$\frac{e^{-ik_E\sqrt{B^2+\varrho^2}}}{\sqrt{B^2+\varrho^2}} \quad \text{or} \quad I_0(\alpha)K_0(\beta)$$

where B is any function of z, I_0 is a modified Bessel function, K_0 is a modified Hankel function, $\alpha = \frac{ik_E}{2}(\sqrt{B^2+\varrho^2} - B)$, $\beta = \frac{ik_E}{2}(\sqrt{B^2+\varrho^2} + B)$. If, as on page II-10, the distances

$$R^2 = x^2 + y^2 + (z-h)^2 \quad \text{and} \quad R'^2 = x^2 + y^2 + (z+h)^2$$

between the dipole and its mirror image are introduced, the following expressions are obtained for $\vec{\pi}_E$

$$\pi_{Ex} = a_E \left(\frac{e^{-ik_E R}}{R} - \frac{e^{-ik_E R'}}{R'} \right)$$

$$\pi_{Ez} = a_E \cdot \frac{2}{k_E^2} \frac{\partial^2}{\partial x \partial z} \left(\frac{e^{-ik_E R'}}{R'} + \frac{\delta}{\partial z} I_o(\alpha) K_o(\beta) \right)$$

and the following for the horizontal components H_x and H_y of the magnetic strength:

$$H_x = a_E \left\{ k_E^2 \left(\frac{e^{-ik_E R}}{R} - \frac{e^{-ik_E R'}}{R'} \right) + \frac{\partial^2}{\partial x^2} \left[\frac{e^{-ik_E R}}{R} - \frac{e^{-ik_E R'}}{R'} + \right. \right.$$

$$\left. \left. + \frac{2}{k_E^2} \frac{\partial^2}{\partial z^2} \frac{e^{-ik_E R'}}{R'} + \frac{\partial}{\partial z} I_o(\alpha) K_o(\beta) \right) \right] \right\} \qquad (5)$$

$$H_y = a_E \frac{\partial^2}{\partial x \partial y} \left[\frac{e^{-ik_E R}}{R} - \frac{e^{-ik_E R'}}{R'} + \frac{2}{k_E^2} \frac{\partial^2}{\partial z^2} \left(\frac{e^{-ik_E R'}}{R'} + \frac{\partial}{\partial z} I_o(\alpha) K_o(\beta) \right) \right]$$

The third derivation of $I_o(\alpha)K_o(\beta)$ for z, which is necessary for calculating H_x and H_y, is arrived at by using the recursion formulas

$$\frac{dI_o(\alpha)}{d\alpha} = I_1(\alpha) \qquad \frac{dK_o(\beta)}{d\beta} = -K_1(\beta)$$

$$\frac{dI_1(\alpha)}{d\alpha} = I_o - \frac{I_1}{\alpha} \qquad \frac{dK_1(\beta)}{d\beta} = -K_o(\beta) - \frac{K_1(\beta)}{\beta}$$

and appears as follows:

$$\frac{\partial^3}{\partial z^3} I_o(\alpha)K_o(\beta) = \frac{ik_E}{2} \Big\{ I_oK_o \Big[ik_E \frac{3q}{R'} (1 - q^2) + \frac{k_E^2}{4\alpha} (q - 1)^3 +$$

$$+ \frac{k_E^2}{4\beta} (q + 1)^3 \Big] + I_1K_o \Big[k_E^2 (1 - q^3) - \frac{k_E^2}{2\alpha^2} (q - 1)^3 -$$

$$- \frac{3}{2} \frac{1}{\alpha R'} ik_E (q - 1) (1 - q^2) - \frac{3}{R'^2} q (1 - q^2) \Big] + \qquad (6)$$

$$+ I_oK_1 \Big[\frac{3}{2} \frac{1}{\beta R'} ik_E (q + 1) (1 - q^2) + k_E^2 (q^3 + 1) +$$

$$+ \frac{k_E^2}{2\beta^2} (q + 1)^3 + \frac{3}{R'^2} q (1 - q^2) \Big] + I_1K_1 \Big[ik_E \frac{1}{R'} (q^2 - 1)(3q) -$$

$$- \frac{3}{4} \frac{k_E^2}{\beta} (q - 1) (q^2 - 1) - \frac{3}{4} \frac{k_E^2}{\beta} (q + 1)^2 (q - 1) \Big] \Big\}$$

On inserting (6) into (5) and making a brief intermediate calculation the following simple expression is found for the horizontal component of $\vec{H}$ in the direction of the main

radiation from the magnetic dipole:

$$H_{x|x=o} = a_E \left\{ \frac{e^{-iM_1}}{R^3} (-1 - iM_1 + M_1^2) + \right.$$

$$\frac{e^{-iN_1}}{R'^3} \frac{1}{N_1^2} \left[-N_1^4 + iN_1^3 - N_1^2 + 6iN_1 + 6 - 2q^2(15+15iN_1-6N_1^2-iN_1^3) \right]$$

$$\frac{1}{R'^3} \left[I_o K_o \ (3q - 15q^3 + q^3 N_1^2) \right.$$

$$I_o K_1 \ iN_1 (-1 + 3q - q^2 - 6q^3 - \frac{1}{N_1^2}(1 - q)(3 - 15q^2))$$

$$I_1 K_o \ iN_1 (-1 - 3q - q^2 + 6q^3 - \frac{1}{N_1^2}(1 - q)(3 - 15q^2))$$

$$\left. \left. I_1 K_1 \ (-13q + 15q^3 - q^3 N_1^2) \right] \right\} \qquad (7)$$

with $M_1 = k_E R$, $N_1 = k_E R'$, $q = (z + h)/R'$

Apart from the VLF approximation nothing else is left out of account in this equation for H_x. A glance at the expressions included in brackets within the second and third summation groups shows that for $h \longrightarrow \infty$ and for a finite R these expressions tend to zero by reason of the e-power vanishing and owing to the Hankel function, so that (7) transforms itself exactly into the equation for the field strength of a magnetic dipole in a

homogeneously dissipative medium. This result, as well as the fact that the field strength decreases as the conductance increases, is trivial as it can at once be inferred from the initial equations. It is possible, therefore, to write (7) in the form: $H_x = H_{x\ hom} + H_{x\ suppl}$

where $H_{x\ suppl}$ represents the additional field attributable to the influence of the earth-air interface behaving symmetrically with regard to z and h: that is to say, independently of whether for instance the transmitter is 300 m and the receiver 50 m below the earth's surface or conversely the receiver 300 m and the transmitter 50 m below.

Obviously no such symmetry applies to $H_{x\ ges}$. Simplifications can be made in (7) if the distance of measurement notably exceeds the height covered by the transmitter and receiver ($q \longrightarrow 0$) or if, on the contrary, the height covered notably exceeds the distance of measurement ($q \longrightarrow 1$). These two limiting cases are, however, only of theoretical interest, since only the intermediate range is amenable to experiment.

For practical evaluation of the formula (7) it is best to divide

H_x into a real and an imaginary part, as the apparatus available at present allows only of measuring the amount and not the phase angle. Since the arguments of the cylindrical functions arising make an angle of 135° in the complex planes, I and K can be expressed by the Kelvin functions ber, ber_1, bei, bei_1, her, her_1, hei, hei_1 whose argument is purely real: the functions ber, bei have the argument $\varkappa_I \equiv (1-q)R'k_3/\sqrt{2}$, and the functions her, hei the argument $\varkappa_{II} \equiv (1+q)R'k_3/\sqrt{2}$, where k_3 has the value $k_3 = \sqrt{\frac{\omega\mu_2\sigma}{2}}$. A short intermediate calculation then leads from (7) to the real and imaginary parts of E_x as follows:

$$\mathrm{Re}H_{x|x=o} = \frac{A}{R^3} e^{-M} (B_8 \cdot \cos M - B_9 \sin M) + \qquad (8)$$

$$+ \frac{A}{R'^3} \Big[-e^{-N}(C_1 \cos N + C_2 \sin N) + B_o A_1 + C_3(A_2 - A_8) +$$

$$+ B_5 A_7 + N(A_3(B_1+B_2) + A_4(B_2-B_1) + A_5(B_3+B_4) +$$

$$+ A_6(B_4 - B_3)) \Big]$$

$$\mathrm{Im}H_{x|x=o} = \frac{A}{R^3} e^{-M} (-B_9 \cos M - B_8 \sin M) +$$

$$+ \frac{A}{R'^3} \Big[-e^{-N}(C_2 \cos N + C_1 \sin N) + B_o A_2 + C_3(A_7 - A_1) +$$

$$+ B_5 A_8 + N(A_3(B_1 - B_2) + A_4(B_1 + B_2) + A_5(B_3 - B_4) + A_6(B_4 + B_3)) \Big]$$

$$M = k_3 R$$

$$N = k_3 R'$$

$$q = \frac{z+h}{R'}$$

$$A_1 = -\frac{\pi}{2}(ber_o hei_o + bei_o her_o) \qquad A_5 = -\frac{\pi}{2}(bei_1 hei_o - ber_1 her_o)$$

$$A_2 = -\frac{\pi}{2}(bei_o hei_o - ber_o her_o) \qquad A_6 = \frac{\pi}{2}(bei_1 her_o + ber_1 hei_o)$$

$$A_3 = -\frac{\pi}{2}(ber_o her_1 - bei_o hei_1) \qquad A_7 = -\frac{\pi}{2}(bei_1 her_1 + ber_1 hei_1)$$

$$A_4 = -\frac{\pi}{2}(ber_o hei_1 + bei_o her_1) \qquad A_8 = \frac{\pi}{2}(ber_1 her_1 - bei_1 hei_1)$$

$$B_o = 3q - 15q^3 \qquad B_4 = (1-q)(3-15q^2)/2N^2$$

$$B_1 = -1-q^2-(6q^3-3q) \qquad B_5 = -13q + 15q^3$$

$$B_2 = (1+q)(3-15q^2)/2N^2 \qquad B_8 = -M-1$$

$$B_3 = -1-q^2+(6q^3-3q) \qquad B_9 = 2M^2 + M$$

$$C_1 = -N + 1 + \frac{3}{N} - 2q^2N - 12q^2 - 15q^2/N$$

$$C_2 = -2N^2 - N - (3/N) - (3/N^2) - 2q^2N + (15q^2/N) + (15q^2/N^2)$$

$$C_3 = 2N^2q^3$$

The result of the numerical calculation for $\sigma = \frac{3\pi}{10}, \frac{6\pi}{10}$ and 3π can be seen from Table 2,5.

Table 2,5

R =	10	$10\sqrt{10}$	10^2	$10^2\sqrt{10}$	10^3	[m]
	10^{-3}	$3.16\cdot10^{-5}$	$1.025\cdot10^{-6}$	$7.96\cdot10^{-8}$	$2.3202\cdot10^{-9}$	$\omega\sigma=3\pi\cdot10^{-1}$
$H_x\vert_{x=0}$	10^{-3}	$3.1\cdot10^{-5}$	$1.009\cdot10^{-6}$	$7.78\cdot10^{-8}$	$3.335\cdot10^{-9}$	$\omega\sigma=\frac{6\pi}{10}$
	10^{-3}	$3.14\cdot10^{-5}$	$8.39\cdot10^{-7}$	$7.76\cdot10^{-8}$	$5.25\cdot10^{-9}$	$\omega\sigma=3\pi$

2,8 Another approach to the solution for a magnetic dipole

(2,6) and (2,7) gave expressions for the field strengths of magnetic dipoles whose numerical evaluation is somewhat difficult and can only be simplified by restrictions with respect to the distance. Besides, in the expressions of (2,7), rather complex Kelvin functions occur which are tabulated only in a bounded region of arguments. In order to avoid this we again turn to the integral method giving an expression similar to that which has been derived in a thesis of the Cornell University [11]. In the latter case, however, the problem of propagation in sea water is dealt with, where the parameters ε (relative dielectric constant) and σ (conductivity) assume much higher values. As $\varkappa \gg \varepsilon$ may be assumed to hold for the quantity $\varkappa = \frac{\sigma}{\omega\varepsilon_0}$ in the VLF range, the approximation in the above thesis can be shown to be valid also in this case. Furthermore, the effect of the ionosphere shall be discussed in the present paper. We derive the field strengths $\vec{E}$ and $\vec{H}$ (oriented as in 2,6, Fig. 2,a) from a Hertzian vector $\vec{\pi} = (\pi_x, 0, \pi_z)$:

$$\vec{H} = k^2\vec{\pi} + \text{grad div } \vec{\pi}$$
$$\vec{E} = -i\omega\mu_0 \text{rot } \vec{\pi} \qquad (1)$$

Let the time dependence be neglected and let it be $\exp(i\omega t)$. $\vec{\pi}$ has to satisfy the differential equation

$$\Delta\vec{\pi} + k^2\vec{\pi} = 0 \qquad k^2 = \frac{\omega^2}{c^2}\left[\varepsilon - \frac{i\sigma}{\omega\varepsilon_0}\right]$$

The condition of continuity of the tangential components of $\vec{H}$ and $\vec{E}$ make the following relations necessary for the boundary surface $z = 0$:

$$\frac{\partial\pi_{Ex}}{\partial z} = \frac{\partial\pi_{Ax}}{\partial z}; \qquad -i\varkappa\pi_{Ex} = \pi_{Ax}; \qquad \pi_{Ez} = \pi_{Az};$$

$$\text{dis } \vec{\pi}_E = \text{dis } \vec{\pi}_A$$

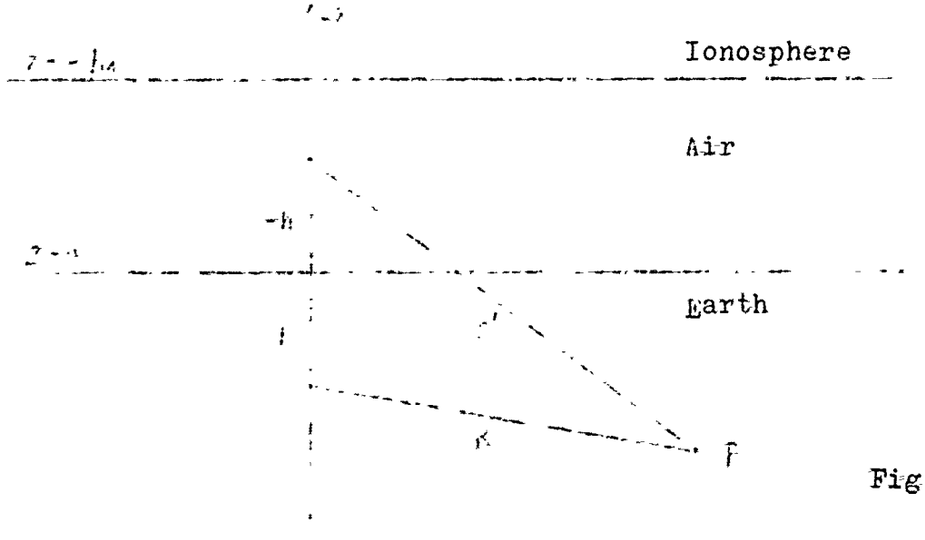

Fig. 2,a

$$r = \sqrt{x^2 + y^2} \qquad R = \sqrt{x^2 + y^2 + (z-h)^2} \qquad R' = \sqrt{x^2 + y^2 + (z+h)^2}$$

If a homogeneous, isotropic and infinitely high ionosphere with a smooth boundary at $z = -h_1$ is taken into account, the equations (2) are to be supplemented by another four relations at the point $z = -h_1$ (the subscripts E, A, J refer to Earth,

air, and ionosphere, respectively).

$$\frac{\partial \pi_{Ax}}{\partial z} = \frac{\partial \pi_{Jx}}{\partial z} \qquad \pi_{Az} = \pi_{Jz}$$
$$k_A^2 \pi_{Ax} = k_J^2 \pi_{Jx} \qquad \operatorname{div} \vec{\pi}_A = \operatorname{div} \vec{\pi}_J \tag{3}$$

The conductivity of air was put zero and the relative dielectric constant of earth was neglected as compared to the quantity $\varkappa = \frac{\sigma_E}{\omega \varepsilon_0}$. We thus confine ourselves to a parameter region in which the displacement current may be neglected. Thus, the following integrals required for calculating the field below ground are obtained by means of the well known integral representation [9]. In the case of earth-air:

$$\pi_{Ex} = a_E \left[\frac{e^{-ik_E R}}{R} - \frac{e^{-ik_E R'}}{R'} + \int_{-\infty}^{\infty} \frac{e^{-U_E(z+h)} H_0^{(1)}(\lambda r)\lambda d\lambda}{U_E - i\varkappa U_A} \right]$$
$$\pi_{Ez} = (1+i\varkappa) a_E \cos\varphi \frac{\partial}{\partial r} \int_{-\infty}^{\infty} \frac{e^{-U_E(z+h)} H_0^{(1)}(\lambda r)\lambda d\lambda}{(U_E+U_A)(U_E - i\varkappa U_A)} \tag{4}$$

In the case of earth-air-ionosphere:

$$\pi_{Ex} = a_E \left[\frac{e^{-ik_E R}}{R} - \frac{e^{-ik_E R'}}{R'} + \int_{-\infty}^{\infty} \frac{e^{-U_E(z+h)} H_0^{(1)}(\lambda r)\lambda d\lambda}{U_E - i\varkappa U_A \operatorname{tgh}(U_A h_1)} \right]$$
$$\pi_{Ez} = a_E i\varkappa \cos\varphi \frac{\partial}{\partial r} \int_{-\infty}^{\infty} \frac{e^{-U_E(z+h)} H_0^{(1)}(\lambda r)\lambda d\lambda}{(U_E - i\varkappa U_A)(U_E+U_A)(1-F(\lambda))} \tag{5}$$

$$U_E = (\lambda^2 - k_E^2)^{1/2} \qquad k_0^2 = \frac{\omega^2}{c^2} \qquad F(\lambda) = \frac{2U_A}{U_E+U_A} \frac{1}{e^{2U_A h_1} - 1}$$

$$U_A = (\lambda^2 - k_o^2)^{1/2} \qquad a_E = \frac{IF}{4\pi}$$

are valid.

$H_o^{(1)}$ means the Hankel function of the first kind $Re(U_E) > 0$ is assumed to guarantee the convergence of the integrals for $z \to \infty$, and $Re^{(U_A)} > 0$ is assumed so that the factor $U_E + U_A$ in the denominator of π_{Ez} does not vanish in infinity of the λ-plane. A comparison of (4) with (5) shows that the two representations differ by the factors in the denominator of the integrals of π_{Ex} and π_{Ez}. Since, however, $U_A h_1 = h_1(\lambda^2 - k_o^2)^{1/2}$ is real on the path of integration except for the interval $-k_o < \lambda < +k_o$, and is a large number ($h \simeq 7 \cdot 10^4$ m), except in the somewhat expanded interval $\Delta = \left[-\nu - k_o, \ \nu + k_o \right]$ $(\nu < k_o)$, we may put $\tanh(U_A h_1)$ everywhere equal to unity by approximation. Similarly, we put $F(\lambda)$ in the denominator of π_{Ez} equal to zero. This approximation can be assumed for the distance region in which the primary excitation $\frac{e^{-ik_E R}}{R}$ prevails, since the other terms there only represent corrections, not so in the region $z/r \ll 1$, where the first two terms in π_{Ex} cancel out and the integral expression prevails. For an exact discussion, another way has to be chosen for this region. Since, however, the distance region at present accessible for experimental measurements below ground does not exceed 10^3 m, we certainly may neglect the effect of the ionosphere there. Hence, we apply expression (4) and continue calculating the integrals U and V:

$$U = \int_{-\infty}^{\infty} \frac{H_o^{(1)}(\lambda r) e^{-U_F(z+h)}}{U_F - i\nu U_A}$$

$$V = \frac{1}{2}\frac{\partial}{\partial r}\int_{-\infty}^{\infty} \frac{e^{-U_E(z+h)}H_o^{(1)}(\lambda r)\lambda d\lambda}{(U_E+U_A)(U_E-i\varkappa U_A)} \qquad (6)$$

Substituting

$$k_o N = U_E \qquad \rho = k_o r$$

$$\lambda = k_o \psi \qquad (7)$$

$$k_o M = U_A \qquad H = k_o(z+h)$$

we obtain

$$U = k_o \int_{-\infty}^{\infty} \frac{e^{-NH}H_o^{(1)}(\psi\rho)\psi d\psi}{N - i\varkappa M}$$

$$V = \frac{k_o}{2}\frac{\partial}{\partial\rho}\int_{-\infty}^{\infty} \frac{e^{-NH}H_o^{(1)}(\psi\rho)\psi d\psi}{(N+M)(N-i\varkappa M)} \qquad (8)$$

The path of integration comprises all real values of ψ ranging from $-\infty$ to $+\infty$. In the following calculations, however, it will be more convenient to shift the integration path slightly into the lower semi-plane at the point $\psi = -1$ (Fig. 2,b). Singular points occur for

$$N = 0$$

$$M = 0$$

$$N - i\varkappa M = 0$$

Thus, branching points lie at $\psi = \pm\sqrt{\frac{\varkappa}{2}}(1-i)$ and $\psi = \pm 1$. Since the latter pair of points would lie on the real axis, it is more convenient to write down

$$k_A^2 = \frac{\omega^2}{c^2}\left(1 - i\frac{\sigma_A}{\omega\varepsilon_o}\right) = k_o^2(1 - ig)$$

instead of putting the conductivity of air equal to zero for

the discussion of the branching points.

Then,

$$M = \sqrt{\psi^2 - (1 - ig)} = 0 \Longrightarrow \psi = \pm (1 - i\frac{g}{2})$$

In the upper semi-plane the branching points lie as follows:

$$V_1 = \sqrt{\frac{\varkappa}{2}}\,(-1 + i)$$

$$V_2 = -1 + ig/2$$

Starting from these points we draw sections along the curves Re(M) = 0 and Re(N) = 0 to infinity. The equation N - i$\varkappa$M = 0 gives the poles at

$$P_1 = \left(\frac{1}{1 + 1/\varkappa^2}\right)^{1/2}\left(-1 + \frac{i}{2(g+1/\varkappa)}\right)$$

$$P_2 = \left(\frac{1}{1 + \frac{1}{\varkappa^2}}\right)^{1/2}\left(1 - \frac{i}{2(g + \frac{1}{\varkappa})}\right)$$

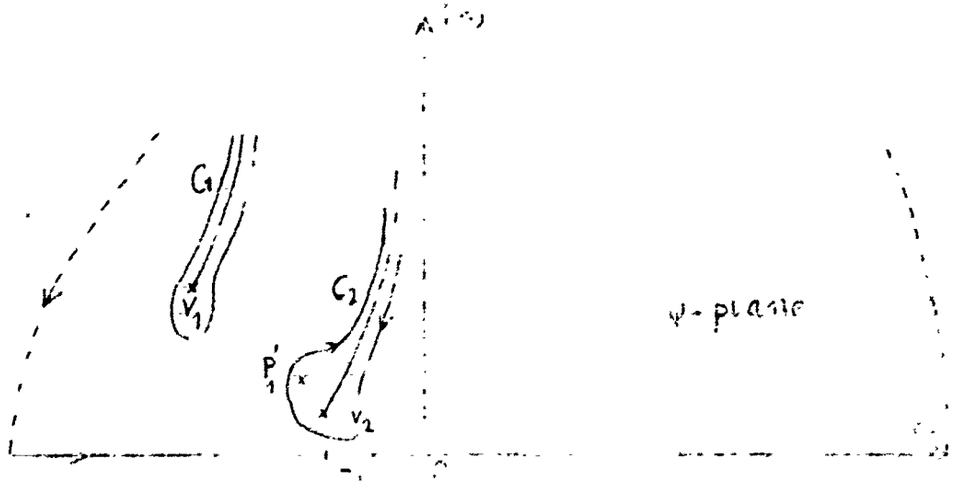

Fig. 2,3

Thus, the pole P_1 lies in the immediate neighborhood of V_2: This confirms the fact (frequently discussed in publications) that the contribution of the pole to the value of the integral cannot be separated from the total expression. Closing the

path of integration in infinity of the upper semi-plane, the branching sections being avoided, we include V_2 and P_1 in the same loop. Since $H_o^{(1)}(\psi\rho)$ for large arguments behaves similarly as $\exp(i\psi\rho)/(\psi\rho)^{1/2}$, the contribution of the branching section V_1 may be neglected. When integrating along C_2, we must consider that the expression $N = (\psi^2 + i\varkappa)^{1/2}$ may be looked upon as being constant owing to the magnitude of $\varkappa$ in the region of the determinative ψ-values. Thus,

$$U = \frac{e^{-H\sqrt{i\varkappa}}}{\sqrt{i\varkappa}} k_o \int_{C_2} \frac{H_o^{(1)}(\psi\rho)\psi d\psi}{1 - \sqrt{i\varkappa}M} \tag{9}$$

$$V = \frac{e^{-H\sqrt{i\varkappa}}}{i\varkappa} \frac{k_o}{2} \frac{\partial}{\partial\rho} \int_{C_2} \frac{H_o^{(1)}(\psi\rho)\psi d\psi}{1 - \sqrt{i\varkappa}M} = \frac{1}{2\sqrt{i\varkappa}} \frac{\partial}{\partial\rho} U$$

is obtained. The problem is thus reduced to the propagation between two points of the earth's surface, $z = 0$. The factor $1/(1 - i\varkappa M)$ still obtained in the integral is thus expanded:

$$\frac{1}{1-i\varkappa M} = \frac{1}{-\sqrt{i\varkappa}\, M(1 - \frac{1}{\sqrt{i\varkappa}M})} = -\frac{1}{\sqrt{i\varkappa}\, M}\left(1 + \frac{1}{\sqrt{i\varkappa}M} + \frac{1}{\sqrt{i\varkappa}\, M}\right)^2 + \ldots)$$

It remains to be shown that the expansion converges for all ψ-values lying outside a certain circle around V_2. The convergence is guaranteed if

$$\left| \frac{1}{\sqrt{i\varkappa}\, M} \right| < 1 \quad , \quad \text{i.e. if} \quad |M| < \frac{1}{\sqrt{\varkappa}} .$$

We show that this is the case already outside a circle with the radius $\frac{1}{\varkappa}$, V_2 being its center:

$$\psi = -1 + i\frac{\varkappa}{2} + \frac{1}{\varkappa}\exp(i\varphi)$$

$$\phi^2 = (1 - ig) + \frac{i\varsigma}{\varkappa}\left[(ig - 2) + \frac{e^{i\varphi}}{\varkappa}\right]$$

$$\left|\sqrt{\phi^2 - (1 - ig)}\right| = \frac{1}{\sqrt{\varkappa}}\left|\sqrt{ig - 2 + \frac{e^{i\varphi}}{\varkappa}}\right| > \frac{1}{\sqrt{\varkappa}}$$

Thus,

$$\int_{C_2} \frac{H_o^{(1)}(\psi\varrho)\psi d\psi}{1 - \sqrt{i\varkappa}\, M} = -\sum_{n=0}^{\infty} V_n \qquad (10)$$

$$V_n = \left(\frac{1}{\sqrt{i\varkappa}}\right)^{n+1} \int_{C_2} \frac{H_o^{(1)}(\psi\varrho)\psi d\psi}{M^{n+1}}$$

is valid.

In the case n+1 = 2k(k=1,2,3,...), the integrand has a pole of the order (n + 1)/2 in $\psi = -1$, if ϱ is again put equal to zero. Hence,

$$V_{2\mu+1} = \left(\frac{1}{i\varkappa}\right)^{\mu+1} \frac{i2\pi}{\mu!}\left[\frac{d^\mu}{d\psi^\mu}\,\frac{H_o^{(1)}(\psi\varrho)}{(\psi^2 - 1)^{\mu+1}}\right]_{\psi=-1}$$

$$V_1 = \frac{2\pi i}{i\varkappa}\,\frac{H_o^{(1)}(-\varrho)}{2}$$

$$V_3 = \frac{2\pi i}{(i\varkappa)^2}\,\frac{H_1^{(1)}(-\varrho)}{4}$$

.
.
.

can be written down.

In the case of integral n, we may refer to a paper by Sommerfeld [9] according to which

$$V_n = -\left(\frac{1}{\sqrt{i\varkappa}}\right)^n \frac{1}{(n-1)!} \int_{\infty}^{0} \frac{d\nu\, \nu^{n-1} e^{-i\sqrt{\rho^2+\nu^2}}}{\sqrt{\rho^2+\nu^2}}$$

$$V_0 = \frac{1}{\sqrt{i\varkappa}} \frac{e^{-i\rho}}{\rho} \qquad V_4 = \frac{i}{\sqrt{i\varkappa}^5} \frac{e^{-i\rho}}{3} (1 + i\rho)$$

$$V_2 = \frac{-i}{\sqrt{i\varkappa}^3} e^{-i\rho} \qquad V_6 = \frac{-e^{-i\rho}i}{5\sqrt{i\varkappa}^7} \left(1 + i\rho + \frac{i\rho^2}{3}\right)$$

This yields:

$$U = \frac{ik_0 e^{-i\rho}}{\rho} \frac{e^{-\sqrt{i\varkappa}H}}{\varkappa} \left[1 + \left(-\frac{\rho}{\varkappa}\right) + \frac{\rho}{(i\varkappa)^2} \frac{i}{3}(1 + i\rho) - \right.$$

$$\left. - \frac{i\rho}{5(i\varkappa)^3}\left(1 + i\rho + \frac{(i\rho)^2}{3}\right) + \frac{i\pi H_0^{(1)}(-\rho)}{\sqrt{i\varkappa}} \rho e^{i\rho} + \right. \qquad (11)$$

$$+ \frac{i\pi H_1^{(1)}(-\rho)\rho^2 e^{i\rho}}{2\sqrt{i\varkappa}^3}$$

for the first terms of U.

Confining curselves to $\rho/\varkappa \ll 1$ which is valid in a wide distance region, the term in parenthesis may be put equal to unity, yielding

$$U = \frac{ik_0 \exp(-i\rho)}{\rho} \frac{\exp(-\sqrt{i\varkappa}\, H)}{\varkappa} = \frac{i \exp(-ik_0 r)}{r} \frac{\exp(-\sqrt{i\varkappa}\, k_0(z+h))}{\varkappa} \qquad (12)$$

The calculation of V has already been reduced to that of U. Hence,

$$V = \frac{-i \exp(-\sqrt{i\varkappa} k_0 (z+h))}{2\varkappa\sqrt{i\varkappa}\, k_0} \frac{\exp(-ik_0 r)}{r^2}(1 + ik_0 r) \qquad (13)$$

$$\pi_{Ex} = a_E \left[\frac{\exp(-ik_e R)}{R} - \frac{\exp(-ik_E R')}{R'} + \frac{i \exp(-ik_o r)}{r} \frac{\exp(-\sqrt{i\varkappa}\, k_o (z+h))}{\varkappa} \right] \tag{14}$$

$$\pi_{Ez} = 2a_E i\varkappa \cos\varphi V = \frac{-a_E i \sqrt{i\varkappa}}{k_o} \cdot \frac{\exp(-\sqrt{i\varkappa}) k_o (z+h)}{k} \cdot \frac{\exp(-k_o r)}{r} (1+ik_o r)$$

The first term in π_{Ex} denotes the direct wave, the second term the wave reflected by the earth's surface. The third term as well as the expression for π_{Ez} can be interpreted such that part of the energy is transferred from the transmitter through the medium, vertical to the earth's surface along which it propagates above ground to the receiving station where it enters the receiver. Formally, the last two terms correspond to the mode denoted as secondary wave in the representation of (2,6), since the exponent of e in I_1'' (2,6)

$$- i k_E (nr - (z+h)\sqrt{1 + n^2})$$

may also be written

$$-ik_o r - \sqrt{i\varkappa}\, k_o (z+h)$$

for $\varkappa \gg \varepsilon$.

This representation differs from that in (2,7) in the following points: In (2,7), the integral U was completely neglected, this is admissible only if transmitter and receiver are not too close to the earth's surface and z/r (for $z = h$) is not too small compared with unity, since in both cases π_{Ex} would vanish altogether. Furthermore, the integral π_{Ez} has not been expressed by the product of modified Bessel and Hankel functions, but by the first term of a rapidly convergent series, which is of great advantage for the numerical evaluation. Thus, the following

expressions are obtained for the field strength components:

$$\frac{Hx}{a_E} = \frac{\exp(-k_E R)}{R}\left(k_E^2 - \frac{ik_E}{R} - \frac{1+k_E^2x^2}{R^2} + \frac{3ik_Ex^2}{R^3} + \frac{3x^2}{R^4}\right) -$$

$$- \frac{\exp(-k_E R')}{R'}\left(k_E^2 - \frac{ik_E}{R'} - \frac{1+k_E^2x^2}{R'^2} + \frac{3ik_Ex^2}{R'^3} + \frac{3x^2}{R'^4}\right) +$$

$$+ \exp\left(-\sqrt{i\varkappa}\, k_o(z+h)\right)\frac{\exp(-ik_o r)}{r}\left(k_o^2 - \frac{ik_o}{r} - \frac{1+k_o^2x^2}{r^2} + \right.$$

$$\left. + \frac{3ik_ox^2}{r^3} + \frac{3x^2}{r^4}\right)$$

$$\frac{Hy}{a_E} = \frac{\exp(-ik_E R)}{R}\left(-\frac{k_E^2}{R^2} + \frac{3ik_E}{R^3} + \frac{3}{R^4}\right) xy$$

$$- \frac{\exp(-ik_E R')}{R'}\left(-\frac{k_E^2}{R'^2} + \frac{3ik_E}{R'^3} + \frac{3}{R'^4}\right) xy \qquad (15)$$

$$+ \exp\left(-\sqrt{i\varkappa}\, k_o(z+h)\right)\frac{\exp(-ik_o r)}{r}\left(-\frac{k_o^2}{r^2} + \frac{3ik_o}{r^3} + \frac{3}{r^4}\right) xy$$

$$\frac{Hz}{a_E} = \frac{\exp(-ik_E R)}{R}\left(-\frac{k_E^2}{R^2} + \frac{3ik_E}{R^3} + \frac{3}{R^4}\right) x\,(z-h)$$

$$- \frac{\exp(-ik_E R')}{R'}\left(-\frac{k_E^2}{R'^2} + \frac{3ik_E}{R'^3} + \frac{3}{R'^4}\right) x\,(z+h)$$

$$\mathrm{Re}Hx = \frac{\exp(-\Delta R)}{R}\left[\cos(\Delta R)A + B\sin(\Delta R)\right] -$$

$$- \frac{\exp(-\Delta R')}{R'}\left[C\cos(\Delta R') + D\sin(\Delta R')\right] + \qquad (16)$$

$$+ \frac{\exp(-\Delta(z+h))}{r}\left[E\cos\phi + F\sin\phi\right]$$

$$\text{Im } H = \frac{\exp(-\Delta R)}{R}\left[B\cos(\Delta R) - A\sin(\Delta R)\right] - \frac{\exp(-\Delta R')}{R'}\left[D\cos(\Delta R') - C\sin(\Delta R')\right] + \frac{\exp(-\Delta(z+h))}{r}\left[F\cos\phi - E\sin\phi\right]$$

In the main direction of emission $H_{x|x=o}$, the functions A, B, ... , F have the simple form:

$$A = -\frac{\Delta}{y} - \frac{1}{y^2} \qquad C = -\frac{\Delta}{R'} - \frac{1}{R'^2} \qquad E = k_o^2 - \frac{1}{y^2}$$

$$B = -2\Delta^2\frac{\Delta}{y} \qquad D = -2\Delta^2 - \frac{\Delta}{R'} \qquad F = -\frac{k_o}{y} \tag{17}$$

$$\phi = \Delta(z+h) + k_o r \qquad \Delta = k_o\sqrt{\frac{\varkappa}{2}} = \frac{\sqrt{\omega\mu_o\sigma}}{2}$$

In order to determine the angular dependence of the value of the field strength in the plane z = h, we calculate:

$$|H|^2 = |H_x|^2 + |H_y|^2$$

at r = R = const. and R' = const. In this case, the following expressions are valid:

$$H_x = A + Bx^2 \qquad H_y = Bxy \tag{18}$$

$$A = a_F\left\{\frac{\exp(-ik_E R)}{R}\left[+k_E^2 - \frac{ik_E}{R} - \right.\right. \qquad B = a_E\left\{\frac{\exp(-ik_E R)}{R}\left[-\frac{k_E^2}{R^2} + \frac{3ik_E}{R^3} + \right.\right.$$

$$\left.\left. - \frac{1}{R^2}\right] - \frac{\exp(-ik_E R')}{R'}\left[k_E^2 - \frac{ik_E}{R'} - + \frac{3}{R^4}\right] - \frac{\exp(-ik_E R')}{R'}\left[-\frac{k_E^2}{R'^2} + \frac{3ik_E}{R^3}\right.\right.$$

$$\left.\left. - \frac{1}{R'^2}\right] + \exp(-\sqrt{i\varkappa}k_o(z+h))\frac{\exp(-ik_o r)}{r}\left[+\frac{3}{R'^4}\right] + \frac{\exp(-\sqrt{i\varkappa}k_o(z+h) - ik_o r)}{r}$$

$$\left.\left[k_o^2 - \frac{ik_o}{r} - \frac{1}{r^2}\right]\right\} \qquad \left.\left[-\frac{k_o^2}{r^2} + \frac{3ik_o}{r^3} + \frac{3}{r^4}\right]\right\}$$

Thus, for $|H|^2$ we obtain

$$|H|^2 = A\tilde{A} + \left\{2\left[\mathrm{Re}(A)\mathrm{Re}(B) + \mathrm{Im}(A)\mathrm{Im}(B)\right] + B\tilde{B}r^2\right\} r^2\cos^2\varphi$$

or $$|H|^2 = |A|^2 + E\,r^2\cos^2\varphi \qquad (19)$$

Re ... real part

Im ... imaginary part, $\tilde{A}$ being the conjugate complex value. Hence, $|H|^2$ in a polar diagram describes the curve (19) whose large semi-axis in the case $E>0$ lies in the dipole axis, and in the case $E<0$ vertical to the dipole axis. $E>0$ corresponds to the short range field. For $\Delta \ll \frac{1}{r}, \frac{1}{R'}$,

$$E = a_E^2\left[\frac{12r^3R'^7 + 9r^{10}}{r^8R'^{10}} + \frac{12R'^{10} - 30r^5R'^5}{r^8R'^{10}}\right] > 0$$

is easily found for E. $E<0$, however, is valid in the long-range field. Neglecting the terms in R and R' (since $R' \approx R$ for $z = h$ and $h/r \ll 1$),

$$|A|^2 = a_E^2\frac{k_o^4}{r^2}\exp(-2\Delta(z+h)) \qquad r^2E = -\frac{k_o^4a_E^2}{r^2}\exp(-\Delta(z+h))$$

hence,

$$|A|^2 = -Er^2$$

and

$$|H|^2 = a_E^2\frac{k_o^4(1-\cos^2\varphi)}{r^2}\exp(-2\Delta(z+h)) \qquad (20)$$

is obtained for $\Delta \ll \frac{1}{r}, \frac{1}{R'}$.

Qualitatively, the result is the same as in the case of a dipole in a homogeneous, unbounded medium. In this case

$$|H|^2 = a_E^2\frac{\exp(-2\Delta r)}{r^6}(1 + 3\cos^2\varphi)$$

is valid for the short-range field, whereas

$$|H|^2 = a_E^2 \frac{4\Delta}{r^2} \exp(-2\Delta r) \quad (1-\cos^2\varphi)$$

is valid for the long-range field.

Thus, a quantitative compa ison is possible. The ratio between the emission into the semi-space that into the full space is

$$\eta = \frac{|H|^2_{HS}}{|H|^2_{FS}} = \frac{\exp(2\Delta r)}{\varkappa^2} \qquad (21)$$

for the long-range field ($h/r \ll 1$). Hence, we may assume that the effect of the surface in the long-range field is of considerable importance. This is also confirmed by (20), since $|H|^2_{HS}$ in the long-range field is represented only by the term which takes the existence of a boundary surface into account.

Tab. 1,6 $H_x|_{x=0}$ z = h = 250 m

σ [mhos/m] \ r [m]	10	$10\sqrt{10}$	10^2	$10^2\sqrt{10}$	10^3	10^4	10^5	
$5\cdot10^{-5}$	10^{-3}	$3,16\cdot10^{-5}$	$1,01\cdot10^{-6}$	$3,19\cdot10^{-8}$	$1,21\cdot10^{-9}$	$5,75\cdot10^{-14}$	$4,76\cdot10^{-45}$	Dipole in un-
$5\cdot10^{-4}$	10^{-3}	$3,16\cdot10^{-5}$	$1,01\cdot10^{-6}$	$3,85\cdot10^{-8}$	$1,28\cdot10^{-9}$	$3,35\cdot10^{-20}$	$3,47\cdot10^{-115}$	bounded space
$5\cdot10^{-5}$	$1,03\cdot10^{-3}$	$3,4\cdot10^{-5}$	$1,08\cdot10^{-6}$	$2,66\cdot10^{-8}$	$1,13\cdot10^{-4}$	$5,95\cdot10^{-13}$	$2,64\cdot10^{-14}$	dipole follow-
$5\cdot10^{-4}$	$1,1\cdot10^{-3}$	$3,6\cdot10^{-5}$	$1,15\cdot10^{-6}$	$3,48\cdot10^{-8}$	$1,35\cdot10^{-9}$	$2,58\cdot10^{-13}$	$1,15\cdot10^{-14}$	ing TNG
$5\cdot10^{-5}$	10^{-3}	$3,16\cdot10^{-5}$	$1,03\cdot10^{-6}$	$7,96\cdot10^{-8}$	$2,32\cdot10^{-9}$			dipole follow-
$5\cdot10^{-4}$	10^{-3}	$3,14\cdot10^{-5}$	$8,39\cdot10^{-7}$	$7,76\cdot10^{-8}$	$5,25\cdot10^{-9}$			ing TN 5

Tab. 2,7 $H_x|_{y=0}$ z = h = 600 m

σ [mhos/m] \ r [m]	67	140	213	285	460	520	335	
$5\cdot10^{-4}$		$6,81\cdot10^{-7}$	$1,85\cdot10^{-7}$	$7,54\cdot10^{-8}$	$1,58\cdot10^{-8}$	$1,00\cdot10^{-8}$	$9,20\cdot10^{-9}$	Dipole follow-
10^{-3}	$6,5\cdot10^{-6}$	$6,9\cdot10^{-7}$	$1,80\cdot10^{-7}$	$7,07\cdot10^{-8}$	$1,27\cdot10^{-8}$	$7,65\cdot10^{-9}$	$6,75\cdot10^{-9}$	ing TN 6
$5\cdot10^{-3}$		$5,8\cdot10^{-7}$	$1,25\cdot10^{-7}$	$3,73\cdot10^{-8}$	$3,42\cdot10^{-8}$	$1,67\cdot10^{-9}$	$1,39\cdot10^{-9}$	
$5\cdot10^{-3}$	$6,24\cdot10^{-6}$	$5,8\cdot10^{-7}$	$1,21\cdot10^{-7}$	$3,79\cdot10^{-8}$	$3,40\cdot10^{-8}$	$1,65\cdot10^{-9}$	$1,36\cdot10^{-9}$	dipole in un- bounded space

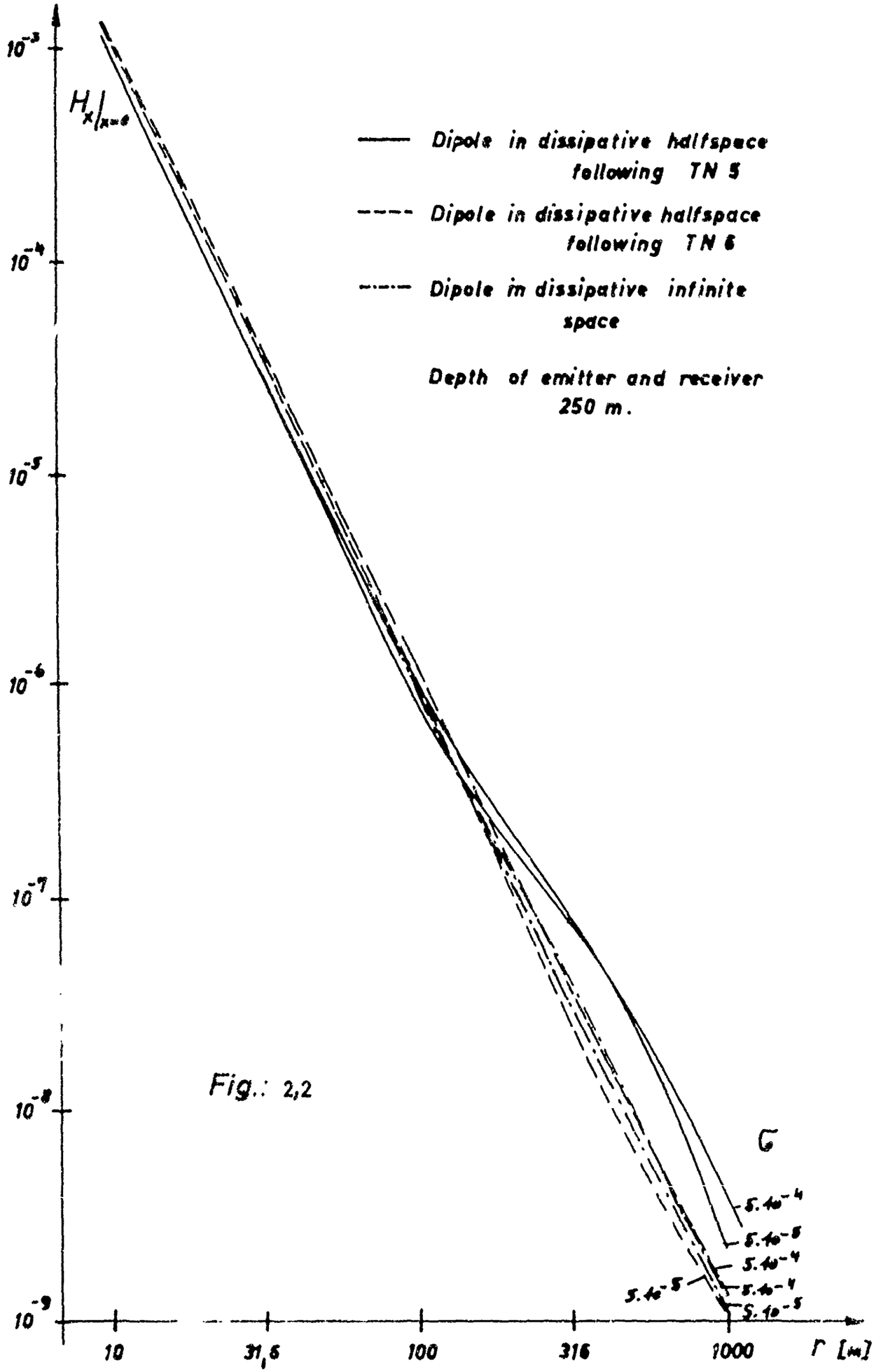
$H_x|_{z=0}$
10^{-3}
10^{-4}
10^{-5}
10^{-6}
10^{-7}
10^{-8}
10^{-9}
10
31,6
100
316
1000
r [m]
—— Dipole in dissipative halfspace following TN 5
---- Dipole in dissipative halfspace following TN 6
-·-·- Dipole in dissipative infinite space
Depth of emitter and receiver 250 m.
σ
5.10^{-4}
5.10^{-5}
5.10^{-4}
5.10^{-5}
5.10^{-4}
5.10^{-5}

Fig.: 2,2

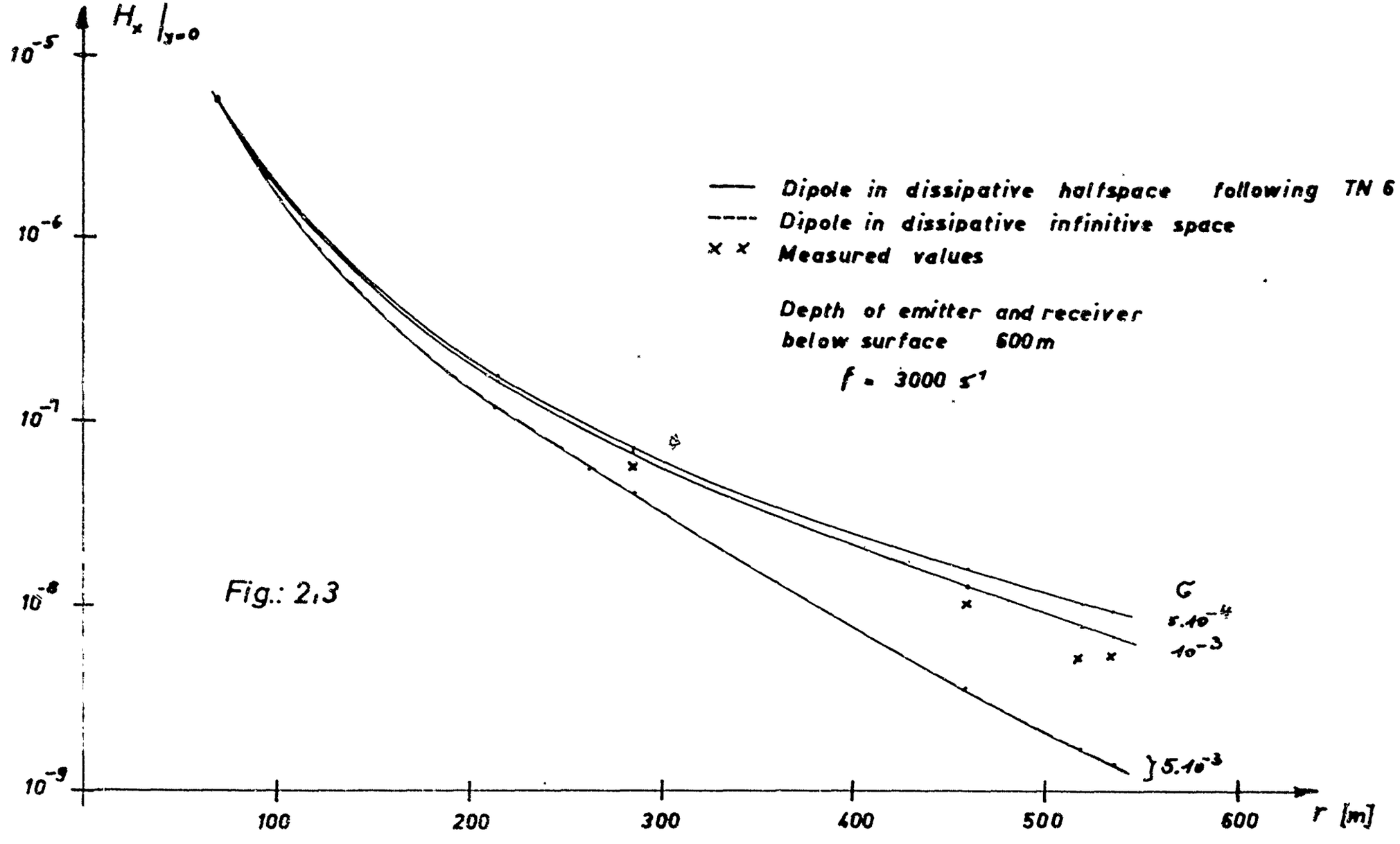
$H_x|_{y=0}$
10^{-5}
10^{-6}
10^{-7}
10^{-8}
10^{-9}
100
200
300
400
500
600
r [m]
Dipole in dissipative halfspace following TN 6
Dipole in dissipative infinitive space
x x Measured values
Depth of emitter and receiver below surface 600m
f = 3000 s⁻¹
G
5.10^{-4}
10^{-3}
5.10^{-3}

Fig.: 2.3

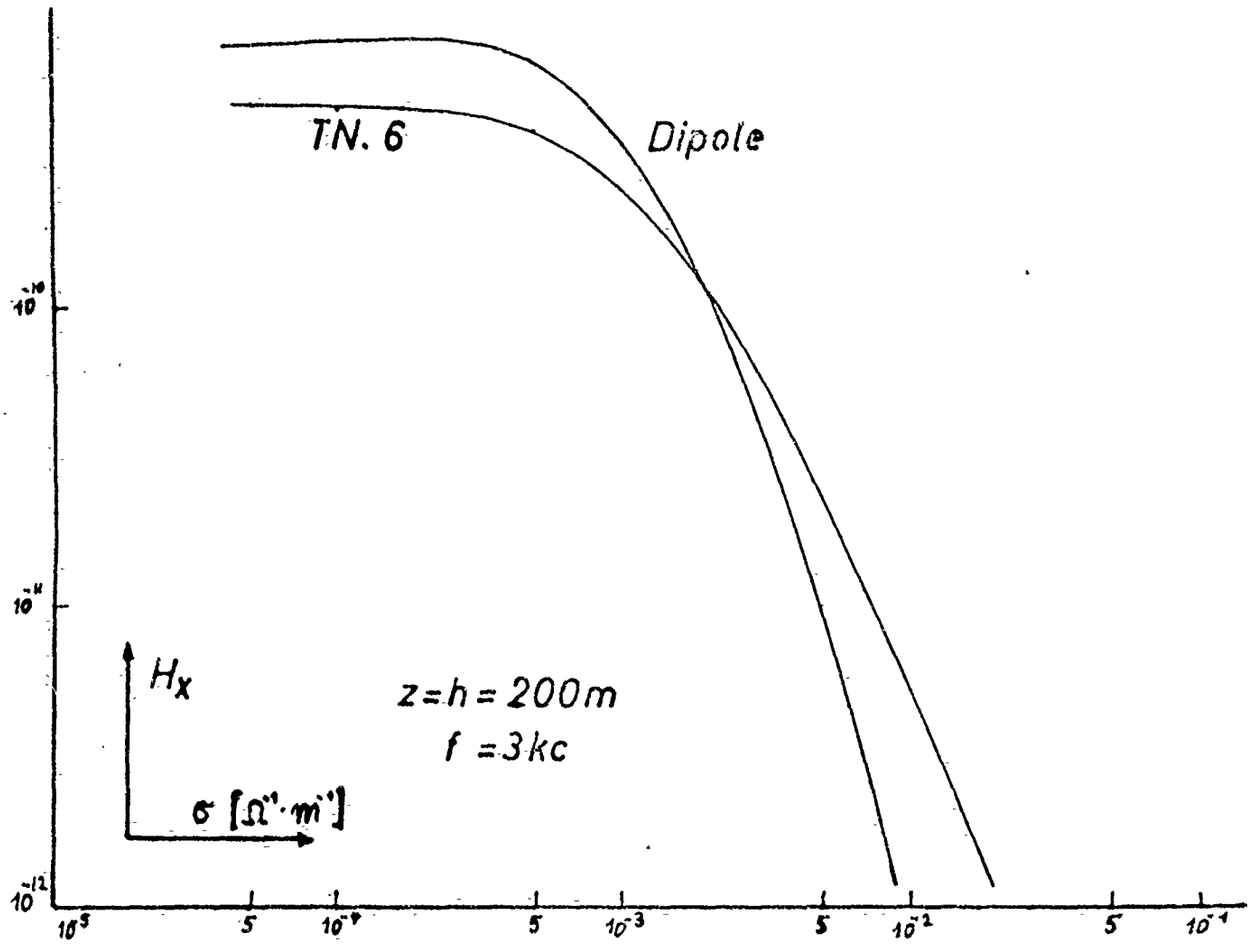
TN. 6
Dipole
10^{-10}
10^{-11}
10^{-12}
H_x
$z=h=200m$
$f=3kc$
$\sigma\ [\Omega^{-1}\cdot m^{-1}]$
10^{-5}
5
10^{-4}
5
10^{-3}
5
10^{-2}
5
10^{-1}

FIG. 2,4

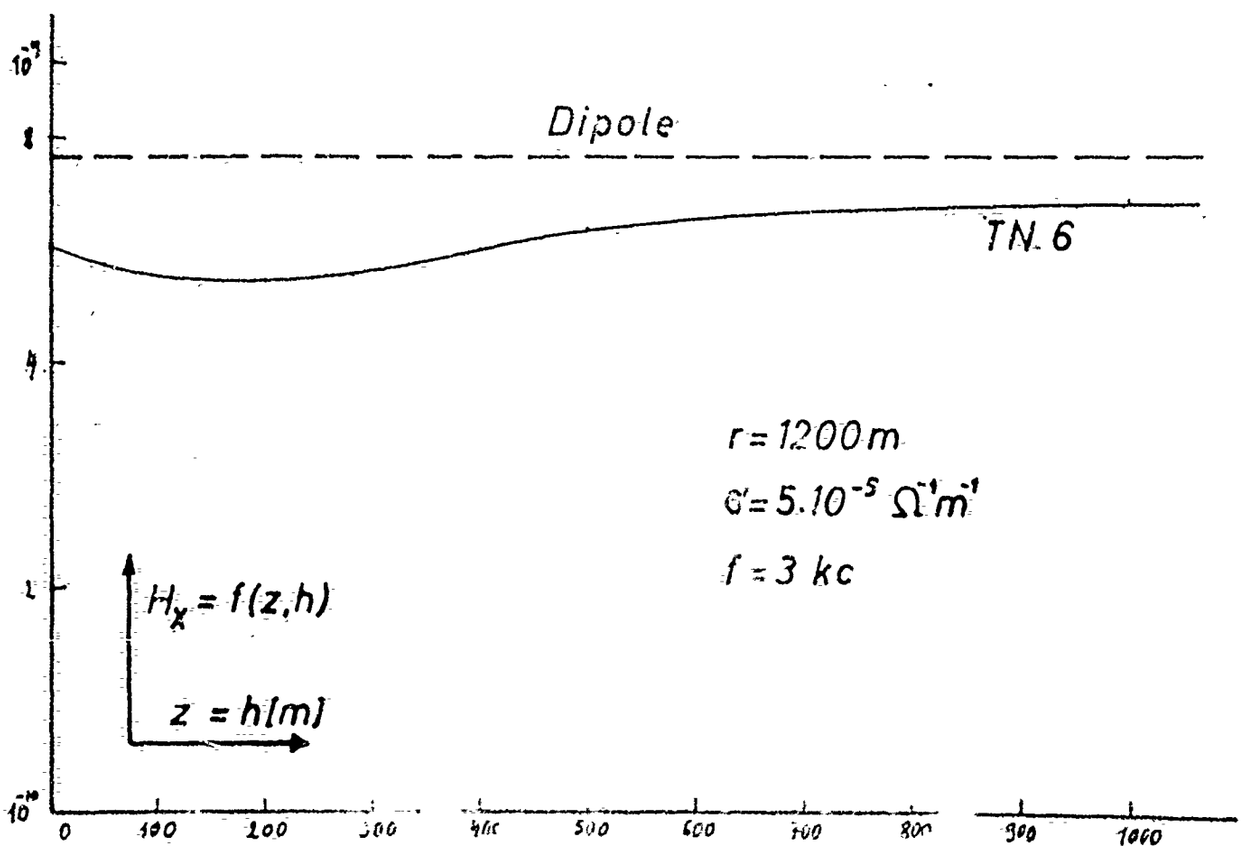
10^{-9}
8
4
2
10^{-10}
Dipole
TN. 6
$r=1200m$
$\sigma=5.10^{-5}\ \Omega^{-1}m^{-1}$
$f=3\ kc$
$H_x=f(z,h)$
$z=h[m]$
0
100
200
300
400
500
600
700
800
900
1000

FIG. 2,5

Fig. (2,3) gives the course of the field strength $H_{x|y=o}$ as dependent on the distance (up to r = 500 m). The depth of transmitter and receiver is 600 m. For comparison, the field strength of a dipole in a homogeneous, unbounded space was plotted (dashed curve). Here, an effect of the surface is not noted; the two curves overlap. The field strength decreases as the product $\omega\sigma$ increases (x are measured points). Fig. 2,2 and Table 2,6 show $H_{x|x=o}$ as dependent on the distance in comparison with the representation according to (2,7) and the Hertzian solution for the unbounded space at a transmitter and receiver depth of 250 m. Fig. 2,2 shows that the earth-air interface hardly has any effect up to a distance of 1000 m. Table 2,6, however, shows that the ground wave U has a decisive effect already from $r = 10^4$ onward, at $r = 10^5$ it yields the 10^{31}-fold field strength in the case $\sigma = 5\cdot10^{-5}$ mhos/m, and the 10^{101}-fold field strength in the case $\sigma = 5\cdot10^{-4}$ mhos/m, as compared to the Hertzian solution. The increase in field strength with σ up to $r = 10^3$ m is consistent with the considerations of [1] (p. 15). The dependence on σ is reversed as the distance increases, the field strength then decreases with increasing σ. The propagation in the range $r \leq 10^3$ m is strongest according to the representation in (2,7). The approximation applied in (2,7) for calculating the integral expressions; [in (2,) the following expressions were obtained:

$$\pi_{Ex} = a_E \left(\frac{\exp(-ik_E R)}{R} - \frac{\exp(-ik_E R')}{R'} \right)$$

$$\pi_{Ez} = a_E \frac{2}{k_E^2} \frac{2}{\partial x \partial z} \left(\frac{\exp(-ik_E R')}{R'} + \frac{\partial}{\partial z} I_o(\alpha) K_o(\beta) \right) \Bigg]$$

is, however, probably not suited for describing the propagation process of dipole excitation, for the following reasons: Owing to the boundary conditions (2) at z = 0, neglecting the integral U in π_{Ex} successively leads to the conclusions:

$$\left.\begin{aligned} \pi_{Ex} &= 0 \\ \pi_{Ax} &= 0 \\ \frac{\partial \pi_{Ex}}{\partial x} &= \frac{\partial \pi_{Ax}}{\partial x} = 0 \\ \operatorname{div}\vec{\pi}_E &= \operatorname{div}\vec{\pi}_A = \frac{\partial \pi_{Ez}}{\partial z} = \frac{\partial \pi_{Az}}{\partial z} \end{aligned}\right\} \quad z = o$$

Introduction of the expressions for π_z of (2,7) into the last expression:

$$\pi_{Ez} = \int_o^\infty g_E(\lambda) \exp(-U_E z) J_1(\lambda r) d\lambda \cos\varphi$$

yields

$$\pi_{Az} = \int_o^\infty g_A(\lambda) \exp(U_A z) J_1(\lambda r) d\lambda \cos\varphi$$

yields

$$\frac{\partial \pi_{Ez}}{\partial Z} \quad \frac{\partial \pi_{Az}}{\partial Z}$$

because of $g_E(\lambda) = g_A(\lambda)$, a discrepancy which cannot be eliminated by the approximation used for π_{Ex} because of

$$-U_E \neq U_A$$

or

$$-\sqrt{\lambda^2 - k_E^2} \neq \sqrt{\lambda^2 - k_o^2} .$$

At distances of $r \geqslant 10^5$ m, R and $r' = \sqrt{r^2 + (z+h)^2} =$

$= r\sqrt{1 + \left(\frac{z+h}{r}\right)^2} \simeq r$ become approximately independent of z for $z = h \lesssim 500$ m. Thus, $R = R' = r$. This again yields

$$\pi_{Ex} = 0$$

$$\pi_{Ez} = \frac{2a_E}{k_E^2} \frac{\partial^3}{\partial x \partial z^2} I_o(\alpha) K_o(\beta)$$

If the asymptotic representations for the modified Bessel or Hankel functions are used

$$I_o(\alpha) = \frac{1}{\sqrt{2\pi\alpha}} \left(e^{\alpha} + e^{-\alpha - i\frac{\pi}{2}}\right)$$

$$K_o(\beta) = \sqrt{\frac{\pi}{2\beta}}\, e^{-\beta}$$

which is possible, since for $|\alpha| = \Delta(R' - (z+h))$ and $|\beta| = \Delta(R' + (z+h))$,

$$|\alpha| \gg 1 \qquad |\beta| \gg 1$$

holds at $r \geq 10^5$ m and $\sigma \geq 10^{-5}$, then the below expressions follow successively:

$$I_o(\alpha) K_o(\beta) = \frac{1}{2\sqrt{\alpha\beta}} \left(\exp(\alpha - \beta) + \exp(-(\alpha + \beta) - i\frac{\pi}{4})\right)$$

$$= -\left(\frac{\exp(-ik_E R')}{k_E r} + i\frac{\exp(-ik_E(z+h))}{k_E r}\right)$$

and

$$H_x = \frac{\partial^2}{\partial x^2} \frac{2}{k_E^2} \frac{\partial^2}{\partial E^2} \left(-\frac{\exp(-ik_E(z+h))}{r}\right)$$

$$= -\frac{2(y^2 - 2x^2)}{r^5} \exp(-ik_E(z+h)),$$

i.e. a plane wave excited in $z = -h$ in ζ-direction, whose amplitude decreases as $1/r^3$. An exact valuation of the theory described in (2,7) will be given later.

III. Comparison of theory and experiment

The measurements described in part I were evaluated from the viewpoints of two different theories, one being the theory for a dipole in an unbounded homogeneous medium, and the second being an elaborate theory developed in chapter 2 and also in [7]. Unfortunately it has not been possible to evaluate this theory accurately and in detail, as for this purpose an electronic computer would be necessary. We shall make these calculations in the near future, as a computer is going to be set up in Innsbruck very soon. So far, we could compute only some special measurements with considerable simplifications.

The measurement in the German mine Füsseberg, dealt with in chapter 1,7, seemed to be well suited for studying the effect of the earth's surface on wave propagation over large distances, because the geometrical conditions are favorable there.

The points of measurement, the curves for a pure dipole, and those according to [7] and chapter 2,8 were plotted in Fig. 2,3, but a statement on the exact course of the experimental curve cannot be made yet because the distance is too small (only 500 m). In this distance range, at a conductivity $\sigma = 10^{-4}\,\Omega^{-1}m^{-1}$ which in this mine can be assumed to be mean value, the two above theoretical curves are practically identical.

The conditions of our measurements in Schwaz are similar - here, the measurement reaches 1200 m, but the effect of the earth's surface cannot be proved with certainty because of the low

conductivity and the great depth (Fig. 3,2).
For our measurements in Schwaz, the surface can no longer be assumed as plane (as e.g. in Füsseberg).
Table 3,1 gives the values calculated according to the theory of a dipole and according to [7].

The transmitter described in chapter 1,3, which was used for measuring over distances up to 3.300 m in the St. Gertraudi mine showed good results (chapter 1,9).
The geometrical conditions of these measurements are given in Fig. 3,3 and the idealization necessary for the evaluation is shown in Fig. 3,4

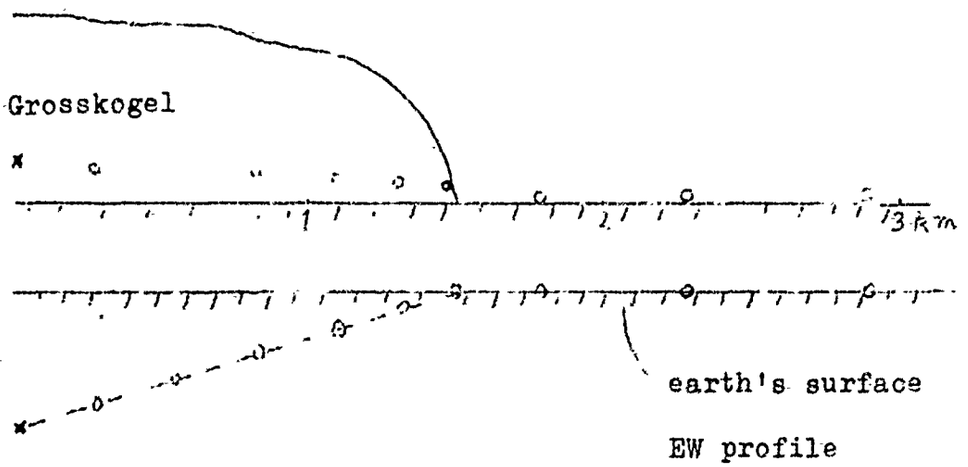

(x) indicates the position of the transmitter and (o) indicates the individual points measured below ground as well as on the earth's surface.

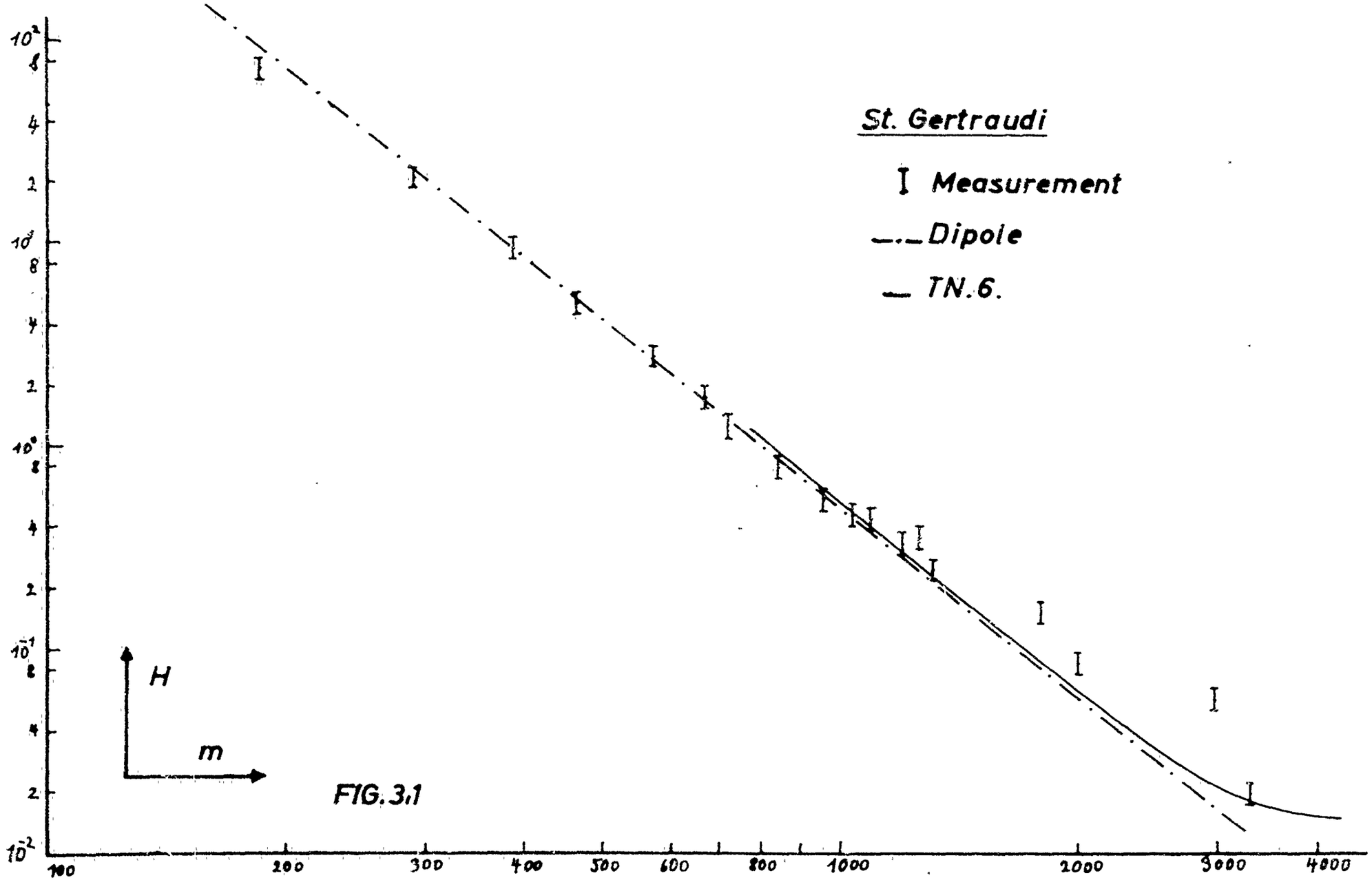
St. Gertraudi
Measurement
Dipole
TN.6.
H
m
100
200
300
400
500
600
800
1000
2000
3000
4000

FIG. 3.1

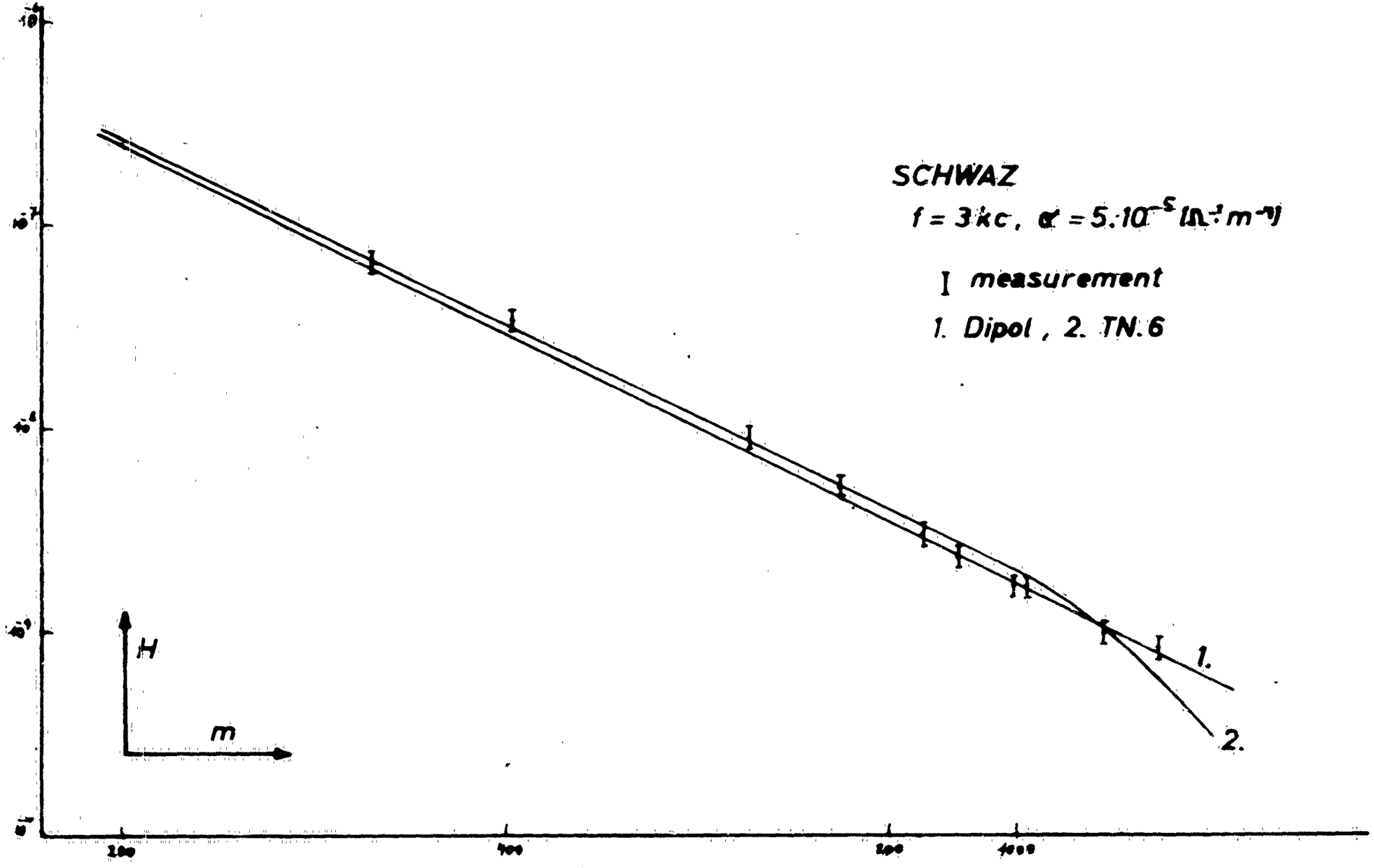

FIG. 3.2

Fig. 3,4 shows that the depth which had to be introduced into the calculation decreases for the individual points of measurement. Despite the considerable idealization of the present problem, the course given in Table 3,2 and Fig. 3,1 shows that the points of measurement at distances of more than 1.5 km are much better described by the new and improved theory (allowing for the sky wave and ground wave) than by the original dipole theory.

It will be the aim of further measurements with a more powerful transmitter antenna which is now being built to study the propagation over very great distances in detail. In this case, only the ground wave yields a considerable contribution to the propagation mechanism.

Table 3,1

$\sigma = 5 \cdot 10^{-5}\ \Omega^{-1}\ m^{-1}$; transmitter - earth's surface 1000 m; f = 3 kc.

r [m]	Dipole [1]	TN6 [7]	measurement [Wb/m^2]
200	$2480 \cdot 10^{-10}$	$2670 \cdot 10^{-10}$	$3,8 \cdot 10^{-12}$
316	626	657	2,8
405	306	314	1,5
620	81	92	0,38
740	45	51	0,21
850	31	34,2	0,13
910	23,8	27,8	0,095
1000	17	20,5	0,07
1024	16,6	18,7	0,07
1180	10,3	10,7	0,042
1275	7,87	6,08	0,035

Table 3,2

St. Gertraudi; $h = 400$ m, $\sigma = 10^{-4}\,\Omega^{-1}\,m^{-1}$, $f = 3$ kc, $\delta = 30^{\circ}$

r [m]	$\lvert H \rvert [\gamma] \cdot 10^{-10}$	measurement [μV]
1000	11,5	0,45
1100	8,81	0,445
1200	6,83	0,33
1400	4,23	0,262
1550	3,53	0,348
1800	2,20	0,151
2000	1,5	0,088
2200	1,12	0,197
3000	0,507	0,058
3300	0,408	0,0197
4000	0,130	—

References:

[1] Second Technical Annual Report, PROPAGATION OF VLF-WAVES IN SOLID AND LIQUID MEDIA, 61(052)-490, 26 December 1962

[2] Technical Note No 1 P.o. VLF-W. i.s.a.l. media 61(052)-490, 1 July 1963

[3] Technical Note No 2 P.o. VLF-W. i.s.a.l.m. 61(052)-490, 15 July 1963

[4] Technical Note No 3 P.o. VLF-W. i.s.a.l.m. 61(052)-490, 15 July 1963

[5] Technical Note No 4 P.o.VLF-W. i.s.a.l.m. 61(052)-490, 10 August 1963

[6] Technical Note No 5 P.o. VLF-W. i.s.a.l.m. 61(052)-490, 10 August 1963

[7] Technical Note No 6 P.o. VLF-W. i.s.a.l.m. 61(052)-490, December 1963

[8] Technical Note No 7 P.o. VLF-W. i.s.a.l.m. 61(052)-490, December 1963

[9] A. Sommerfeld, UEBER DIE AUSBREITUNG DER WELLEN IN DER DRAHTLOSEN TELEGRAPHIE, Ann. d. Phys. IV, vol. 28, 1909

[10] A. Sommerfeld, DRAHTLOSE TELEGRAPHIE, published in Frank-Mises: DIE DIFFERENTIALGLEICHUNGEN DER PHYSIK, 1935

[11] H. Ott, BRECHUNG VON KUGELWELLEN, Ann. d. Phys., 41, 1942

[12] W. I. Smirnov, LEHRGANG DER HOEHEREN MATHEMATIK, III 2, 1962, 242

[13] R. Kerr Moore, THE THEORY OF RADIO COMMUNICATION BETWEEN SUBMERGED SUB MARINES.

Ph. D. Thesis, Cornell 1951

Review of publications

In 1963, the collaborators of the VLF research project studied the following publications which they partly discussed in the form of abstracts.

(1) A. Sommerfeld, UEBER DIE AUSBREITUNG DER WELLEN IN DER DRAHTLOSEN TELEGRAPHIE, Ann. d. Physik, vol. 28, 1909

(2) H. Ott, REFLEXION UND BERECHNUNG VON KUGELWELLEN; EFFEKTE ZWEITER ORDNUNG, Ann. d. Physik, vol. 41, 1941

(3) H. Weyl, AUSBREITUNG ELEKTROMAGNETISCHER WELLEN UEBER EINEM EBENEN LEITER, Ann. d. Physik, vol. 60, 1937

(3) A. Sommerfeld u. Renner, STRAHLUNGSENERGIE UND ERD-ABSORPTION BEI DIPOLANTENNEN, Ann. d. Physik, vol. 41, 1941

(5) Kenneth G. Budden, WAVE GUIDE THEORY OF VLF-PROPAGATION, Proceedings of the IRE, June 1957

(6) J. R. Wait, H. H. Howe, THE WAVEGUIDE MODE THEORY OF VLF JONOSPHERIC PROPAGATION, Proceedings of the IRE, January 1957

(7) J. R. Wait, ELECTROMAGNETIC WAVES IN STRATIFIED MEDIA,

(8) Schelkunoff, ADVANCED ANTENNA THEORY,

(9) J. R. Wait, A NEW METHOD IN MODE THEORY OF VLF-WAVES PROPAGATION, Journal of Research of National Bureau of Standards, Jan.-Febr. 1961 65 D

(10) J. R. Wait, MODE THEORY OF VLF-WAVES PROPAGATION FOR FINITE GROUND CONDUCTIVITY, Proceedings of the IRE, June 1951

(11) J. R. Wait and A. Murphy, GEOMETRICAL OPTICS OF VLF SKY WAVE PROPAGATION, Proceedings of the IRE, June 1951

(12) H. Volland, A COMPARISON BETWEEN MODE THEORY AND RAY THEORY OF VLF PROPAGATION, Journal of Research of National Bureau of Standard, 1961/65

(13) J. R. Wait, THE ATTENUATION VS FREQUENCY CHARACTERISTICS OF RADIO WAVES, Proceedings of the IRE, June 1957

(14) R. Kerr Moore, THEORY OF RADIO COMMUNICATION BETWEEN SUBMERGED SUBMARINES, Thesis of the Cornell University, USA

(15) W. O. Schuhmann, UEBER DIE AUSBREITUNG SEHR LANGER ELEKTR. WELLEN UND BLITZENTLADUNGEN UM DIE ERDE, Zeitschrift fuer angewandte Physik, vol. 4. 1952

(16) Janis Galejs, EXCITATION OF VLF AND ELF RADIO WAVES BY A HORIZONTAL MAGNETIC DIPOLE, Journal of Research of National Bureau of Standards, June 1961 65D

(17) D. Dobrett and A. Ishimarn, EAST-WEST EFFECT ON VLF MODE TRANSMISSION ACROSS THE EARTH'S MAGNETIC FIELD, Journal of Research of National Bureau of Standards, Febr. 1961 65D

(18) D. D. Crombie, REFLECTION FROM A SHARPLY BOUNDED IONOSPHERE FOR VLF PROPAGATION PERPENDICULAR TO THE MAGNETIC MERIDIAN, Journal of Research of National Bureau of Standards, Okt. 1961, 65D

(19) Y. L. Alpert, UEBER DIE AUSBREITUNG ELEKTROMAGNETISCHER WELLEN MIT NIEDERER FREQUENZ UEBER DIE ERDOBERFLAECHE, Verlag der akademischen Wissenschaften, Moskau, 1955 (Auszug)

(20) W. O. Schumann, UEBER DIE OBERFELDER BEI DER AUSBREITUNG LANGER ELEKTR. WELLEN IM SYSTEM ERDE - LUFT - JONOSPHAERE, Zeitschrift fuer angewandte Physik 1954/6

(21) W. O. Schumann, UEBER DIE AUSBREITUNG LANGER ELEKTR. WELLEN UND EINIGE ANWENDUNGEN AUF SENDERINTERFERENZ UND BLITZSIGNALE, Zeitschrift fuer angewandte Physik 1954/6

(22) W. O. Schumann, UEBER SPHAERISCHE ELEKTROMAGNETISCHE EIGENSCHWINGUNGEN IN RAEUMEN, DIE PLASMA ENTHALTEN, Zeitschrift fuer Naturforschung 4a 1949

(23) E. T. Pierce, THE PROPAGATION OF RADIO WAVES OF FREQUENCY LESS THAN 1 KC, Proceedings of IRE, March 1960

(24) W. O. Schumann, UEBER DIE STRAHLUNGSLOSEN EIGENSCHWINGUNGEN EINER KUGEL, DIE VON EINER LUFTSCHICHT UND EINER JONOSPHAERENHUELLE UMGEBEN IST, Zeitschrift fuer Naturforschung 7a, 1952

(25) R. King, RADIATION RESISTENCE OF A TRANSMISSION LINE, Proceedings of the IRE, Nov. 1951

(26) J. S. Belrose, FERROMAGNETIC LOOP AERIALS FOR KILOMETRIC WAVES, Wireless Engineer, Feb. 1955

(27) Ch. W. Harrison, AN APPROXIMATE REPRESENTATION OF THE ELECTROMAGNETIC FIELD NEAR A SYMMETRICAL RADIATOR, Journal of applied Physics. 1944, July vol. 15

(28) S. Weinbaum, SOLUTION OF DEFINITE INTEGRALS IN ANTENNA THEORY, Journal of appl. Physics, Jan. 1944. vol. 15

(29) D. D. King and R. King, TERMINAL FUNCTIONS FOR ANTENNAS, Journal of appl. Physics, Febr. 1944, vol. 15

(30) F. F. Fulton, EFFECT OF RECEIVER BANDWITH ON THE AMPLITUDE DISTRIBUTION OF VLF ATMOSPHERIC NOISE, Journal of Research of National Bureau of Standards. June, 1961, vol. 65D

(31) A. S. Orange, L. A. Ames, GEOLOGICAL AND GEOPHYSICAL FACTORS INFLUENCING DEEP STRATA COMMUNICATIONS, AFCRL March 1962

(32) STUDIES IN DEEP STRATA RADIO COMMUNICATIONS, Final report, Oct. 1962. Raytheon Company, Norwood, Massachusetts

(33) R. W. Turner, SUBMARINE COMMUNICATION ANTENNA SYSTEMS, Proceedings of the IRE, May 1959

(34) Rabindra N. Ghose, THE LONG RANGE SUB-SURFACE COMMUNICATION SYSTEM. Sixth national communications symposium, Oct. 1960. Utica, New York

(35) C. W. Pritchett, ATTENUATION OF RADIOFREQUENCY WAVES THROUGH THE EARTH. Geophysics Vol XVII, April 1952, No 2

(36) Krajew, GRUNDLAGEN DER GEOELEKTRIK, VEB Verlag Berlin 1957.

(37) A. G. Tarkhov, ϱ & ε VON GESTEINEN IN EL. WECHSELFELDERN.

(38) Evjen, H. M., THEORY AND PRACTICE OF LOW FREQUENCY ELECTROMAGNETIC EXPLORATION. GEOPHYSICS 13.

(39) Koops, G. C., ON THE DISPERSION OF RESISTIVITY AND DIELECTRIC CONSTANT OF SOME SEMI-CONDUCTORS AT AUDIOFREQUENCIES:. Phys. Review, v. 83

(40) Smith-Rose, ELECTRICAL MEASUREMENTS ON SOIL WITH ALTERNATING CURRENTS. Inst. Elec. Engineers Journ. 75

(41) W. Buchheim, BESTIMMUNG DES SPEZ. WIDERSTANDES VON ANISOTROP LEITENDEN AGGREGATEN NACH DER 4-PUNKTMETH. Geofisica pura e applicata (1947)

(42) Keller and Licastro, DIELECTRIC CONSTANT AND ELECTRICAL RESISTIVITY OF NATURAL STATE CORES Geological Survey Bulletin 1052-H

(43) Keller, George V., ELECTRICAL PROPERTIES OF SANDSTONES OF THE MORRISON FORMATION. Geol. Surv. Bull. 1052-J

(44) Lichtenecker, K., EL. LEITUNGSWIDERST. KUENSTL. UND NAT. AGGREGATE, Phys. Zeitschrift 25

(45) I. Koenigsberger, ZUR MESSUNG DER EL. LEITF. DURCH INDUKTION. Phys. Z. XXXI.

(46) James R. Wait, TRANSIENT COUPLING IN GROUNDED CIRCUITS. Geophysics 18
MUTUAL COUPLING OF LOOPS LYING ON THE GROUND. Geophysics 19.

(47) Kenneth L. Cook and Robert G. van Nostrand, INTERPRETATION OF RESISTIVITY DATA OVER FILLED SINKS. Geophysics 19.

(48) Carpenter, E. W. SOME NOTES CONCERNING THE WENNER CONFIGURATION. Geophysical prospection 3 (1955)

The publications (1) through (4) as well as (14) proved to be of

principal importance. The methods discussed therein were used in Technical Notes Nos. 4 to 6. An exact study of (7) made us acquainted with fundamental methods for the treatment of transmission problems in general, and especially those in the VLF range. The Mode Theory explained in (5), (6), (7), (9), and (10) as well as the methods of VLF transmission in the atmosphere between the earth's surface and the ionosphere explained in (15), (16), and (19) through (24), where the waves are considered to be excited in the atmosphere, will be important for further work because the theory may be extended to excitation of the modes beyond the atmosphere; interesting results are expected to be gained by this extension. A continuation of the above studies is planned but is bound to the use of an electronic computer which will be available at the beginning of 1964. As yet, publications (17) and (18) seem to be of little interest for our work. Publications (25) through (30) as well as (8) deal with antenna problems. In this connection it will be necessary to study an even larger number of publications.

The comprehensive report (82) which we obtained just before going to press naturally was of special interest. It showed on the one hand, that the way we chose independently for describing the propagation of VLF waves, has also been used by other scientists. It proves, on the other hand, that a number of questions must be answered before the problem can be looked upon as being solved, although some problems can be solved by

modifying the existing theory of the propagation and excitation of VLF waves in the atmosphere between earth and ionosphere. This holds both in theory and practice, especially for the antenna problem. A considerable improvement of the efficiency of VLF antennas would be a great advance in this field, which has not yet been made despite great efforts. For further studies of the excitation problem, emphasis must be laid on improving the efficiency of VLF antennas.

(32) solves the problem of the propagation of electromagnetic waves in the interior of the earth in three different ways, depending on the geological structure and on the values of the electrical parameter of the studied region:

(a) by the so-called UP-OVER AND DOWN modes at a small depth of transmitter and receiver, and at high conductivity losses, a form of propagation R. K. Moore described in this thesis.

Here, the direct wave and the wave reflected from the earth's surface are neglected because of high exponential damping. Hence, this theory can describe propagation at high conductivities (approximately that of sea water).

(b) By the so-called SHORT DISTANCE MODES at medium ohmic losses. The field at the point of reception is composed of a direct wave, a reflected wave, and a ground wave (we have already described this form of propagation in [7]).

(c) By the wave guide theory at small ohmic losses, as is the case in propagation in the atmosphere between earth and ionosphere. The geological structure of the earth was assumed to consists of layers of different conductivity (a layer of comparatively poor conductivity between two layers of good conductivity).

(b) has already been worked out in [7] and has been adopted in the present report. (a) and (c) are of less interest for our work, because the geological conditions are not appropriate. Our measurements are mainly carried out with the conditions shown in Fig. 4,1. Therefore we are intended to set up a theory of propagation based on this structure, which will better correspond to the actual conditions.

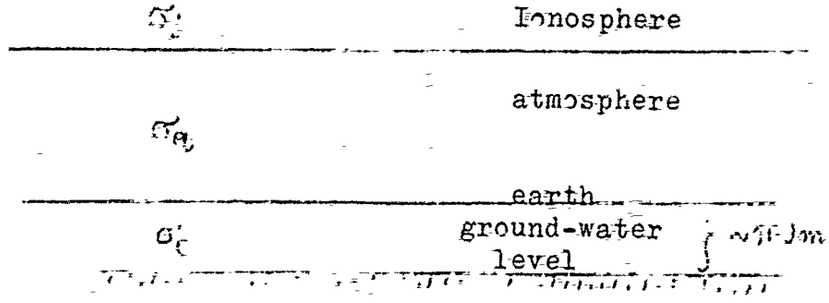

Another problem will be to study the propagation in a layer with a conductivity $\sigma = 10^{-4}$-10^{-1} mhos/m making allowances for the reflection from the ground and by the ground-water level, as well as the influence of the ionosphere which will exist at least for large distances (more than 5000 m) with the transmitter and receiver at comparatively small depths (200 - 1000 m).

A b s t r a c t

The present paper deals with measurements concerning the propagation of VLF waves through inhomogeneous rock, the influence of the earth's surface being taken into account. These measurements are compared with results of theoretical works. Furthermore, conductivity measurements of rock in mines are discussed and compared with the results gained from propagation measurements. The results have been found to agree well.

List of coworkers

team for

theoretical problems	experimental problems
direction: Univ. Prof. Dr. F. Cap	direction: Dr. W. Bitterlich
G. Tinhofer	O. Gröbner
	O. Wörz
	W. Gradl

Other coworkers: T. Elster, Dr. R. Hommel, I. Steinacker, N. Nessler, computation team consisting of 10 students

Contractor: Dr. W. Bitterlich

C O N T E N T S

Preface

		Page
I	Experimental part	
	1,1 Review	I - 1
	1,2 Field strength measuring device	I - 2
	1,3 The amplifier of the transmitter and the transmitting antennas	I - 4
	1,4 Mine laboratory	I - 6
	1,5 Salzgitter mine Konrad I	I - 8
	1,6 Potassium mine Hansa III	I - 13
	1,7 Ore mines of Fuesseberg and Georg	I - 15
	1,8 Oranje Nassau mine in Heerlen	I - 17
	1,9 St. Gertraudi mine	I - 19
	1,10 Determination of the electrical conductivity of rock	I - 22
II	Theoretical part	
	2,1 Effect of quadrupole radiation	II - 1
	2,2 Effect of cavity	II - 3
	2,3 Maximum moment of magnetic antennas	II - 4
	2,4 Sub-scale tests	II - 5
	2,5 Determination of rock conductivity from VLF-propagation measurements	II - 6
	2,6 Horizontal magnetic dipole at the depth h under the earth's surface - Calculation of the radiation field by the integral method	II - 10
	2,7 Calculation of the dipole field using the VLF approximation	II - 25
	2,8 Another approach to the solution for a magnetic dipole	II - 36
III	Comparison of theory and experiment	
IV	Publications	
	References	IV - 1
	Review of publications	IV - 7